Prog. Energy Combust. Sci. 1987, Vol. 13, pp. 293–345
Printed in Great Britain.

0360-1285/87 $0.00 + .50

MIXING, TRANSPORT AND COMBUSTION IN SPRAYS

G. M. FAETH

The University of Michigan, Ann Arbor, MI 41803, U.S.A.

Abstract—Recent advances concerning analysis of sprays and drop/turbulence interactions are reviewed. Consideration is given to dilute sprays and related dilute dispersed flows, which contain well-defined dispersed-phase elements (e.g. spherical drops) and have dispersed-phase volume fractions less than 1%; and to the near-injector, dense spray region, having irregularly-shaped liquid elements and relatively-high liquid fractions.

Early analysis of dilute sprays and other dispersed flows assumed either locally-homogeneous flow (LHF), implying infinitely-fast interphase transport rates, or deterministic separated flow (DSF) where finite interphase transport rates are considered, but interactions between dispersed-phase elements and turbulence are ignored. These limits are useful in some instances; however, recent evidence shows that both methods are deficient for quantitative estimates of the structure of most practical dispersed flows, including sprays. As a result, stochastic separated flow (SSF) methods have been developed, which treat both finite interphase transport rates and dispersed phase (drop)/turbulence interactions using random-walk computations for the dispersed phase. Evaluation of SSF methods for particle-laden jets; nonevaporating, evaporating and combusting sprays; and noncondensing and condensing bubbly jets has been encouraging, suggesting capabilities of current SSF methods to treat a variety of interphase processes. However, current methods are relatively *ad hoc* and many fundamental problems must still be resolved for dilute flows, e.g. effects of anisotropic turbulence, modification of continuous-phase turbulence properties by the dispersed phase (turbulence modulation), effects of turbulence on interphase transport rates, and drop shattering, among others.

Dense sprays have received less attention and are poorly understood due to substantial theoretical and experimental difficulties, e.g. the idealization of spherical drops is not realistic, effects of liquid breakup and collisions are difficult to describe, spatial resolution is limited and the flow is opaque to optical diagnostics which have been helpful for studies of dilute sprays. Limited progress thus far, however, suggests that LHF analysis may provide a useful first-approximation of the structure and mixing properties of dense sprays near pressure-atomizing injectors. Since dense-spray processes fix initial conditions needed to rationally analyze dilute sprays, more research is this area is clearly warranted.

CONTENTS

Nomenclature 294
1. Introduction 295
2. Analysis of Dilute Dispersed Flows 297
   2.1. Formulation 297
   2.2. Analysis of turbulence 298
   2.3. State relationships 299
      2.3.1. Noncombusting flows 299
      2.3.2. Combusting flows 300
   2.4. LHF analysis 302
   2.5. DSF analysis 303
   2.6. SSF analysis 304
      2.6.1. Background 304
      2.6.2. Turbulence/dispersed-phase interactions 306
      2.6.3. Dispersed-phase trajectory analysis 306
      2.6.4. Continuous-phase source terms 308
3. Structure of Dilute Dispersed Flows 309
   3.1. Introduction 309
   3.2. Particle-laden gas jets 309
      3.2.1. Measurements of Yuu *et al.*[25] 309
      3.2.2. Measurements of McComb and Salih[26,27] 310
      3.2.3. Measurements of Laats and Frishman[28,29] 310
      3.2.4. Measurements of Levy and Lockwood[30] 312
      3.2.5. Measurements of Shuen *et al.*[31] 313
   3.3. Nonevaporating sprays 315
   3.4. Evaporating sprays 317
   3.5. Combusting sprays 319
   3.6. Particle-laden water jets 322
   3.7. Bubbly jets 323
      3.7.1. Measurements of Sun and Faeth[37,38] 323
      3.7.2. Measurements of Sun *et al.*[39] 324

4. Turbulence Modulation 326
4.1. Background 326
4.2. Modulation of turbulence spectra 327
5. Alternative Analysis of Dilute Dispersed Flows 330
5.1. Introduction 330
5.2. Interpenetrating continua analysis 330
5.2.1. Introduction 330
5.2.2. Mixing-length methods 330
5.2.3. One-equation methods 331
5.2.4. Higher-order methods 331
5.3. Discrete-element analyses 333
6. Dense-Dispersed Jets 335
6.1. Introduction 335
6.2. Background 335
6.2.1. Breakup regimes 335
6.2.2. Flow patterns 336
6.2.3. Breakup processes 338
6.2.4. Collisions 340
6.3. Dense-Spray Analysis 340
6.3.1. LHF analysis 340
6.3.2. Separated-flow analysis 341
7. Conclusions 342
Acknowledgements 342
References 343

NOMENCLATURE

a acceleration of gravity
C_c empirical constant, Eq. (46)
C particle concentration
C_D drag coefficient
C_i parameters in turbulence model
C_p specific heat in constant pressure
d injector diameter
d_p particle diameter
D coefficient of mass diffusion, drop diameter (Figs 21 and 36)
$E(K)$ turbulence energy spectrum
f mixture fraction
$f(\omega)$ Lagrangian frequency function
g square of mixture fraction fluctuations
G particle mass flux
h_{fg} enthalpy of vaporization
k turbulence kinetic energy
K wave number
L_{fc} length of liquid core
L_e dissipation length scale
L_L Lagrangian length scale
LR loading ratio
L_s total enthalpy rise of vaporization
$\dot{m}_0$ injector mass flow rate
m_p particle mass
M_A acceleration modulus
n number of particle groups
n_i number of particles per unit time in group i
$\dot{n}''$ particle number flux
$\dot{n}_p$ drop collision rate, Eq. (51)
N forced-convection correction factor
N_{vib} dimensionless frequency, Eq. (24)
$P(f)$ probability density function of mixture fraction
Pr Prandtl number
r radial distance
Re Reynolds number
R_N deviation of dispersed-phase velocity, Eq. (25)
SMD Sauter mean diameter
S_ϕ continuous-phase source term
$S_{p\phi}$ source term due to dispersed phase
t time
t_b drop breakup time, Eq. (49)
t_e eddy lifetime
t_p characteristic dispersed-phase response time
T temperature
T_L streamwise Lagrangian integral time scale
T'_L macro time scale

T_{WB} wet-bulb temperature
u, U axial velocity
u_{ri} component i of relative velocity
v radial velocity
V_j volume of computational cell j
w tangential velocity
W dispersed-to-continuous-phase mass ratio
We jet Weber number, Eq. (45)
We_p drop Weber number, Eq. (48)
x axial distance
y cross-stream distance
Y_i mass fraction of species i
α particle number intensity, void fraction
β property-reference-state factor, Eq. (23)
δ_{ij} Kronecker delta
Δ_A correction for virtual mass force
Δ_H correction for Bassett-history force
Δx_p relative path length of particles in an eddy
Δt_p time of particle residence in an eddy
ε rate of dissipation of turbulence kinetic energy
ε_p rate of dissipation due to dispersed phase
η Kolmogorov microscale
λ thermal conductivity, Eulerian microscale
μ viscosity
μ_t turbulent viscosity
ν kinematic viscosity
ξ variable of integration, energy spectrum constant, mixture fraction
ϱ density
σ surface tension
σ_t turbulent Prandtl/Schmidt number
ϕ generic property, fuel-equivalence ratio
ω angular frequency of oscillation
Ω_1, Ω_2 dispersed-phase spectral response functions

Subscripts

c centerline property
f liquid property
F evaporating fluid
p particle property
ref reference state
s particle surface property
0 injector exit condition
∞ ambient condition

Superscripts

$\overline{(\ )}, (\ )'$ time-averaged mean and root-mean-square fluctuating quantity
$\tilde{(\ )}, (\ )''$ Favre-averaged mean and root-mean-square fluctuating quantity
$(\rightarrow)$ vector quantity

1. INTRODUCTION

In spite of many practical applications, our understanding of sprays is relatively limited, since interactions between phases must be resolved in addition to the ususal problems of analyzing turbulence. In spite of the difficulties, however, there has been progress in the field. This has led to the development of new theoretical methods for treating sprays and the availability of measurements of flow structure to both evaluate analysis and to highlight features of the flow. The objective of this paper is to review these findings and to suggest areas where additional research is needed. While the main interest of this review is sprays, other dispersed flows (particle-laden jets, bubbly jets) are considered as well, since they offer simplified situations to test concepts useful for spray analysis.

Aspects of sprays have been considered during several earlier reviews. Soo[1] presents a comprehensive treatment of early work on dispersed flows and sprays. Particle-laden flows, which are closely related to sprays, are considered by Hinze,[2,3] Goldschmidt *et al.*,[4] Peskin,[5] Marble[6] and Lumley.[7] Interphase transport properties of drops, emphasizing nonturbulent effects, are considered by Faeth,[8] Clift *et al.*,[9] Law[10] and Sirignano.[11] Finally, Bracco,[12,13] Chigier,[14] Crowe,[15] Faeth,[16,17] Lefebvre,[18,19] Elkotb,[20] Drew[21] and Williams[22] review various aspects of spray structure and methods for analyzing sprays. The present paper is an extension of Refs 16 and 17, discussing recent work on analysis of sprays and related dispersed flows, and the evaluation of analysis with measurements.

Sprays and other dispersed flows are normally divided into dilute and dense flow regimes, cf. Faeth[8]

TABLE 1. Summary of measurements used for evaluation*

Source: configuration	Loading ratio	Reynolds number§	Continuous phase	Dispersed phase: Substance	Dispersed phase: Diameter‖ (μm)	Dispersed phase: Density (kg/m^3)
Hinze[3]: one-dimensional flow, isotropic turbulence	Single particles	–	Theoretical	Theoretical	0	0
Snyder and Lumley[24]: grid-generated turbulence in a duct	Single particles	11,000 (grid) 176,000 (channel)	Air	Hollow glass	46	260
				Corn pollen	87	1,000
				Glass	87	2,500
				Copper	47	8,900
Yuu *et al.*[25]: round particle-laden jet	0.0008–0.004†	11,000–56,000	Air	Fly Ash	20	2,000
McComb and Salih[26,27]: round particle-laden jet	Small†	5,000–15,000	Air	Titanium dioxide	2	4,260
				Tungsten	6	19,300
Laats and Frishman[28,29]: round particle-laden jet	0.3–1.4†	66,000–137,000	Air	Corundum	17–80	4,022
Levy and Lockwood[30]: round particle-laden jet	1.14–3.50†	20,000	Air	Sand	215–1,060	2,250
Shuen *et al.*[31]: round particle-laden jet	0.20–0.66†	14,600–18.700	Air	Sand	79–207	2,620
Solomon *et al.*[32,33]: round nonevaporating spray	1.78, 6.48†	30,000 and 24,000	Air	Vacuum pump oil	30, 87	878
Solomon *et al.*[34]: round evaporating spray	7.71, 15.8†	41,000 and 36,000	Air	Freon-11	31, 58	1,476
Shuen *et al.*[35]: ultradilute round combusting spray	0.018–0.036†	11,700	Methane flame	Methanol	105, 180	792
Parthasarathy and Faeth[36]: round particle-laden jet	0, 0.54, 0.108† 0, 0.024, 0.048‡	8,530	Water	glass	500	2,450
Sun and Faeth[37,38]: noncondensing bubbly round jet	2.4–9.1‡	8,740–9,380	Water	Air	1,000–1,200	1.14
Sun *et al.*[39]: condensing bubbly round jet	2.4, 4.8‡	8,740 and 8,860	Water	Carbon dioxide	900 and 1.050	1.73

*Round jets were injected into still media.
†Mass flow rate of dispersed phase per unit mass flow rate of continuous phase.
‡Volume flow rate of dispersed phase/unit volume flow rate of continuous phase.
§Reynolds number based on injector momentum and continuous-phase properties.
‖Initial SMD given for nonevaporating and evaporating sprays; rest were initially monodisperse.

for estimates of the regions where these flows are observed in sprays. Both regimes are considered in this review, although dilute flows are emphasized since more attention has been devoted to them in the past. Dilute dispersed flows contain well-defined dispersed-phase elements, e.g. spherical drops or bubbles, and have relatively small local dispersed-phase volume fractions (generally $< 1\%$). As a result, taking a dilute spray as an example, drop collisions are infrequent and heat transfer, mass transfer and drag coefficients of individual drops are not directly influenced by adjacent drops, i.e. correlations of drop heat transfer, mass transfer and drag coefficients are independent of liquid volume fraction or drop spacing.[12,13] A dilute spray, however, does not correspond to the behavior of isolated drops in a known environment, since transport from the drops influences the structure of the continuous phase, e.g. there is two-way coupling between the phases,[15] Our understanding of dilute dispersed flows has developed rapidly during the last decade, due to the emergence of optical diagnostics and new methods for analyzing turbulence. Major unresolved issues for dilute dispersed flows involve dispersed-phase/turbulence interactions,. e.g. the turbulent dispersion of the dispersed phase, the modification of continuous-phase turbulence properties by the presence of the dispersed phase (called turbulence modulation by Al Taweel and Landau),[23] and the direct effect of turbulence on interphase transport rates. These issues will be emphasized in the present review.

Dense dispersed flows are typified by the dense-spray region near the exit of an injector. This region involves the transition between an all-liquid flow in a passage and the dilute dispersion of drops which marks the start of the dilute-spray region. Thus, large liquid volume fractions are an important feature of dense sprays. Dense sprays are also characterized by irregularly-shaped, rather than spherical, liquid elements, e.g. ligaments and the long liquid core associated with pressure-atomized sprays.[12,13] Other complex phenomena are important in dense sprays as well, e.g. collisions of liquid elements, effects of liquid volume fraction in interphase transport rates, and breakup of liquid elements. Finally, measurements are problematical in dense sprays, due to the need for high spatial resolution and the opacity of the flow to optical diagnostics. The limited information available

today concerning dense sprays will be discussed in the review, including suggestions for circumventing some of the difficulties.

The paper begins with a description of common methods curently used to analyze dilute sprays. Simplified or baseline versions of these procedures are then used to interpret recent measurements of the structure of dilute sprays and related dispersed turbulent jets. The following flows are considered: particle-laden homogeneous turbulent flows; particle-laden gas jets; nonevaporating, evaporating, and combusting sprays; particle-laden liquid jets; and noncondensing and condensing bubbly jets. The actual data base to be considered is summarized in Table 1. The comparison between the predictions and the measurements also serves as an initial evaluation of these baseline analyses for a wide range of conditions. Work undertaken by the author and his associates is emphasized, since it provides a common basis of analytical and experimental methods for all these flows. Next, some general findings concerning dispersed-phase/turbulence interactions are considered, to provide background to help interpret aspects of dilute dispersed flows. Several recent alternative methods that have been proposed to treat dilute dispersed flows are then discussed. The paper concludes with a consideration of dense sprays, where existing information is far more limited.

2. ANALYSIS OF DILUTE DISPERSED FLOWS

2.1. *Formulation*

In order to provide perspective for the analytical methods considered in this review, various formulations used for dilute dispersed flows will be briefly considered in the following. Additional discussion of theoretical methods employed for these flows is provided by Soo,[1] Peskin,[5] Marble,[6] Bracco,[12,13] Crowe,[14] Faeth,[16,17] Elkotb,[20] Drew[21] and Williams,[22] and references cited therein.

Virtually every analysis used to treat dilute dispersed flows has unique features; however, some general categories can still be defined.[13,15,17] First of all, the methods can be broadly separated into two categories which identify the approach used to treat interphase transport rates, as follows: (1) locally homogeneous flow (LHF) analysis, where interphase transport rates are assumed to be infinitely fast; and (2) separated-flow analysis where finite interphase transport rates are considered. LHF analysis implies that the phases are in dynamic and thermodynamic equilibrium, i.e. at each point in the flow, all phases have the same velocity and temperature and are in phase equilbrium. This implies that dispersed flow processes are mixing controlled. LHF analysis only accurately represents dispersed flows whose dispersed-phase elements are infinitely small; therefore, fundamental errors are always present when LHF calculations are applied to practical systems. Nevertheless, uncertainties in prescribing parameters for more complete analysis are frequently quite large and LHF analysis becomes a viable alternative. Major advantages of LHF analysis are as follows: relatively little information is required to specify initial conditions for computations, since initial dispersed-phase size and the velocity distributions play no role in the computations; the formulation is equivalent to a single-fluid analysis, which simplifies computations; and very complex flows, involving the appearance and disappearance of a variety of phases, can be handled with relative ease.[17] These features make the use of LHF analysis attractive in many instances, in spite of the crude treatment of interphase transport rates; therefore, LHF analysis is one of the methods that will be considered in the following.

Separated-flow analysis has the potential to treat a broader class of dispersed flows, since effects of finite interphase transport rates are considered. Separated-flow models generally average over processes on scales comparable to the size of dispersed-phase elements, since resolving such phenomena would exceed practical limitations of computer storage and costs. Therefore, exchange processes between phases must be modeled independently, usually by employing empirical transport expressions. Separated flow-analyses invariably treat the continuous phase as continuous; however, both continuum and discrete formulations have been used for the dispersed phase. Two types of continuum formulations of the dispersed phase have been used. One involves treating both phases as interpenetrating continua, in conjunction with empirical interphase transport rates,[5,21] cf. Drew,[21] Gany *et al*,[40] and Harlow and Amsden[41] for early examples. Several recent analyses using this formulation will be considered in Section 5.2. An alternative is to describe dispersed-phase properties by a continuous distribution function, defined at all positions in the flow field, as described by Williams.[22] Both methods are convenient for isothermal monodisperse flows; however, the number of phases that must be considered, or the dimensions of the statistical distribution function, become awkwardly large for polydisperse flows involving both heat and mass transfer.[17] Furthermore, methods used to treat dispersed phase/turbulence interactions with these analyses have not been evaluated to a great extent. Therefore, present considerations will be limited to discrete formulations of the dispersed phase (discrete element formulations) since they overcome these difficulties—returning to the interpenetrating continuum methods in Section 5.2.

The discrete-element formulation involves dividing the dispersed phase into representative groups (samples), whose motion and transport are tracked through the flow field using a Lagrangian formulation. A Eulerian formulation is used to solve the governing equations for the continuous phase, similar to the solution of the flow equations for LFH calcula-

tions. However, separated-flow analysis also involves inclusion of source terms due to finite-rate transport from the dispersed phase in the governing equations for the continuous phase. There are two formulations of this type, as follows: (1) deterministic separated-flow (DSF) analysis, where finite interphase transport rates are considered, but dispersed-phase/turbulence interactions are ignored; and (2) stochastic separated-flow (SSF) analysis, where both finite interphase transport rates and effects of dispersed-phase/turbulence interactions are considered using random-walk computations for the motion and transport of the dispersed phase. DSF analysis has been the most popular approach used to treat dispersed flows in the past, particularly for sprays.[17] SSF analysis, however, is also of interest, since it provides a convenient formalism to consider dispersed-phase/turbulence interactions. Therefore, both methods will be considered in the following.

To recapitulate, three types of analysis of dilute dispersed flow will be examined, as follows: (1) LHF analysis, where interphase transport rates are assumed to be infinitely fast; (2) DSF analysis, where finite interphase transport rates are considered but dispersed-phase/turbulence interactions are ignored; and (3) SSF analysis, where both finite interphase transport rates and dispersed-phase/turbulence interactions are considered using random walk computations for the dispersed phase. The three methods provide a convenient way of highlighting effects of mixing (LHF analysis), finite interphase transport rates (DSF analysis), and dispersed-phase/turbulence interactions (SSF analysis), at least within the limitations inherent in the current state of the development of these methods.

2.2. *Analysis of Turbulence*

Subsequent development of the analysis is specific to the flows to be considered (summarized in Table 1). The formulation was developed using three general guidelines, as follows: (1) the methodology should be sufficiently general to accommodate the flows listed in Table 1 within a single formalism, e.g. the approach should be capable of dealing with flows as disparate as particle-laden jets and combusting sprays; (2) the formulations should be baseline analyses, designed to highlight features of specific importance for sprays and related dispersed flows, while minimizing empiricism as much as possible; and (3) the methods must be computationally tractable, yielding grid-independent, numerically-closed results with acceptable computation costs.

The continuous phase is invariably turbulent for practial sprays and other dispersed flows. Consistent with the objectives of the present analysis, turbulence properties of the continuous phase are modeled, while averaging over processes on the scale of dispersed-phase elements, as noted earlier. More exact numerical simulations of dispersed flows are beginning to appear which avoid the approximations and empiricism of turbulence models, cf. Peskin and Kau,[42] Moore and Davis,[43] and Davis *et al.*[44] However, these methods are currently limited to relatively simple, idealized problems due to limitations of computation time and costs; therefore, they do not offer a viable approach for most practical dispersed-flow problems or for evaluation using existing experimental results.

Present computations employ a density-weighted (Favre)-averaged k–ε–g turbulence model, in conjunction with the conserved-scalar formalism for scalar properties. This tactic is convenient since the full range of processes summarized in Table 1 can be considered with a single methodology, while minimizing empiricism. The turbulence modeling procedure originated with workers at Imperial College, cf. Lockwood and Naguib[45] and references cited therein, with subsequent development by Bilger[46,47] and Liew *et al.*[48,49] The use of Favre averages, rather than time (Reynolds) averages, is helpful for present purposes, since the formulation is simplified considerably for variable density flows.[46]

Improved methods of analyzing turbulence are being sought, and questions have been raised concerning the use of k–ε models for round jet-like flows similar to those listed in Table 1.[50] Nevertheless, the present formulation has been extensively evaluated for a variety of axisymmetric single-phase flows, yielding encouraging results with all empirical parameters kept constant. The evaluation has considered constant and variable density jets,[51,52] with data for evaluation drawn from Wygnanski and Fiedler,[53] Becker *et al.*,[54] Hetsroni and Sokolov,[55] Birch *et al.*,[56] Chevray and Tutu,[57] Shearer *et al.*[58] and Mao *et al.*[59] The evaluation has also extended to gaseous jet diffusion flames in still air, burning the following fuels: hydrogen,[60] carbon monoxide,[61] methane and natural gas,[51,62] propane[63] and ethylene.[64]

Several major assumptions of the continuous-phase analysis are appropriate for all the flows listed in Table 1. First of all, all the flows are axisymmetric and steady (in the mean) with no swirl. Next, the flows generally sastisfy the boundary layer approximations, which substantially reduces computation costs needed to obtain numerically accurate solutions. Mach numbers of all the flows are small, less than 0.1, therefore, mean kinetic energy can be neglected with little error. Flames which are considered are non-premixed. Effects of radiation are small for the flows listed in Table 1 and can be neglected. Radiation is most important for the combusting flow; however, even in this case, radiative losses are relatively small and the flames are optically thin; therefore, energy losses due to radiation could be treated as a perturbation of the adiabatic approximation.[51,62] Interactions between density fluctuations and pressure gradients, essentially buoyancy/turbulence interactions, were

ignored in the governing equations for turbulence quantities. This was done in the spirit of a baseline analysis, since including these effects substantially increases the complexity and empiricism of the analysis. Past work has shown that effects of buoyancy/turbulence interactions are relatively small for present flows in any event.[62]

A final major assumption of the continuous-phase analysis is that the exchange coefficients of all species and heat are the same. This implies that all laminar and turbulent diffusivities are identical. This is reasonable at high Reynolds numbers, typical of present test conditions, where laminar transport is small in comparison to turbulent transport. At low Reynolds numbers, however, differences between laminar diffusivities are frequently significant and other methods must be used; Bilger[65] proposes a perturbation technique for such conditions. Assuming equal exchange coefficients of all species and heat is also inappropriate for low Reynolds number flows when the LHF approximation is used, since the laminar diffusivities of even finely-divided dispersed phases are much smaller than those of gas molecules.[17] Fortunately, such circumstances are not often encountered for practical sprays and other dispersed flows.

Under these assumptions, the conserved-scalar formalism provides a convenient way to find scalar properties of the continuous phase, particularly if local thermodynamic equilibrium can be applied to the flow. This additional approximation implies that instantaneous scalar properties of the continuous phase are only a function of mixture fraction. Expressions relating scalar properties to mixture fraction are called state relationships.[17] Methods for determining state relationships are central to the development of the conserved-scalar formalism and are discussed in the next section.

2.3. *State Relationships*

2.3.1. *Noncombusting flows*

Applications of the conserved-scalar formalism to dispersed flows have generally involved two-stream problems, e.g. mixing of an injected fluid with an ambient stream. In this case, a single conserved scalar is sufficient to fix all scalar properties. The mixture fraction (the fraction of mass at a point which originated from the injector) is often chosen for this purpose. For two-stream problems, computation of state relationships varies, depending on whether the flow is noncombusting or combusting and whether the analysis is based on the locally homogeneous flow or separated flow approximations. The different circumstances will be briefly considered in the following.

State relationships for concombusting flows can be found by simple adiabatic mixing computations under the assumption of equal exchange coefficients of all species and heat, and negligible potential and kinetic energies and effects of radiation, cf. Faeth[17] for

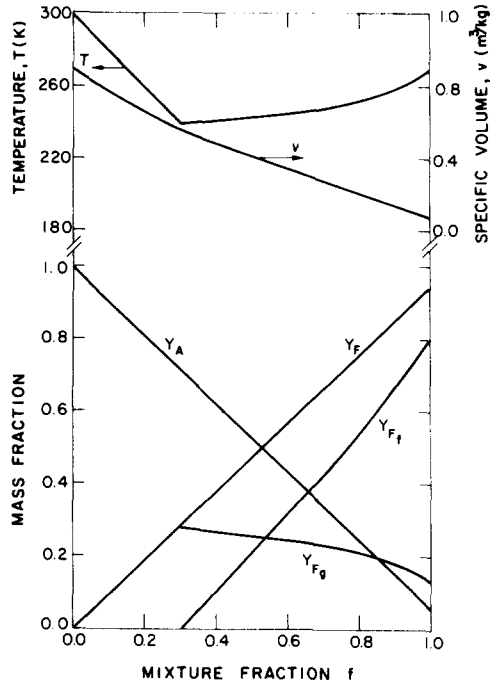

FIG. 1. Scalar properties as a function of mixture fraction for LHF analysis of an air-atomized Freon-11 spray evaporating in air at atmospheric pressure. From Shearer *et al.*[58]

the formulation of a number of examples. Results are the same for LHF and separared-flow analysis for conditions of mixing where only the continuous phase is present. When both phases are present, the LHF approximation implies that the temperature is uniform throughout both phases, and that phase equilibrium is maintained at the surface of the dispersed phase, for each mixture fraction. This allows straightforward computation of all scalar properties as a function of mixture fraction to provide the state relationships.[17]

An example of state relationships for a noncombusting flow, under the LHF approximation, is illustrated in Fig. 1 from Shearer *et al.*[58] These conditions involved air-atomizing injection of Freon-11 into still air at atmospheric pressure, with all flows initially at 300K. Since thermodynamic equilibrium is assumed throughout the flow, adiabatic saturation of air and Freon-11 in the injector causes the flow leaving the injector to have a temperature below 300K. The mass fraction of liquid Freon-11 decreases with decreasing mixture fraction, reaching zero at $f \sim 0.3$. At this point, the mass fraction of Freon-11 vapor reaches a maximum while the temperature is a minimum. With continuing reduction of f, the vapor mixture becomes more diluted in a straightforward manner, eventually reaching the properties of pure air at $f = 0$. Density is a relatively nonlinear function of mixture fraction, due to the presence of liquid for $f > 0.3$, e.g. both liquid and gas contribute to the density under the LHF approximation.

For separated-flow calculations, state relationships are only relevant for the continuous phase. Solomon

et al.[34] point out that this introduces a conceptual problem for the conserved-scalar formalism when the flow involves energy exchange between the phases. For example, drops undergo some bulk heating or cooling as they pass through the flow for the Freon-11 spray considered in Fig. 1, causing direct energy losses or gains by the continuous phase. This implies that both total enthalpy and mixture fraction are needed to specify instantaneous scalar properties of the continuous phase, which substantially complicates the continuous-phase analysis. In many instances, however, the sensible energy change of the bulk liquid is small in comparison to enthalpies of vaporization and combustion; therefore, this energy exchange can often be ignored with little error, retrieving the conserved-scalar formalism.

The energy exchange problem of separated flow analysis can also be circumvented by using the thin-skin approximation for drop heatup.[17,34] This implies that the bulk liquid remains at its initial condition, while only an infinitely-thin layer at the drop surface is heated (or cooled) during evaporation. This removes the energy exchange problem, since the evaporating substance always enters the continuous phase from the same thermal state; therefore, the properties of the continuous phase are once again fully defined by the mixture fraction. Sirignano and coworkers[11] have studied energy transport within drops, finding significant property variations within the drop througout most of its lifetime; therefore, the thin-skin approximation seems more appropriate than the more widely used uniform-drop-temperature approximation in any event.[8] In highly-loaded flows, however, this energy transport within the dispersed phase is important and the conserved-scalar formalism must be extended to consider conservation of energy and the correlation between total enthalpy and mixture fraction—a substantial complication.

2.3.2. *Combusting flows*

The present conserved-scalar formalism is limited to diffusion flame conditions for combusting flows. Early work found state relationships for combusting flows using procedures analogous to noncombusting flows,[17] assuming local thermodynamic equilibrium at all mixture fractions. Thermodynamic equilibrium at all mixture fractions is satisfied for some reactants,

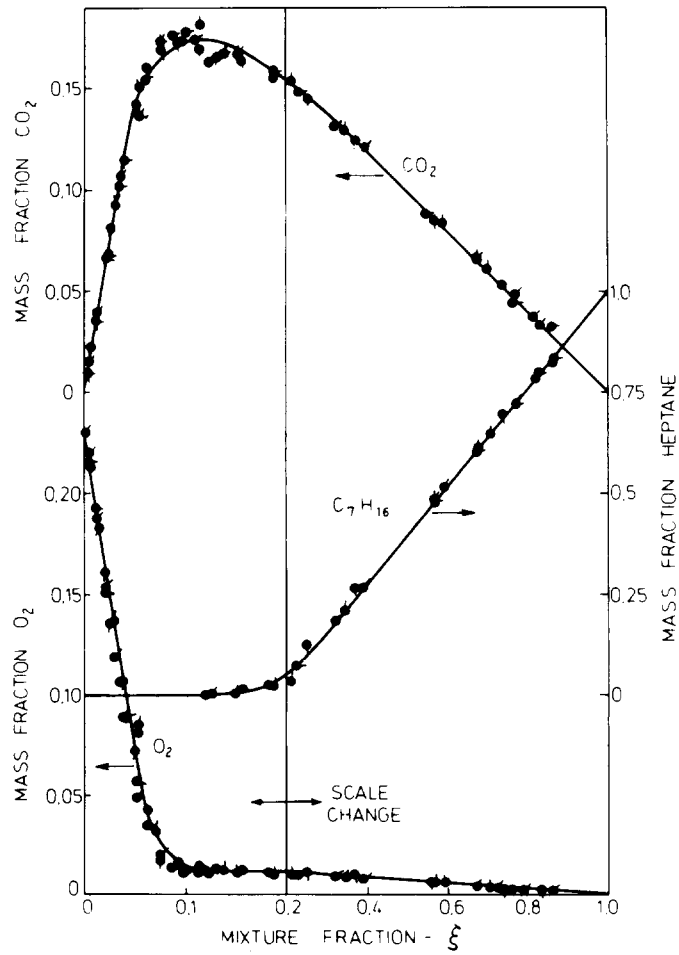

FIG. 2. Concentrations of major gas species as a function of mixture fraction for laminar *n*-heptane/air diffusion flames. From Bilger.[47]

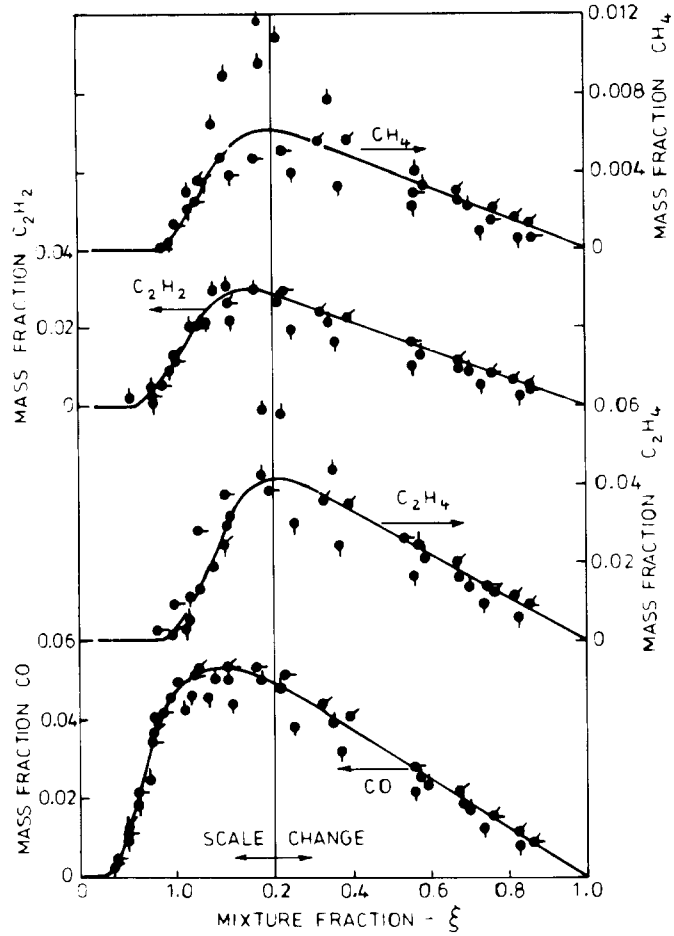

FIG. 3. Concentrations of minor gas species as a function of mixture fraction for laminar *n*-heptane/air diffusion flames. From Bilger.[47]

like hydrogen/air and carbon monoxide/air, except near regions of flame attachment.[60,61,66] The approach is also effective at fuel-lean conditions for hydrocarbon fuels. However, there are substantial departures from thermodynamic equilibrium for hydrocarbons at fuel-rich conditions, due to effects of finite-rate chemistry associated with the decomposition of the fuel and the formation and oxidation of soot.

Bilger[47] and Liew *et al.*[48,49] have proposed the laminar-flamelet approximation to circumvent the problem of loss of thermodynamic equilibrium for hydrocarbons at fuel-rich conditions. They note that scalar properties in laminar flames (for wide ranges of length scales, residence times and levels of flame stretch) are nearly universal functions of mixture fraction, even though these functions depart from thermodynamic equilibrium estimates at fuel-rich conditions. Thus, correlations of measurements made in laminar flames are used for state relationships, viewing scalar properties in turbulent flames as the result of a succession of laminar flamelets passing a given position (or a wrinkled laminar flame fluctuating within the flow).

Results using the laminar flamelet technique have been encouraging for analysis of turbulent single-phase hydrocarbon diffusion flames. This inlcudes turbulent methane or natural gas,[51] propane[48,63] and ethylene[64] flames burning in air.

The laminar flamelet hypothesis has not been tested for combusting sprays; however, available information supports its use.[47] During development of the laminar flamelet concept, Bilger[47] considered results for liquid *n*-heptane burning in air. This involved correlating scalar properties as a function of mixture fraction, based on measurements of Abdel-Khalik *et al.*[67] These measurements were obtained for laminar combustion around a porous sphere, continuously fed with liquid fuel (the boundary conditions of this flow are formally equivalent to the thin-skin approximation). The resulting correlations are illustrated in Figs 2 and 3. Tick marks on the data indicate positions of various radial traverses around the cylinder. Nearly universal correlations are found for major gas species (Fig. 2), at all positions around the cylinder, clearly supporting the laminar flamelet concept. There is greater scatter for the minor species (Fig. 3) suggesting some loss of universality; however, these departures are relatively small in comparison to uncertain-

ties generally associated with predictions of the structure of turbulent flames.

State relationships like those of Figs 2 and 3 are sufficient for separated-flow analysis of liquid hydrocarbons under the thin-skin approximation of drop heatup, e.g. the needed range of fuel-equivalence ratios is completely accessible from the experiment. However, LHF analysis using this data presents problems for the high mixture fraction regions, since mixture fractions are encountered which are difficult to simulate using stationary experiments. Examination of measurements like those of Figs 2 and 3, however, shows that results at high mixture fractions only involve mixing, e.g. fuel breakdown occurs at mixture fractions relatively near the stoichiometric mixture fraction while properties at higher mixture fractions essentially result from quenched adiabatic mixing. Thus, once the properties of the quenched state are known, properties at higher mixture fractions can be found by adiabatic-mixing computations (with frozen chemistry) for the fuel inlet and quenched states.

An example of state relationships found in this manner for LHF analysis is illustrated in Fig. 4. These results are for a pressure-atomized *n*-pentane spray burning in air (at 3 MPa with all reactants initially at 300K), from Mao *et al.*[68] Laminar flame data were not available for these conditions; therefore, the low mixture fraction region was computed assuming local thermodynamic equilibrium, using the Gordon and McBride[69] algorithm. For lack of other information

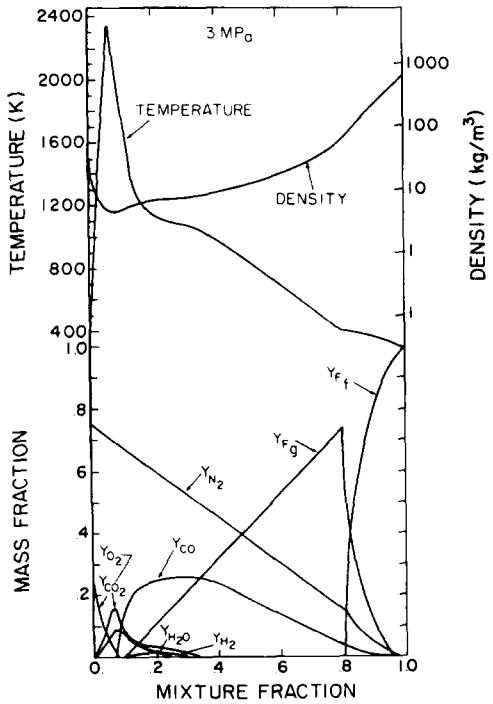

FIG. 4. Scalar properties as a function of mixture fraction for LHF analysis of a pressure-atomized n-pentane spray burning in air at 3 MPa. From Mao *et al.*[68]

the process was assumed to be quenched at $f \sim 0.4$ (gas temperature $\sim$ 1000K), with properties at higher mixture fractions computed assuming adiabatic mixing. For these high-pressure conditions, real-gas effects, involving appreciable quantities of ambient gas dissolved in the liquid phase, become important. This was considered using the Redlich–Kwong equation of state with multicomponent mixing rules due to Prausnitz and Chueh.[70] Fuel-rich properties at low mixture fractions are likely to be in error due to the loss of chemical equilibrium, discussed in connection with Figs 2 and 3; however, the results illustrated in Fig. 4 show that complex phenomena can be handled with relative ease within the LHF approach—one of its major advantages.

In summary, the conserved-scalar formalism, along with the laminar flamelet concept for hydrocarbon combustion, provides a convenient approach for finding scalar properties using either LHF or separated flow analysis. Major advantages are that the approach can accommodate a wide range of flows within a single procedure, and that the methodology conforms to the recognized structure of turbulent flames—at least when the wrinkled laminar flame structure is appropriate. These conditions are satisfied for the flows to be considered here; therefore, the approach is adopted in the following.

2.4. *LHF Analysis*

Portions of the analysis have been described in an earlier review.[17] However, at that time, analysis of the continuous phase was based on the time-averaged approach of Lockwood and Naguib,[45] and many features of the SSF analysis were not considered. Subsequent work has involved use of a Favre-averaged formulation and additiional modification of SSF analysis; therefore, curent features of the baseline LHF, DSF and SSF analyses, used in connection with the measurements of Table 1, are described in the next three sections.

LHF analysis will be considered first since the same formulation is used for the continuous phase for all three methods. The LHF approximation implies local kinematic and thermodynamic equilibrium (extended by the laminar flamelet concept when needed), including both phases; therefore, multiphase flows correspond to a variable-property single-phase fluid due to variations in the concentration of the dispersed phase, even in instances when the properties of each phase are constant. This generally causes continuous-phase density variations; therefore, properties are represented as Favre averages, defined as follows:[46]

$$\tilde{\phi} = \overline{\varrho\phi}/\bar{\varrho}. \qquad (1)$$

In Eq. (1), ϕ is a generic property and an overbar denotes a conventional time average.

The conserved-scalar formalism, in conjunction with a k–ε–g turbulence model, requires solution of

TABLE 2. Continuous-phase source terms in governing equations

ϕ	S_ϕ
1	0
$\tilde{u}$	$\alpha(\varrho_\infty - \bar{\varrho})$
$\tilde{f}$	0
k	$\mu_t\left(\frac{\partial\tilde{u}}{\partial r}\right)^2 - \bar{\varrho}\varepsilon$
ε	$C_{\varepsilon 1}\mu_t\frac{\varepsilon}{k}\left(\frac{\partial\tilde{u}}{\partial r}\right)^2 - C_{\varepsilon 2}\bar{\varrho}\frac{\varepsilon}{k}$
g	$C_{g1}\mu_t\left(\frac{\partial\tilde{f}}{\partial r}\right)^2 - C_{g2}\bar{\varrho}\frac{\varepsilon}{k}$

C_μ	$C_{\varepsilon 1}$	C_{g1}	$C_{\varepsilon 2} = C_{g2}$	σ_κ	σ_ε	$\sigma_f = \sigma_g$
0.09	1.44	2.8	1.87	1.0	1.3	0.7

governing equations for conservation of mass, momentum and mixture fraction, along with modeled governing equations for the turbulence quantities, k, ε and g. These equations can all be written in a common form as follows:

$$r\partial/\partial x(\bar{\varrho}\tilde{u}\phi) + \partial/\partial r(r\bar{\varrho}\tilde{v}\phi) = \partial/\partial r((r\mu_t/\sigma_\phi)\partial/\partial r(\phi)) + rS_\phi. \quad (2)$$

The parameters ϕ and S_ϕ appearing in Eq. (2) are summarized in Table 2, along with appropriate empirical constants. The constants are the same as earlier work,[17,45] except $C_{\varepsilon 2} = C_{g2} = 1.87$ for all flows, rather than the two different values for non-combusting and combusting flows used earlier (1.87 is roughly the average of the two). Reynolds numbers of present flows are relatively large; therefore, laminar transport can be ignored with little error and the turbulent viscosity becomes

$$\mu_t = C_\mu\bar{\varrho}k^2/\varepsilon. \quad (3)$$

Mean scalar properties are found from the state relationships and the probability density function of mixture fraction. The formulation can accommodate any two-parameter PDF. Within this class (e.g. clipped Gaussian, beta, etc.), past results suggest that scalar property predictions are relatively insenitive to the specific formula used for the PDF.[45] Present results employ a clipped-Gaussian Favre-averaged PDF, $\tilde{P}(f)$. The two parameters needed to specify this distribution can be found by noting the following identities:

$$\tilde{f} = \int_0^1 f\tilde{P}(f)\,df \quad (4)$$

$$g = \int_0^1 (f - \tilde{f})^2\tilde{P}(f)\,df. \quad (5)$$

Since both $\tilde{f}$ and g are known, from solving Eq. (2), Eqs (4) and (5) provide two implicit equations to find the two parameters of the Favre PDF. This step must be carried out frequently during computations; therefore, tables developed by Shearer *et al.*[58] were used to speed parameter determination.

Given the state relationships, $\phi(f)$, the Favre-averaged mean and variance of scalar properties can be computed from the following equations.[46]

$$\tilde{\phi} = \overline{\varrho\phi}/\bar{\varrho} = \int_0^1 \phi(f)\tilde{P}(f)\,df \quad (6)$$

$$\tilde{\phi}''^2 = \overline{\varrho\phi''^2}/\bar{\varrho} = \int_0^1 (\phi(f) - \tilde{\phi})^2\tilde{P}(f)\,df. \quad (7)$$

$\bar{\varrho}$ is needed to solve Eq. (2) and it is frequently convenient to have estimates of time-averaged scalar properties as well. Time averages can be found by noting that density is only a function of mixture fraction under present approximations; therefore, the time- and Favre-averaged PDFs of mixture fraction are related as follows;[46]

$$\bar{P}(f) = \bar{\varrho}\tilde{P}(f)/\varrho(f). \quad (8)$$

As a result, the time-averaged mean and variance of scalar properties become:

$$\bar{\phi} = \bar{\varrho}\int_0^1 (\phi(f)/\varrho(f))\tilde{P}(f))\,df \quad (9)$$

$$\bar{\phi}'^2 = \bar{\varrho}\int_0^1 ((\phi(f) - \bar{\phi}(f))^2/\varrho(f))\tilde{P}(f)\,df. \quad (10)$$

The value of $\bar{\varrho}$, needed to integrate Eq. (2), can be found by setting $\phi = 1$ in Eq. (9).

LHF analysis is not limited to dilute dispersed flows and requires relatively little information concerning initial conditions; therefore, LHF computations were initiated at the jet exit in all cases considered here. The prescription of initial conditions and methods used to solve the governing equations are described elsewhere.[17]

2.5. *DSF Analysis*

Both separated-flow analyses adopt the main features of the LHF analysis for the continuous phase. Present methods are limited due to dilute dispersed flows; therefore, volume fractions of the continuous phase are near unity and the basic formulation of Eq. (2) and the flow source terms in Table 2 can be retained. The main extension of the continuous-phase analysis for the separated-flow methods involves the appearance of source terms due to transport from the dispersed phase. Initial conditions are prescribed at the point nearest to the injector where all needed properties can be measured. At this point, the dispersed phase is divided into groups (defined by initial position, size, velocity and

TABLE 3. Dispersed-phase source terms in governing equations

ϕ	$S_{p\phi}$
1	$\bar{S}_{pm} = \sum_{i=1}^{n} n_i \Delta m_i / V_j$
$\tilde{u}$	$\bar{S}_{pu} = \sum_{i=1}^{n} \dot{n}_i(\Delta(m_i u_{pi}) + m_{im} a(1 - \bar{\varrho}/\varrho_p)\Delta t_{pi})/V_j$
$\tilde{f}$	$\bar{S}_{pm}$
k	$\tilde{u}\bar{S}_{pu} - \tilde{u}\bar{S}_{pu}$
ε	$-2C_{\varepsilon 3}\mu_t \frac{\varepsilon}{k}\frac{\partial \bar{S}_{pu}}{\partial r}$
g	$2(\widetilde{f S}_{pm} - \tilde{f}\bar{S}_{pm})$

direction). Lagrangian computations then track the subsequent life history of each group in the flow field.

Transport from the dispersed phase introduces new source terms, $S_{p\phi}$, in the governing equations for the continuous phase. These are found by computing property changes for each dispersed-phase group, i, as it crosses a computational cell, j, and then summing over all groups intersecting a particular cell. Expressions for the $S_{p\phi}$ are summarized in Table 3. DSF analysis ignores all phase/turbulence interactions; therefore, the source terms appearing for k, ε and g in Table 3 are not used with this approach.

While mass and momentum exchange between the phases can be handled directly by the conserved-scalar formalism, there is a conceptual problem with respect to energy transfer, as noted earlier. This was handled during construction of state relationships by adopting the thin-skin approximation of drop heat-up, described in Section 2.3. The mixture fraction used in the state relationships for separated flows is the mixture fraction of the continuous phase.

The formulation of the equations governing trajectories or life histories of dispersed-phase groups will be deferred until the SSF approach is discussed. This aspect of DSF and SSF analysis is the same, except that DSF computations are based on mean continuous-phase properties while the SSF approach seeks to account for the instantaneous properties experienced by the dispersed phase. Formally, mean interphase transport rates should be found by finding the time average of each interphase transport expression, considering variations of scalar properties with mixture fraction and the effect of relative velocity, as well as the correlation between mixture fraction and velocity. For example, if $F_D\ (f,\ u_{ri})$ represents the functional form of the drag for a particular dispersed-phase group, and $P\ (f,\ u_i)$ represents the time-averaged joint probability function of the local mixture fraction and continuous-phase velocity, then the proper time-averaged drag of the group is given by

$$\overline{F_D} = \int_0^1 \int_{-\infty}^{\infty} F_D(f,\ u_{ri})\bar{P}(f,\ u_i)\ \mathrm{d}f\ \mathrm{d}u_i. \qquad (11)$$

Finding $F_D\ (f,\ u_{ri})$ is relatively straightforward, after adopting a model for interphase transport of momentum; however, finding $P\ (f,\ u_{ri})$ substantially increases the complexity of the continuous-phase analysis. A form for the joint PDF must be specified. Then finding the parameters of the joint PDF requires information on correlations between mixture fraction and all the velocity components. Progress is being made in developing higher-order turbulence models capable of providing information of this nature, cf. Jones;[71,72] however, reliable methods to find these variables have not been reported for multiphase flows. Furthermore, DSF analysis has more serious sources of errors, as we shall see. Therefore, ad hoc property averages are generally adopted to find mean interphase transport rates for DSF analyses.

The procedure adopted in the DSF computations reported here is to compute interphase transport rates using time-averaged mean scalar properties found from Eq. (9), and Favre-averaged mean continuous-phase velocities from the solutions of Eq. (2). This choice is convenient since these properties are provided directly by the analysis (use of mean scalar properties at f also could be used, reducing computation times since the integrals of Eq. (9) would not have to be evaluated, but this approach has not been tested). Time-averaged velocities are more appropriate than Favre averages; however, this requires knowledge of density/velocity correlations which are not provided by the continuous-phase turbulence model, e.g.

$$\tilde{u}_i = \tilde{u}_i - \overline{\varrho' u_i'}/\bar{\varrho}. \qquad (12)$$

Such a modification is unlikely to result in significant changes in predictions, however, since differences between time- and Favre-averaged mean velocities are relatively small, even in flames.[66] Thus, in the spirit of baseline analysis, the more-approximate approach is adopted for present computations.

2.6. *SSF Analysis*

2.6.1. *Background*

There is abundant evidence that both finite interphase transport rates and dispersed phase/turbulence interactions are important in most practical dispersed flows.[16,17] Finite interphase transport rates are ignored during LHF analysis while dispersed-phase/turbulence interactions are ignored during DSF analysis; therefore, neither approach is sufficiently complete. The SSF method was developed in order to circumvent these limitations, by extending the DSF method.

There are three main types of dispersed-phase/turbulence interactions, as follows: (1) turbulent

transport or dispersion of the dispersed phase itself; (2) modification of continuous-phase turbulence properties by transport from the dispersed phase, called turbulence modulation by Al Taweel and Landau;[23] and (3) modification of the properties of interphase transport rates by turbulent fluctuations, e.g. the fact that nonlinear interphase transport rate expressions cannot be properly represented using mean properties in the interphase transport rate expressions, as discussed in connection with the DSF analysis.

Initial work on these problems concentrated on turbulent dispersion at the small-particle limit e.g. Tchen,[73] Hjelmfelt and Mockros,[74] and Hinze.[2,3] This implies linear interphase transport (Stokes flow), and that particles remain within a single fluid element (eddy) during their motion. Later, Elghobashi and Abou-Arab[75] extended these ideas to treat turbulence modulation as well. The small-particle limit provides a logical approach for developing a better understanding of dispersed-phase/turbulence interactions but the assumptions involved are too restrictive for most practical dispersed flows—particularly sprays. First of all, typical drop Reynolds numbers in sprays are on the order of 100, which is well beyond the Stokes regime. As a result, drops have significant velocities relative to the continuous phase and do not remain associated with a particular fluid element. This phenomenon, recognized by Yudine[76] and Csanady,[77] is called the crossing-trajectories effect, e.g. representing the fact that dispersed-phase elements and turbulent eddies follow different trajectories and only interact for a time.

Jurewicz and Stock[78] propose a more general approach for treating turbulent dispersion, using a gradient diffusion approximation within the Lagrangian formulation for the motion and transport of the dispersed phase. This involves definition of an effective diffusion velocity, or diffusion force, in the equation of motion of the dispersed phase. The diffusion velocity was found using an empirical turbulent diffusivity in conjunction with the concentration gradient of the dispersed phase.[15] Abbas *et al.*[79] use a similar approach. Dukowicz[80] also proposes a related procedure based on a stochastic representation of dispersed-phase diffusion. However, these methods are of limited value since they do not provide a means of estimating the dispersed-phase diffusivities. Dispersed-phase diffusivities depend on the properties of both the turbulence and the dispersed phase, e.g the rates of turbulent dispersion of small and large particles (or even the same sized particles if they have different relative velocities with respect to the continuous phase) differ in the same turbulence field, even when other properties of the particles are the same. Therefore, the accumulation and correlation of appropriate data for these methods are substantial tasks which have not proceeded very far.

Stochastic separated-flow methods have been proposed by a number of workers, as a means of predicting dispersed-phase/turbulence interactions without recourse to empirical data for properties like dispersed-phase turbulent diffusivities. Hutchinson *et al.*[81] report one of the earliest studies along these lines, proposing many of the ideas used in current SSF analysis. They treat turbulent dispersion of particles in a pipe, in an attempt to predict particle deposition rates. The approach involved random-walk computations of particles interacting with a succession of eddies having statistically-independent properties. It was assumed that the energy-containing eddies of the flow exerted primary influence on particle motion and that the time of interaction between a particle and a particular eddy was governed by the characteristic lifetime of the eddies. The flow was assumed to be ultradilute; therefore, only one-way coupling was considered, i.e. eddy properties were specified from existing correlations for single-phase turbulent pipe flows. The results of this procedure were compared with the data for particle deposition in turbulent pipe flows available at that time, yielding encouraging agreement.[81]

Subsequently, Brown and Hutchinson[82] extended the approach of Hutchinson *et al.*[81] Two types of interactions between eddies and particles were recognized, involving times of interactions between particles and eddies controlled by either the eddy lifetime or the time required for a particle to traverse an eddy—whichever is shorter. In a sense, the latter time limit attempts to account for effects of crossing trajectories.

Yuu *et al.*[25] independently adopted a procedure similar to Hutchinson *et al.*,[81] in order to analyze turbulent diffusivities in particle-laden jets. One-way coupling, continuous-phase-to-particle, was assumed with interaction times governed only by eddy lifetimes. Eddy properties were found using existing empirical correlations for jet properties. Later work revealed problems with these computations, associated with neglect of mean relative velocities between the phases and use of the Stokes drag law; however, the results were still encouraging. Subsequently, Dukowicz[80] proposed a similar approach for analysis of turbulent dispersion in dilute sprays.

Gosman and Ioannides[83] extended these ideas to obtain an SSF analysis which treats two-way coupling between the phases and incorporates a k–ε–g model to estimate eddy properties and phase interaction parameters. Their approach has been modified only slightly during subsequent evaluation by the author and his associates,[31–39, 84–86] and forms the basis of the baseline SSF analysis described in the following.

With SSF analysis, as dispersed-phase elements move through the flow, they are assumed to interact with a succession of turbulent eddies, simulating actual conditions by a random-walk computation. Properties within a particular eddy are assumed to be uniform, but change in a random manner from one eddy to the next. Eddy properties are obtained from the continuous-phase analysis, which includes source

terms to provide for transport from the dispersed phase, e.g. there is two-way coupling between the phases. The dispersed-phase computations are the same as the DSF approach, except that instantaneous eddy properties are used for the local environment of the dispersed-phase elements, rather than mean properties. Thus, in principle, the method can treat all aspects of dispersed-phase turbulence interactions, subject to the limitations of the continuous-phase turbulence model and the uniform-eddy approximation. In a sense, the method is an exact simulation of dispersed-phase properties. However, current limitations concerning physical understanding and numerical simulation of continuous-phase turbulence properties for practical dispersed flows requires the use of a model of turbulence for the continuous phase.

2.6.2. *Turbulence/dispersed-phase interactions*

For the present SSF Analysis, properties of each eddy at the start of interaction with a dispersed-phase element are found by making a random selection compatible with the PDFs of velocity and mixture fraction. The distinction between Favre- and time-averaged velocities must be ignored, similar to the DSF analysis, due to the limitations of the current simplified continuous-phase turbulence model. This is not a serious problem for mean velocities, as noted earlier. However, differences between Favre- and time-averages are greater for velocity fluctuations—particularly in flame environments. For example, existing measurements of streamwise velocity fluctuations in jet diffusion flames suggest that time-averaged velocity fluctuations can be up to 50% greater than Favre-averaged velocity fluctuations.[66] Evidence of this effect will be presented later; however, the approximation will be used in conjunction with the present baseline continuous-phase analysis.

Jet-like flows, similar to those listed in Table 1, usually have anisotropic turbulence properties, e.g. Wynanski and Fieldler[53] find $\tilde{u}'^2:\tilde{v}'^2:\tilde{w}'^2 = k:k/2:k/2$ near the axis of single-phase turbulent jets. Nevertheless, work to date has invariably assumed that velocity fluctuations are isotropic and have statistically-independent Gaussian PDFs in each coordinate direction. The most probable values and variances of these distributions are taken to be the local mean velocities in each direction and $2k/3$—obtained from the continuous-phase solution. Extension of this approach to consider anisotropic turbulence properties will be considered in connection with particle-laden liquid jets.

Scalar properties of each eddy are found by assuming that velocities and mixture fractions are statistically independent, for lack of a rational alternative under the approximations of the present k–ε–g model. This effect is only relevant when mixing of different substances or combustion occurs in the continuous phase. In such cases, errors are incurred by this approximation, since the correlation between mixture fraction and velocity fluctuations is on the order of one-half in portions of most boundary layer flows.[66] The time-averaged PDF of mixture fraction is available from Eq. (8), and random samples consistent with this PDF are used to select values of f for each eddy. Scalar properties of the eddy are then found from the state relationships, using the sampled value of f.

A dispersed-phase element is assumed to interact with an eddy as long as the relative displacement of the element with respect to the eddy does not exceed the characteristic eddy size, L_e, and the time of interaction does not exceed the characteristic eddy lifetime, t_e, e.g.

$$|\Delta\vec{x}_p - \vec{u}\Delta t_p| \leq L_e, \qquad \Delta t_p \leq t_e. \tag{13}$$

Thus, the limit with respect to eddy size also incorporates isotropic ideas, e.g. only the total relative displacement is measured to find the interaction time, with no concern for different eddy dimensions in the different coordinate directions. The characteristic eddy parameters are taken to be the dissipation-length and time scales which can be obtained from the continuous-phase solution, as follows:

$$L_e = C_\mu^{3/4}k^{3/2}/\varepsilon, \qquad t_e = L_e/(2k/3)^{1/2}. \tag{14}$$

The prescriptions given by Eqs (13) and (14) differ somewhat from Gosman and Ioannides,[83] who employ an approach similar to Hutchinson *et al.*[81] However, calibration of the SSF analysis yielded better results with Eqs (13) and (14), which are also more convenient to evaluate.[84–86]

The selections of L_e and t_e in Eqs (14) are clearly arbitrary, since only one scale out of the entire turbulent spectrum is used to represent interactions with the dispersed phase. Furthermore, predictions of turbulent dispersion are sensitive to the values of L_e and t_e used in the simulation.[35] Therefore, following Gosman and Ioannides,[83] these choices were evaluated by comparing predictions with the fundamental dispersion results of Hinze[3] and Snyder and Lumley.[24]

Hinze[3] developed an expression for the diffusion of "marked" fluid particles introduced at a constant rate from a point source in a homogeneous and isotropic turbulent flow. He obtains an analytical dispersion expression for this situation, assuming a constant turbulent diffusivity. Comparable results were obtained from the stochastic model by fixing values of u, k and ε and computing the turbulent diffusivity used in the analytical solution as $C_\mu\bar{\varrho}^2k^2/\varepsilon$, which is consistent with the present turbulence model.[84] A typical comparison between the analytical and stochastic predictions is illustrated in Fig. 5. The agreement between the two methods is reasonably good, with only a slight tendency for the present approach to underestimate the rate of dispersion. Since the particles were assumed to be infinitely small, they are always "captured" by eddies for these conditions, e.g. interactions times are governed by eddy lifetimes.

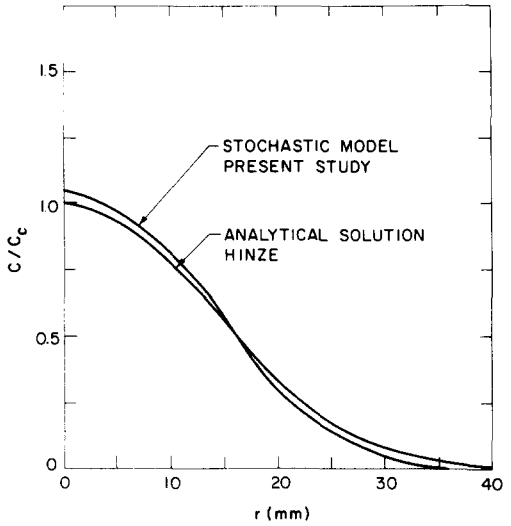

FIG. 5. Analytical and numerical solutions for the transverse distribution of infinitely small particles from a point source. Adapted from Shuen *et al.*[84]

Therefore, this calibration primarily tests the prescription for t_e.

The measurements of Snyder and Lumley[24] involved dispersion of various types of individual solid particles which were injected isokinetically (in the mean) into a uniform turbulent flow downstream of a grid. The results of the present predictions,[84] and these measurements are illustrated in Fig. 6. The SSF predictions are in reasonably good agreement with the measurements for both light particles (hollow glass beads) where t_e controls the interaction time, and heavy particles (glass and copper beads) where L_e controls the interaction time.[84]

Results for the calibration flows, where turbulence properties are nearly uniform over the flow field, are seen to be reasonably satisfactory. Subsequent evaluation in Section 3 will consider shear flows where there are significant variations of turbulence properties with position.

2.6.3. *Dispersed-phase trajectory analysis*

Assumptions of the dispersed-phase trajectory calculations vary since flows as disparate as particles (drops) in gases and bubbles in liquids will be considered; therefore, individual sources should be consulted for details. Assumptions common to all, which are typical of past analysis of dilute sprays,[8,17] are briefly summarized here. In addition, the formulation used for evaporating sprays is described, since it involves features used in most of the cases listed in Table 1.

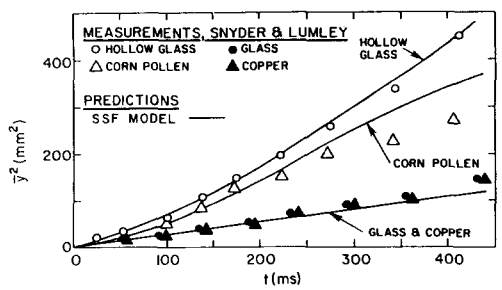

FIG. 6. Particle dispersion in a uniform, grid-generated turbulent flow. Adapted from Shuen *et al.*[84] Measurements from Snyder and Lumley.[24]

First of all, interphase transport is assumed to be quasisteady, e.g. at each instant transport rates are taken to be steady-state transport rates for the same boundary conditions. Past evaluations have generally shown that characteristic times of transient development of the flow field around dispersed-phase elements are small in comparison to other characteristic times of dispersed flows, justifying this assumption.[8,17] Dispersed-phase elements are assumed to be spheres, which is a condition of the experiments for the particle-laden jets and bubbly jets of Table 1; drops deform from spherical shapes but interphase transport expressions for drops naturally incorporate this effect. Heat transfer, mass transfer and drag coefficients (transfer coefficients) are assumed to be independent of the volume fraction of the dispersed phase, e.g. the transfer coefficients are taken to be equivalent to those of dispersed-phase elements in an infinite environment having the same properties as the eddy. O'Rourke and Bracco[87] consider effects of finite volume fractions of the dispersed phase on transfer coefficients, using results developed for fluidized beds. They conclude that this effect is not important for dispersed-phase volume fractions less than 10%, which is the range of interest for dilute dispersed flows. Effects of Magnus and Saffman-lift forces are ignored. Magnus forces are difficult to quantify since the initial spin of dispersed phase elements is generally unknown; however, strong effects of this phenomenon have only been suspected in a few instances, e.g. the results of Laats and Frishman.[28,29] Past evaluation has shown that Saffman-lift effects are generally small for multiphase jets.[17] The surface of the dispersed-phase element is assumed to be in thermodynamic equilibrium, which is satisfactory for evaporation of drops having diameters greater than 1 μm at atmospheric pressure and above, even for combusting conditions.[17] Empirical expressions are used to treat drag, virtual mass and Basset history forces. Interphase energy and mass transfer are treated using stagnant film theory, which allows for finite mass transfer rates, with empirical correction for effects of forced convection. As noted earlier, such modeling of interphase transport coefficients is currently necessary due to computational limitations. These methods, of course, are widely accepted during analysis of transport. Finally, only hydrostatic pressure variations are considered, which is a condition of the experiments.

Under these assumptions, the motion of the dispersed phase can be determined using the formulation of Odar and Hamilton,[88] which was reviewed later by Clift *et al.*,[9] as follows:

$$(\varrho_p/\varrho + \Delta_A/2)\, \mathrm{d}/\mathrm{d}t(u_{ri}) = a(1 - \varrho_p/\varrho)\,\delta_{ji} - 0.75 C_D |u_{ri}| u_{ri}/d_p + \Delta_H (81\nu/\pi \mathrm{d}_p^2)^{1/2} \int_{t_0}^{t} (t - \xi)^{-1/2} \mathrm{d}/\mathrm{d}\xi\,(u_{ri})\,\mathrm{d}\xi \quad (15)$$

where δ_{ji} is the Kroneker delta function and $i = 1$ represents the free fall (or rise) direction of the dispersed phase. The two-terms on the LHS of Eq. (15) represent accelerations due to particle and virtual mass. Only the former is important for particle (drop)/gas flows; only the latter for bubble/liquid flows. However, both are important for particle/liquid flows. The terms on the RHS of Eq. (15) represent buoyancy, drag and Basset history forces. The Bassett history force is important for bubble/liquid and particle/liquid flows but can be ignored for particle (drop)/gas flows with little error. The parameters Δ_A and Δ_H were empirically correlated by Odar and Hamilton[88] as a function of the acceleration modulus, defined as follows:

$$M_A = \mathrm{d}/\mathrm{d}t(u_r) d_p/u_r^2. \quad (16)$$

The values of Δ_A and Δ_H vary between 0.1–2.1 and 1.00–0.48—the former values being the correct limit for the classical Basset–Boussinesq–Oseen (B–B–O) formulation of Eq. (15). Drag coefficients were obtained either from the values for solid spheres (particles/drops) summarized by Faeth,[8,17] or for bubbles, summarized by Moore[89] and Clift *et al.*[9] The position of each dispersed-phase group is found by integrating the group velocity as a function of time.

The approach used to formulate interphase transport of mass and energy will be illustrated using drop vaporization as an example, following Solomon *et al.*[34] Original sources should be consulted for other cases. In addition to previous assumptions the gas-phase Lewis number is assumed to be unity; only concentration diffusion is considered with equal binary diffusivities of all species; and the Chapman gas property approximations are used, e.g. we assume an ideal gas mixture with $\varrho^2 D$, $\varrho\lambda$ and C_p constant. These assumptions are removable, at the expense of a more complex formulation, cf. Law.[10] In the present case, they are adopted for simplicity, with the resulting procedure calibrated using measurements for individual drops in environments typical of conditions within the spray.[34]

Based on these assumptions, the rate of change of mass of a drop in group i is given by

$$\mathrm{d}/\mathrm{d}t\,(m_{pi}) = -2\pi(\varrho D)_{\mathrm{ref}} d_p N \ln((Y_{FS} - Y_{F\infty})/(1 - Y_{Fs})) \quad (17)$$

where Y_{Fs} is the mass fraction of drop vapor at the liquid surface and N is a correction factor allowing for drop motion with respect to the gas phase (forced convection correction), as follows[17]

$$N - 1 = 0.276\, Re^{1/2} Pr^{1/3}/(1 + 1.232/(Re\, Pr^{4/3})^{1/2}. \quad (18)$$

For mass transfer, the Schmidt number should be used instead of the Prandtl number in Eq. (18); however, this distinction is not made since $Sc = Pr$ according to the unity Lewis number assumption. Under the thin-skin approximation, all the heat reaching the liquid surface is used to preheat the liquid to the surface temperature and vaporize it, e.g. no bulk heating is considered. This yields the following relationship between surface temperature and mass fraction

$$Y_{Fs} = (C_p(T_\infty - T_s) + Y_{F\infty} L_s)/(C_p(T_\infty - T_s) + L_s) \quad (19)$$

where L_s is the total enthalpy rise of vaporization

$$L_s = C_{pf}(T_s - T_0) + h_{fgs}. \quad (20)$$

A second expression, relating the vapor mass fraction and the surface temperature is provided by the vapor pressure characteristics of the liquid, as follows:

$$Y_{Fs} = f(T_s, \text{pressure}). \quad (21)$$

Simultaneous solution of Eqs (19) and (21) yields T_s and Y_{Fs} for any imposed ambient conditions. Since bulk heating has been ignored, drop diameter and mass are related, as follows:

$$d_{pi} = (6 m_{pi}/\pi \varrho_{f0})^{1/3}. \quad (22)$$

Life-history computations are strongly influenced by reference conditions used to determine transport properties and the specific correlations of the properties themselves. During work reported here, properties were selected by matching predicted and measured life histories for single dispersed-phase elements (particles, drops or bubbles) at test conditions representative of the multiphase flow. This involves selecting an optimum weighting parameter, β, to define the property reference state, as follows:

$$\phi_{\mathrm{ref}} = \beta\phi_s + (1 - \beta)\phi_\infty \quad (23)$$

where ϕ is a generic factor representing either species mass fraction or temperature.

Equations (15)–(23) were solved numerically, using a second-order Runge–Kutta algorithm. Details of these computations are presented elsewhere.[85] Numerical convergence with respect to the number of dispersed-phase groups needed to obtain statistically-significant results varies with the flow. Typical values are ~1000 groups for the DSF approach and ~5000 groups for the SSF approach.

2.6.4. *Continuous-phase source terms*

Once the properties of all dispersed-phase groups are found, the dispersed-phase source terms needed in

the governing equations for the continuous-phase can be found. These terms are listed in Table 3. The source terms in the governing equations for mean quantities are exact, and are used in all DSF and SSF computations considered in the following.

Derivation of the source terms in the governing equations for turbulence quantities (the turbulence modulation terms) is described by Shuen *et al.*[90] This analysis follows conventional procedures for turbulence models.[3,91] Under the SSF formulation, the dispersed-phase source terms in the k and g equations are formally exact and closed, since correlations like $\overline{uS_{pu}}$ and $\overline{fS_{pm}}$ can be computed from the simulation of the dispersed phase (although both are contaminated by problems of Favre- and time-averaged velocities using the present simplified analysis, as noted earlier). The term in the ε equation, however, must be modeled, and this involves all the approximations typical of $-\varepsilon$ models.[91] Furthermore, a new model constant, $C_{\varepsilon 3}$, is introduced, which must be determined empirically.

Work to date has not provided an adequate evaluation of the turbulence modulation portion of the present SSF analysis. It has also not been possible to obtain an accurate determination of $C_{\varepsilon 3}$. The problem has been that dense dispersed flows having significant effects of turbulence modulation are difficult to measure accurately. On the other hand, turbulence properties are largely established by other phenomena in dilute flows where accurate measurements are more feasible. As a result, evaluation of the turbulence modulation proposal summarized in Table 3, is judged to be premature. Thus, the approach taken in the following is to ignore the turbulence modulation terms, in the spirit of baseline analysis with minimum empiricism. The comparison between the baseline analysis and measurements, however, does provide indication of potential effects of turbulence modulation seen in the measurements. After studying these results, we shall reconsider turbulence modulation, as well as some alternative formulations proposed to treat this phenomena, in Sections 4 and 5.

3. STRUCTURE OF DILUTE DISPERSED FLOWS

3.1. *Introduction*

In the following we shall consider measurements of the structure of the flows listed in Table 1. This involves the the following dilute dispersed flows: particle-laden gas jets, nonevaporating sprays, evaporating sprays, combusting sprays, particle-laden liquid jets and bubbly noncondensing and condensing jets. Predictions obtained using the present LHF, DSF and SSF analyses will be compared with the measurements. These comparisons help interpretation of the measurements, since they highlight effects of interphase transport rates and dispersed-phase/turbulence interactions. The comparison also provides an initial evaluation of the methods, within the limitations of the relatively simplified turbulence model used here, and the fact that effects of turbulence modulation have been ignored during present computations.

Original sources should be consulted for specific estimates of experimental uncertainties. Typically, measurements reported by the author and his associates have uncertainties (95% confidence) $< 10\%$ for mean quantities and $< 20\%$ for quadratic turbulence quantities, like $\overline{u'v'}$ and k (this uncertainty is representative of the maximum values of the Reynolds stress with proportionately higher values elsewhere).

3.2. *Particle-Laden Gas Jets*

3.2.1. *Measurements of Yuu* et al.[25]

Yuu *et al.*[25] considered a particle-laden jet containing fly-ash particles. Information needed to estimate initial conditions for separated flow analysis was not reported and had to be estimated. The jet nozzle was designed to provide uniform exit properties; therefore, the assumed initial condition was taken to be slug flow, except for a shear layer having a thickness = 1% of the jet exit radius at the passage wall. In the uniform region, properties were specified as follows: $\bar{u}_0 = 4\dot{m}_0/(\varrho_0/\pi d^2)$; $\bar{f}_0 = 1$; $k_0 = (0.02\bar{u}_0)^2$; $\varepsilon_0 = 2.84 \times 10^{-5}\bar{u}_0^3/d$; and $g_0 = 0$. Quantities $\bar{u}_0$ and $\bar{f}_0$ were assumed to be linear in the shear layer. Initial values of k, ε and g in the shear layer were found by solving their transport equations, while neglecting convection and diffusion terms. Mean particle properties at the jet exit were computed using particle-trajectory computations based in the particle/gas mixing system and the nozzle geometry. Particles were assumed to be distributed uniformly across the jet exit.

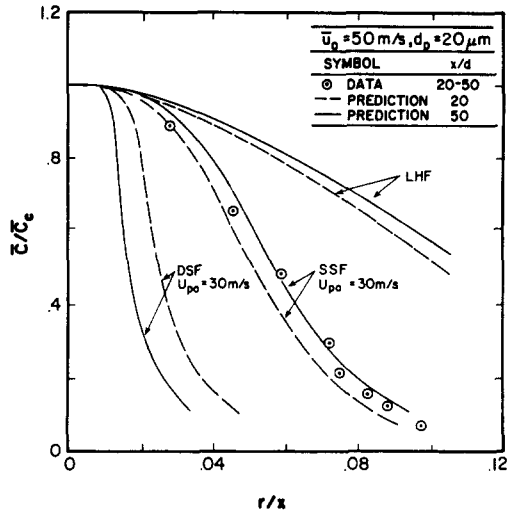

FIG. 7. Particle concentrations in a particle-laden round jet. Measurements from Yuu *et al.*[25]

The significance of turbulent dispersion in particle-laden jets can be seen from the results appearing in Fig. 7, from Shuen *et al.*[84] A portion of the particle concentration measurements of Yuu *et al.*[25] is illustrated along with LHF, DSF and SSF predictions of the flows. Only the range of streamwise positions where data were measured was reported; therefore, predictions are illustrated for the limits of this range. Estimated initial particle velocities also appear on the figure.

The rate of particle spread is overestimated using the LHF analysis, since effects of relative velocities between the phases (slip) are ignored. Neglecting slip causes the particle response to turbulent fluctuations, the mechanism of turbulent dispersion, to be overestimated. This also reduces streamwise particle velocities in the flow field, and the increased residence time causes further overestimation of particle spread rates.

The DSF analysis is seen to underestimate particle spread rates in Fig. 7. In this case, particle spread is caused only by the initial radial velocities of the particles and by drag in the radial direction from the mean radial velocity of the gas phase. Both of these velocities are small in comparison to the fluctuating gas-phase radial velocities which are responsible for turbulent dispersion. Furthermore, since the radial velocities of particles eventually are dominated by gas-phase radial velocities, particles tend to acumulate in regions where $\bar{v} = 0$, e.g. their behaviour is similar to particles in laminar flow, cf. Soo.[1] In jets, $\bar{v} = 0$ at the centerline (an unstable accumulation point) and roughly half-way between the axis and the flow edge (a stable accumulation point), It takes time for this process to develop, and effects of gravity modify the effect. Thus, the trend can only be seen indirectly in Fig. 7, by a tendency for the profiles of particle concentration to become progressively narrower (in terms of r/x) with increasing streamwise distance, rather than the opposite trend given by the LHF and SSF analyses.

In contrast to the LHF and DSF methods, SSF predictions are in reasonably good agreement with the measurements illustrated in Fig. 7. Additional comparisons between predictions and these measurements, yielding the same conclusion, can be found in Ref. 84. This suggests that both finite interphase transport rates and turbulent dispersion were important for this flow. Evaluation of the SSF method with these data, however, is not very definitive due to the uncertainties of the estimated initial conditions of the flows.

3.2.2. *Measurements of McComb and Salih*[26,27]

McComb and Salih[26,27] used relatively small particles in their experiments. Initial conditions for these flows were estimated similar to the procedure used for the measurements of Yuu *et al.*,[25] except that initial slip between the phases was neglected due to small particles used in these tests.

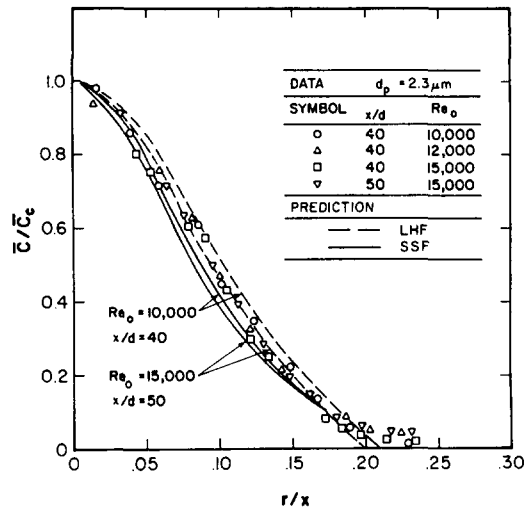

FIG. 8. Particle concentrations in a particle-laden round jet. Measurements from McComb and Salih.[26,27]

Test conditions of McComb and Salih[26,27] provided conditions more conducive to predictions based on LHF analysis. This is borne out by a portion of their data which is illustrated in Fig. 8. These results were obtained using titanium dioxide particles having a diameter of 2.3 μm. Predictions are shown for the LHF and SSF methods (the NSSF designation appearing in Fig. 8 represents the present SSF analysis). The small particles in this flow act nearly like tracer particles; therefore, the LHF approximation yields reasonably good results. The SSF method tends to underestimate particle dispersion slightly, similar to findings when the method was calibrated at the exact LHF limit, seen in Fig. 5.

McComb and Salih[26,27] also carried out tests where effects of particle inertia were more significant. This was done by decreasing the characteristic mixing times of the flow, u_0/d, by using larger initial velocities and smaller injector diameters; and by increasing the characteristic response times of the particles, by increasing particle densities and diameters. A portion of these results is illustrated in Fig. 9, along with LHF and SSF predictions. A range of characteristic mixing times is considered for a single characteristic particle response time. Effects of particle inertia can be seen by comparing the measurements with LHF predictions. It would be difficult to anticipate the trends of this data as operating conditions are changed; however, the SSF approach is seen to provide reasonably good estimates of the measurements for all conditions shown.

3.2.3. *Measurements of Laats and Frishman*[28,29]

Results considered thus far were limited to relatively low particle loadings. This implies that while the gas flow influences particle dispersion, the effect of the particles on the structure of the continuous phase is small, e.g. the test conditions have emphasized one-

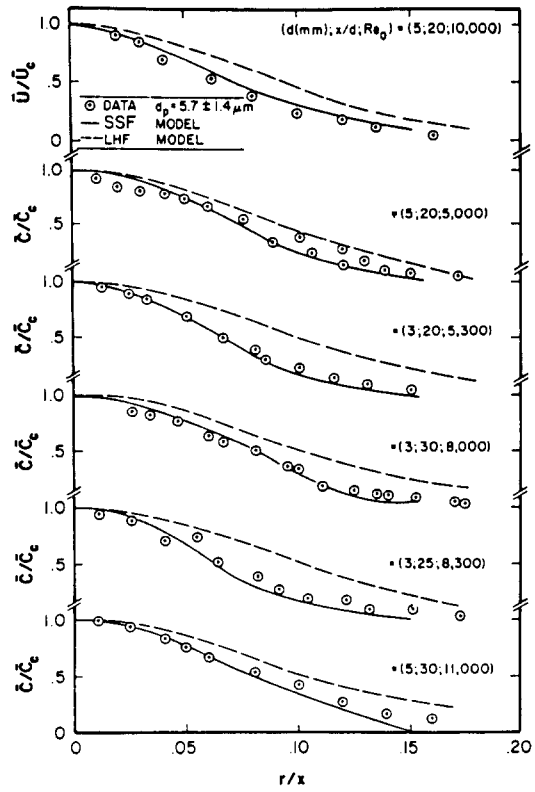

FIG. 9. Gas velocities and particle concentrations in particle-laden round jets. Measurements from McComb and Salih.[26,27]

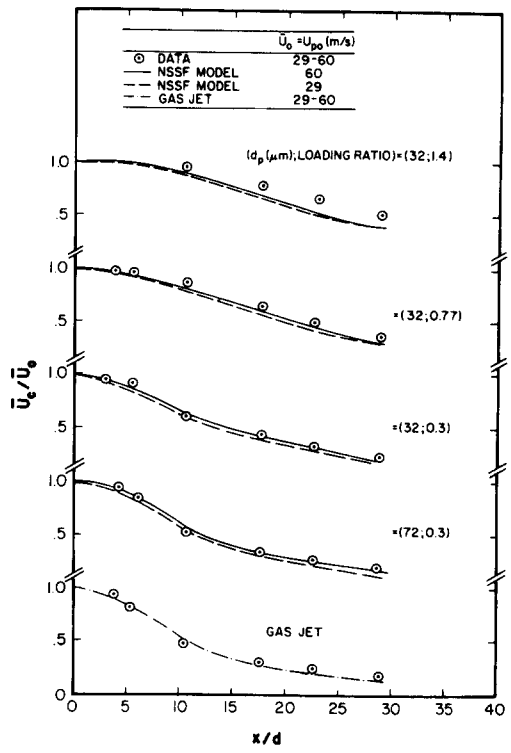

FIG. 10. Gas velocities in particle-laden round jets. Measurements from Laats and Frishman.[28,29]

way coupling from the gas to the particles. In contrast, the measurements of Laats and Frishman[28,29] involve relatively large particle loadings, resulting in significant effects of particles on the structure of the continuous phase.

A disconcerting feature of these measurements is that particle mass fluxes along the axis increased for a time for a portion of the data. This behavior could be due to redistribution of the flow from fully-developed pipe flow conditions, to particle-laden jet conditions. However, Laats and Frishman[28,29] attribute this phenomenon to Magnus forces introduced by the particle/gas mixing and injection processes. This effect could not be prescribed adequately to include it in the calculations; therefore, data having such trends are not considered in the following.

Initial conditions were not measured for these flows and had to be estimated. A constant-area pipe was used for an injector. In the absence of other information, fully-developed pipe flow was assumed at its exit. Quantity $\tilde{f}_0$ is unity by definition while $\tilde{u}_0$ was obtained from the conventional power law expressions for pipes—allowing for the variation of the power with Reynolds number.[3] Initial values of k_0 and ε_0 were also obtained from Hinze,[3] for fully-developed pipe flow in the same Reynolds number range as the experiments. The quantity $g_0 = 0$ by definition. For lack of other information, it was assumed that there was negligible slip between the phases at the jet exit. Particle concentrations were assumed to be uniform at the jet exit.

Predictions and measurements for the Laats and Frishman[28,29] tests are illustrated in Figs 10 and 11. As

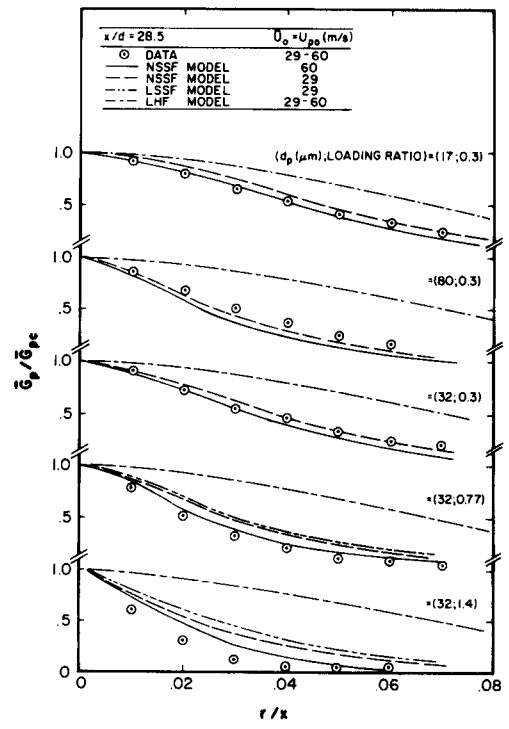

FIG. 11. Particle mass fluxes in particle-laden round turbulent jets. Measurements from Laats and Frishman.[28,29]

noted earlier, the NSSF designation refers to the present SSF analysis. The LSSF designation refers to a preliminary version of the separated flow analysis,[84,85] based on the prescription of particle/eddy interaction time of Gosman and Ioannides,[83] which has not been subsequently pursued. Only a range of initial gas velocities was specified for the data; therefore, predictions are shown for the limits of the velocity range. Predicted effects of initial velocity changes are small, in agreement with observations.

Predicted and measured mean gas velocities along the axis for both an air jet and the particle-laden jets are illustrated in Fig. 10. The gas flow is only influenced by the particles at higher loadings, greater than 0.3, where the presence of particles tends to reduce the rate of decay of centerline velocity.

Predicted and measured particle mass fluxes are illustrated in Fig. 11. The results are for $x/d = 28.5$, which is beyond the range where Laats and Frishman[28,29] observed Magnus effects directly, although this phenomena would still influence the development of the flow to the position shown. The large particles used in these tests have significant inertia; therefore, finite interphase transport rates are significant and the LHF analysis does not perform very well. The SSF predictions are more satisfactory except at the highest particle loadings, similar to Fig. 10. It was suggested that this could be due to initial relative velocities of the large particles, which were neglected, as noted earlier. For example, reduction of the particle velocities at the jet exit by 30% from the gas velocity would essentially match predictions and measurements for the particle loading of 1.4 in Fig. 11. Magnus forces and effects of turbulence modulation, both of which were not considered in the predictions, were also advanced as potential sources of the discrepancies between predictions and measurements at high loading ratios.[85]

3.2.4. *Measurements of Levy and Lockwood*[30]

The measurements of Levy and Lockwood[30] include mean and fluctuating phase velocities, found using laser–Doppler anemometry (LDA). Initial conditions were not reported for these tests and had to be estimated. The flow was produced in a constant area pipe; therefore, initial conditions were estimated assuming fully developed flow, following the procedure used for the measurements of Laats and Frishman.[28,29] These tests involved rather large particles; therefore, the initial mean velocities of the particles at the jet exit were estimated by carrying out particle trajectory computations for the flow in the pipe. Particle concentrations across the exit of the pipe were assumed to be constant. Present predictions (SSF method) and the measurements are illustrated in Figs. 12 and 13. In this case, predictions of streamwise velocity fluctuations were obtained assuming isotropic turbulence, e.g. $\bar{u}'^2 = 2k/3$. If levels of anistropy usually observed in jets, e.g. $\bar{u}'^2 = k$, were assumed, predictions would be 20% higher.

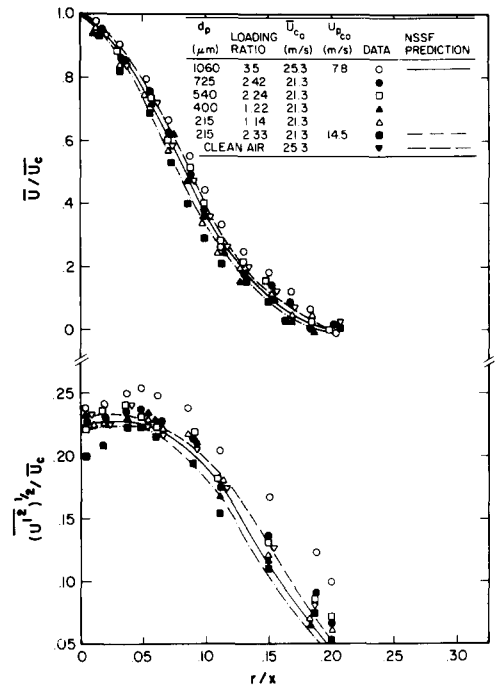

FIG. 12. Mean and fluctuating gas velocities in particle-laden round jets. Measurements from Levy and Lockwood.[30]

Both predictions and measurements indicate relatively small effects of particle size and loading ratio on the gas properties illustrated in Fig. 12. This follows since large particles were used to generate large particle loadings, and momentum exchange from these particles to the continuous phase was relatively

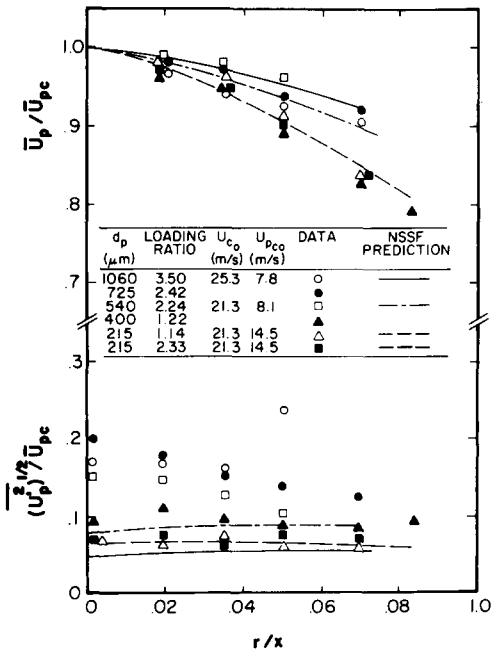

FIG. 13. Mean and fluctuating particle velocities in particle-laden round jets. Measurements from Levy and Lockwood.[30]

small for the limited axial distance considered during these experiments.

Predicted and measured mean and fluctuating particle velocities are illustrated in Fig. 13. Predictions of mean particle velocities are in good agreement with measurements at all conditions. Predictions of particle velocity fluctuations, however, are underestimated except for the smallest particles. This behavior was attributed to effects of the particle/gas mixing and injection system, which was a worm gear particle feeder followed by a short length of pipe. Such an arrangement would introduce relatively high particle velocity fluctuations at the jet exit. Since large particles exchange relatively little momentum as they pass to the measuring station in this flow, these fluctuations would be preserved. In contrast, small particles interact with the flow field to a greater degree, so that effects of the injection system are damped. For lack of other information, initial particle velocity fluctuations were ignored in the computations; therefore, the results are only satisfactory for small particles where effects of initial conditions are less persistent.

3.2.5. *Measurements of Shuen* et al.[31]

Results considered this far have illustrated some aspects of the structure of dispersed jets and effects of turbulent dispersion of the dispersed phase. However, evaluation of analysis and interpretation of some of these measurements is compromised, since initial conditions of the flows were not adequately documented. It was found that computed results were significantly influenced by initial mean and fluctuating phase velocities and the initial distribution of the dispersed phase in the flow.[85]

Boundary conditions can also be a problem when using measurements to evaluate a particular method of analysis.[66] For example, Modarress *et al.*[92] report very complete measurements of particle-laden jets in a coflowing stream within a duct. Attempts to compare these measurements with predictions were not very successful, however, since small streamwise pressure gradients encountered in ducts ($\sim$ 1–10 Pa/m) were not reported, but they can significantly influence continuous-phase properties.[66,86]

Many of these difficulties were resolved in the particle-laden jet study reported by Shuen *et al.*[31] Particles in these flows were nearly monodisperse and a free jet configuration was used to provide a known ambient pressure field. Mean and fluctuating phase velocities were measured at the jet exit, using laser-Doppler anemometry. Distributions of particle mass fluxes were meausured as well, using isokinetic sampling at the mean streamwise velocity. Initial values of ε were estimated from measurements of Reynolds stress and the mean velocity gradient in the radial direction. Particle drag properties were also assessed during calibration experiments for individual particles moving in still air.

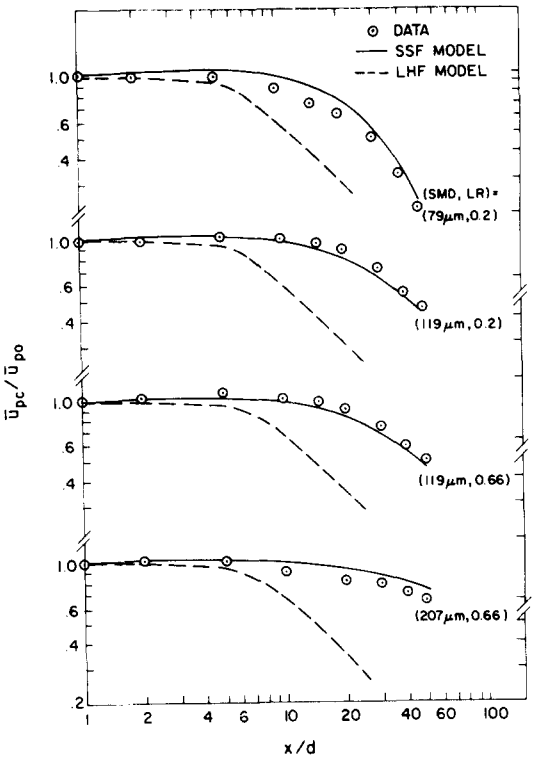

FIG. 14. Mean particle velocities along the axis of a particle-laden round turbulent jet. From Shuen *et al.*[31]

In spite of these precautions, two concerns have been raised concerning the use of these measurements for the evaluation of analysis. First of all, only amplitude discrimination was used to distinguish particles from the seeding particles in the gas phase for the LDA measurements. LDA seeding particles had diameters $\sim 1\,\mu$m, while the smallest flow particles used were 79 μm in diameter; therefore, pedestal signals from the flow particles were generally much larger than from the seeding particles, providing a reliable scheme for measuring particle velocities. It has been pointed out, however, that this approach is less effective for continuous-phase velocities, since grazing collisions of the large particles with the LDA measuring volume yield small pedestal signals which could be interpreted as coming from seeding particles in the continuous phase.[92] In fact, Modarress *et al.*[92] employ a phase-discriminating LDA to avoid this difficulty. Recent measurements of a similar flow using a phase-discriminating LDA, however, suggest that this effect was small for the measurements of Shuen *et al.*,[31] since their flows were very dilute.

A second difficulty with the measurements of Shuen *et al.*[31] involves the specification of initial values of ε for computations of the flow. Mostafa and Mongia[93] report an influence of these estimates on their predictions. Shuen *et al.*[31] report sensitivities of their predictions to this and other parameters of the analysis, finding that 100% changes in ε_o yield on the order of 10% changes of predicted continuous- and dispersed-phase properties. Furthermore, estimates used in Ref.

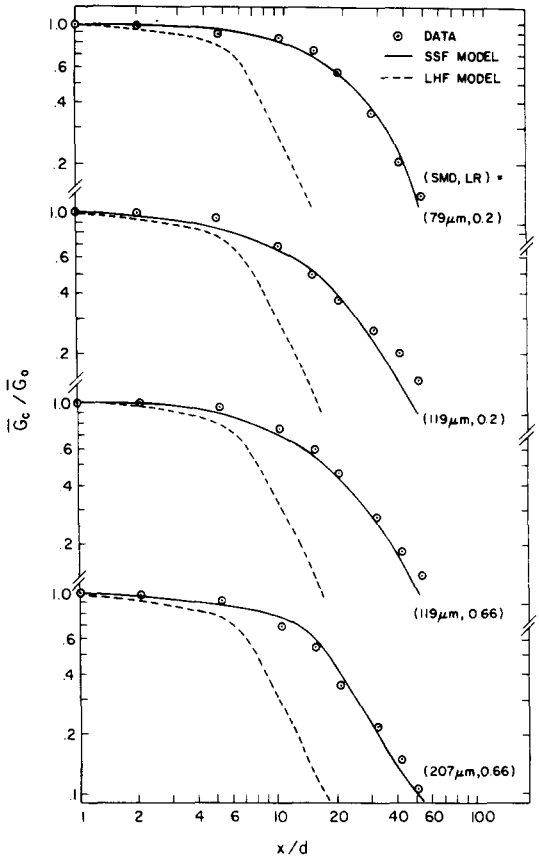

FIG. 15. Axial variation of mean particle mass flux in a particle-laden round turbulent jet. From Shuen *et al.*[31]

31 were able to provide reasonanly good predictions of k along the axis, which is sensitive to the selection of ε_o. Thus, while uncertainties of ε_o might be large, perhaps 100%, it seems unlikely that results discussed in the following are influenced by this effect to a greater degree than the uncertainties of the measurements noted earlier.

Only a portion of the results of Shuen *et al.*[31] will be considered. Measured and predicted (LHF and SSF methods) mean particle velocities along the axis are illustrated in Fig. 14. Mean gas velocities for these conditions roughly correspond to the LHF predictions illustrated in Fig. 14. Clearly, there are significant differences between particle and gas velocities in the regions just beyond the end of the potential core. This behaviour is typical of many multiphase jets, including spray injection processes at high pressures.[17] The rapid deceleration of the flow beyond the end of the potential core (or near the jet exit if there is no core) can only be followed by small particles—typically less than 10 μm in diameter for particle (drop)/gas flows. Naturally, each case must be evaluated for slip effects independently; however, most multiphase flows studied to date exhibit this property, suggesting that finite interphase transport rates are rarely unimportant in multiphase dispersed jets.

Predicted (LHF and SSF method) and measured particle mass fluxes along the axis of the jets are illustrated in Fig. 15. This variable is a sensitive indicator of the importance of turbulent dispersion of particles. LHF predictions overestimate the rate of decay of particle mass flux, since ignoring finite-interphase transport rates overestimates the response of the particles to continuous-phase turbulence and, thus, turbulent dispersion. The present SSF approach, however, provides reasonably good estimates of the measurements.

Typical radial profiles of mean and fluctuating particle properties are illustrated in Fig. 16. DSF predictions are illustrated for mean properties (the only particle properties that this approach provides), while LHF and SSF predictions are illustrated for all properties. The radial variation of particle mass flux is similar to the trends observed in Fig. 7. The substantial overestimation of particle dispersion using the LHF approach is very evident due to the relatively large particles used in these tests. SSF and LHF predictions of the radial profiles of normalized mean particle velocities fortuitously agree; recall, however, that particle velocities along the axis are substantially underestimated by the LHF approach; therefore, the absolute comparison between LHF predictions and measurements is not very good. DSF predictions of

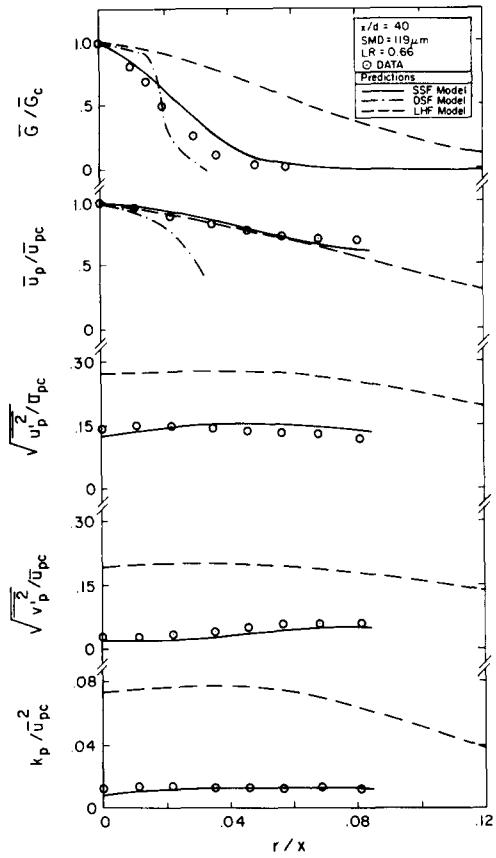

FIG. 16. Radial variation of mean and fluctuating particle properties in a particle-laden round turbulent jet. From Shuen *et al.*[31]

mean particle velocities underestimate the measurements. This is caused by neglecting turbulent dispersion, so that the particles are confined near the axis of the flow. Predictably, the LHF model overestimates particle velocity fluctuations due to neglect of slip. The SSF predictions of particle velocity fluctuations are reasonably good, which is consistent with its representation of turbulent particle dispersion.

An interesting effect seen in Fig. 16 is that particle velocity fluctuations are anisotropic, with streamwise fluctuations being much larger than radial fluctuations, even though the analysis used to predict particle fluctuations assumes isotropic velocity fluctuations for the continuous phase. This is caused by radial transport of particles from regions having different mean streamwise particle velocities, followed by relatively slow relaxation to the new state via the indirect mechanism of drag from the continuous phase. This mechanism is somewhat similar to the phenomena causing anisotropic velocity fluctuations in single-phase turbulent jets. For the conditions of Fig. 16, the SSF approach gives nearly quantitative predictions of levels of anisotropy of particle velocity fluctuations; however, we shall see that this is not always the case.

3.3. *Nonevaporating Sprays*

Consideration of sprays vastly complicates both measurements and predictions, since drop properties must be segregated by size. Results from Solomon *et al.*[32,33] for nonevaporating sprays will be considered

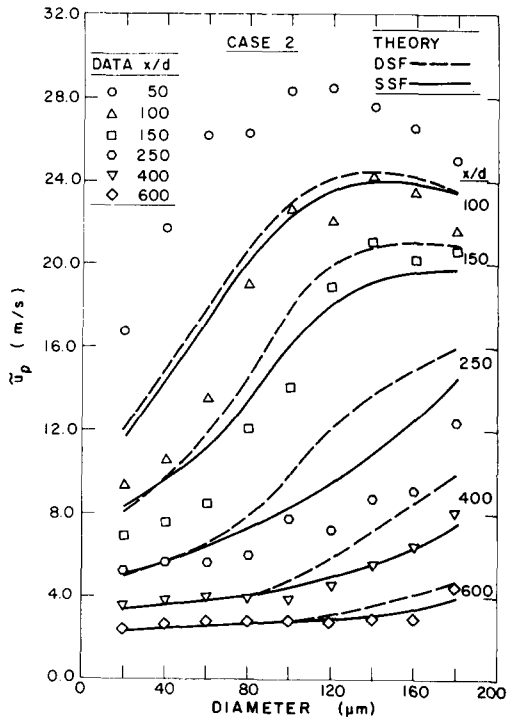

FIG. 17. Mean streamwise drop velocities in a round nonevaporating spray. From Solomon *et al.*[32,33]

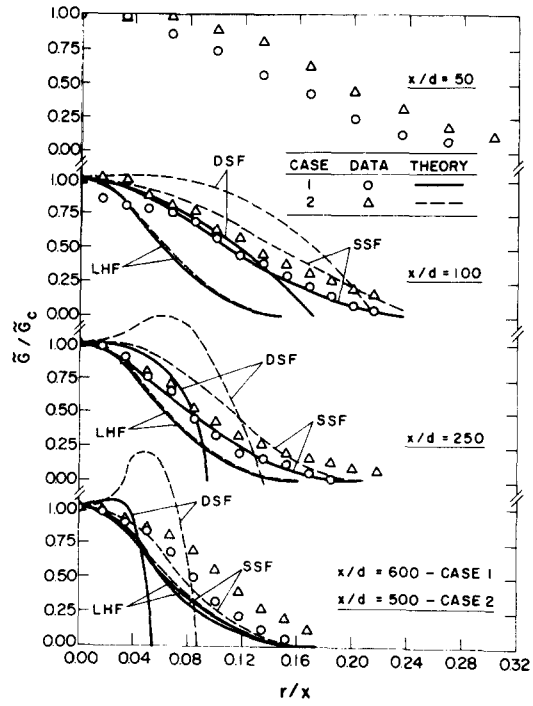

FIG. 18. Mean liquid flux distributions in a round nonevaporating spray. From Solomon *et al.*[32,33]

since they are reasonably complete. The measurements involved air atomization of vacuum pump oil (insuring negligible evaporation) to yield a free spray. Mean and fluctuating gas-phase velocities were measured with an LDA, while drop size and velocity distributions were measured using multiflash photography. Mean drop mass flux was measured by isokinetic sampling at the mean streamwise gas velocity. The dense-spray region near the injector was not considered, due to lack of adequate spatial resolution, opacity to optical diagnostics, and the presence of irregularly-shaped liquid elements (ligaments, etc.); therefore, both measurements and predictions were confined to $x/d \geq 50$.

Initial conditions for separated flow calculations were measured at $x/d = 50$. Direct measurements included mean and fluctuating velocities, Reynolds stress and turbulence kinetic energies of the gas phase; and mean mass flux, drop size distributions and mean and fluctuating streamwise velocities of the liquid phase. The ε distributions were computed using the turbulence model. Initial conditions for LHF calculations were prescribed at the jet exit, assuming slug flow and following the procedure used for the measurements of Yuu *et al.*[25]

Some of the complexities of polydisperse sprays are illustrated in Fig. 17. Predicted (DSF and SSF methods) and measured mean streamwise drop velocities along the axis are plotted as a function of drop size and x/d. Drop velocities decrease with both size and distance from the injector. At $x/d = 50$ and 100, drops with $d_p < 30\,\mu$m had velocities up to 30% less than the gas velocity while the largest drops had

velocities up to twice the has phase value. Far downstream, however, at $x/d = 600$, velocity differences become small—approximating LHF flow. SSF predictions in Fig. 17 yield a more rapid deceleration than DSF predictions for each drop size. This is due to the nonlinearity of the drag law interacting with turbulent fluctuations—one of the dispersed-phase/turbulence interactions discussed earlier. The SSF method yields better predictions than the DSF method, since it uses instantaneous properties and only averages over particle groups. O'Rourke and Bracco[87] propose an alternative for use with DSF analysis, which allows for a nonlinear drag law; however, this approach has not been evaluated as yet.

Predictions (all three models) and measurements of mean liquid flux for the nonevaporating sprays are illustrated in Fig. 18. An interesting property of these results is the extraordinary width of the flow just downstream of the dense-spray region at $x/d = 50$, where initial conditions for the separated-flow analyses were specified. A single-phase flow, which should spread more rapidly than the dispersed-phase, would roughly have a concentration profile similar to the LHF predictions illustrated in Fig. 18. The spray is roughly twice as wide near $x/d = 50$ and only approaches the LHF profile in the far field. The fact that the unusual width is associated with the near-injector regions suggests a dense-spray mechanism, although some unmonitored instability of the injector passage cannot be ruled out. Drop collisions and drop breakup phenomena, which are frequent in polydisperse dense sprays, could be responsible since this provides a means of efficiently converting streamwise to radial drop momentum. The phenomenon deserves further study since it strongly influences the initial conditions of the dilute portion of the spray.

The unusual width of the dense spray region cannot be sustained. As the spray becomes dilute the liquid mass flux distributions evolve toward LHF predictions as x/d increases for the results pictured in Fig. 18. Effects of turbulent dispersion are significant

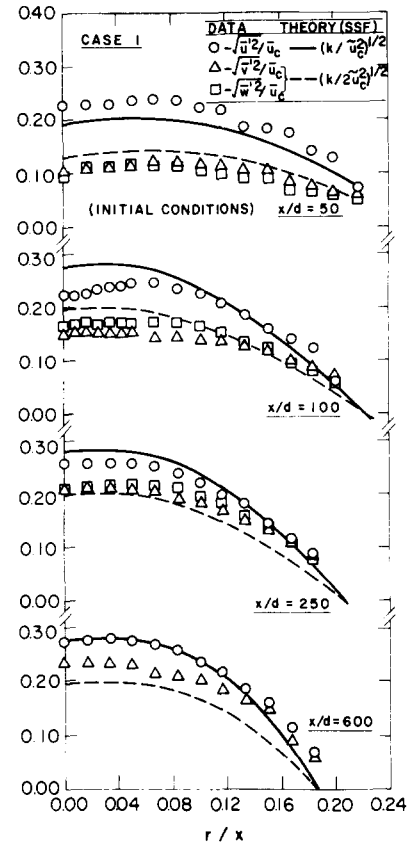

FIG. 20. Gas-phase velocity fluctuations in a round nonevaporating spray. From Solomon *et al.*[32,33]

during this evolution; therefore, DSF predictions show a more rapid narrowing of the flow than SSF predictions. The latter are in better agreement with measurements. DSF predictions also yield pathological concentrations of drops at radial distances where $v = 0$, e.g. for $r/x = 0.06$–0.10 at $x/d = 600$. This behavior was discussed earlier, cf. Section 3.2.1. SSF predictions of mean liquid fluxes are also poorer than for other properties of these flows. Computations

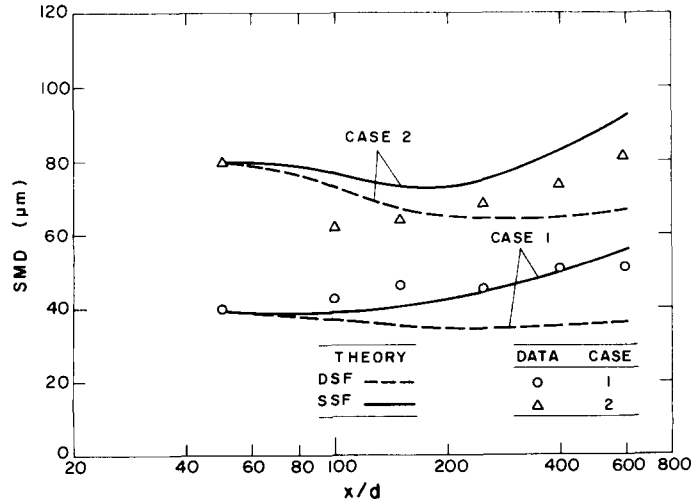

FIG. 19. SMD along the axis of round nonevaporating sprays. From Solomon *et al.*[32,33]

showed that this was due to the very high sensitivity of liquid fluxes to uncertainties of initial conditions.[32,33]

Turbulent dispersion and relative velocities vary with drop size; therefore, the size distribution of drops changes as the flow develops in polydisperse sprays. This is illustrated in Fig. 19, where the Sauter Mean Diameter (SMD) along the axis of the nonevaporating sprays is plotted as a function of distance from the injector exit. The fact that large drops pass through the flow more rapidly, and are less influenced by turbulent dispersion than small drops, causes a progressive increase of SMD along the axis. SSF analysis appears to represent this effect reasonably well.

Effects of turbulence modulation can be seen in the predictions and measurements of gas phase velocity fluctuations which are plotted in Fig. 20. The present continuous-phase anlysis only provides k; therefore, velocity fluctuation predictions were obtained assuming the usual levels of anisotropy found near the axis of single-phase jets, e.g. $\tilde{u}'^2:\tilde{v}'^2:\tilde{w}'^2 = k:k/2:k/2$, cf. Wygnanski and Fiedler.[53] Recall that $x/d = 50$ is the initial condition for predictions, where k is matched to the measurements. It is evident that measured levels of anisotropy are much larger than the usual levels seen in jets at this position near the dense-spray region. Farther into the dilute spray region, however, effects of drops on turbulence properties decrease and anisotropy levels approach those of single-phase jets.

Another effect, attributable to turbulence modulation, is the relatively low level of turbulent fluctuations near the dense spray region seen in Fig. 20. This is particularly noticeable near the axis of the flow. One reason for this behavior is the relatively broad mean velocity profiles near the dense spray region, which reduces turbulence by shear forces. The predictions model this effect, which is not due to turbulence modulation, but still overestimate turbulence levels near the dense-spray region. Calculations considering turbulence modulation provide better results.[32,33] The empirical constant $C_{\varepsilon 3}$, needed in the terms representing turbulence modulation in Table 3, is not known very well, as noted earlier. Available evidence, however, suggests that its value is small, ca. 0.01–0.1.[37-39] Including the turbulence modulation terms in the SSF analysis and using values of $C_{\varepsilon 3}$ in this range yields reductions in k_c, and thus the components of velocity fluctuations, which improves the comparison between predictions and measurements.[33] The quantitative effect of turbulence modulation in the dilute spray region, however, was comparable to uncertainties in predictions due to uncertainties in initial conditions. Thus, the measurements of Solomon *et al.*[32,34] are not adequate to definitively study turbulence modulation phenomena.

3.4. *Evaporating Sprays*

Solomon *et al.*[34] extended their work on nonevaporating sprays to evaporating sprays, using the same apparatus and test methods. Evaporation influences scalar properties of the gas phase; therefore, even the separated flow models must employ the conserved-scalar formulation. These experiments involved injection of liquid Freon-11 into still air, using an air atomizing injector.

Initial conditions for LHF calculations were specified at the injector exit, assuming slug flow and following the procedures used for the measurements of Yuu *et al.*[25] Initial conditons for separated-flow calculations were established at $x/d = 50$, using procedures similar to Solomon *et al.*[32,33] The total mean concentration of Freon-11 was also measured including both phases, yielding the mean mass fraction of Freon-11 vapor from overall conservation of mass. Profiles of concentration fluctuations were not measured directly; therefore, this parameter was estimated using results from the LHF solution. Fortunately, predictions were not very sensitive to this estimate.

Measurements of the life histories of stationary drops in a well-defined environment were used to calibrate the drop transport analysis. This involved drops supported on a thermocouple bead and subjected to an ambient air flow at several different velocities. These test drops were large ($\sim 1000\,\mu$m initial diameter) in comparison to the drops in the test sprays; however, operating conditions of the calibration tests were selected so that the Reynolds number range of the calibration experiments spanned the range encountered by drops in the spray.

Typical results of the calibration experiments are illustrated in Fig. 21. On this figure, D denotes drop diameter. To match predictions, the parameter β in Eq. (23) was taken to be 0.75. The resulting comparison between predicted and measured drop diameters as a function of time is seen to be quite good. Freon-11 is quite volatile; therefore, the drops cool down to a relatively low wet-bulb temperature, T_{WB} are also summarized in Fig. 21.; the values agree

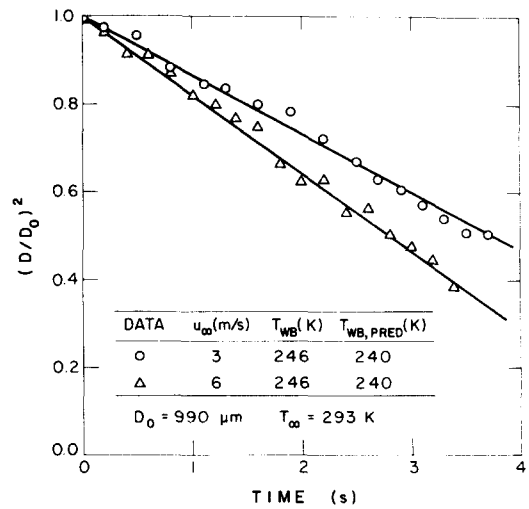

FIG. 21. Drop-life-history calibrations for evaporating Freon-11 drops. From Solomon.[94]

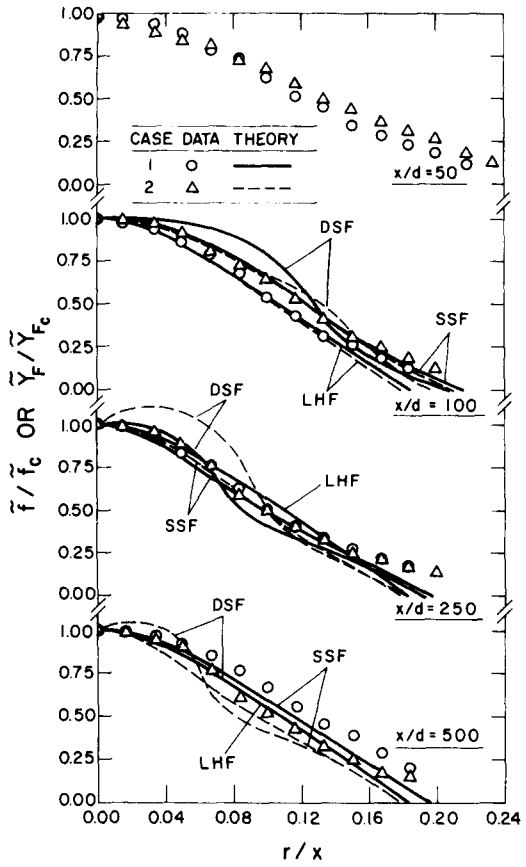

FIG. 22. Distributions of total Freon-11 concentrations in round evaporating sprays. From Solomon *et al.*[34]

within experimental uncertainties. However, no universality of the matched value of β should be assumed from these results, since the values depend on a variety of property calculations which are all subject to uncertainties. Instead, calibration results similar to Fig. 21 should be used to assess drop-life-history calculations wherever possible.[17]

Predicted and measured profiles of total (gas and liquid) mean Freon-11 concentrations are illustrated in Fig. 22. Similar to the nonevaporating sprays, the flow is unusually wide near the dense spray region. The behavior is somewhat less pronounced, than for nonevaporating sprays, however, since drops rapidly evaporate as they reach the edge of the flow—limiting their penetration into the surroundings.

DSF predictions illustrated in Fig. 22 exhibit peaked profiles, due to neglect of turbulent dispersion of drops. LHF and SSF predictions are in better agreement with the measurements. LFH analysis yields better results in this case since Freon-11 vapor tends to dominate the total concentration measurements for present test conditions. Gosman and Ioannides[83] encountered similar reduced effects of turbulent dispersion in connection with evaporating and combusting spray measurements of Tishkoff *et al.*[95] and Founti *et al.*[96] They concluded that effects of turbulent dispersion were small in comparison to uncertainties in distributions of drop size, velocity and direction at the injector exit. If this continues to be the case for evaporating and combusting sprays, the more extensive computations of SSf analysis could be avoided in preference to DSF analysis. However, additional study is needed to establish the universality of this simplification for practical spray processes.

Predicted (DSF and SSF analysis) and measured SMD along the axis of the sprays are illustrated in Fig. 23. For nonevaporating sprays, SMD increased with increasing distance from the injector, cf. Fig. 19, due to higher rates of turbulent dispersion of small drops. For evaporating sprays, however, this is counteracted by drop evaporation, tending to decrease drop diameters. Thus, the SMD remains relatively constant along the axis until the last stages of drop vaporization for these test conditions. These trends are represented reasonably well by both theories, since SMD is dominated by the largest drops in the flow, which have low rates of dispersion.

Predictions and measurements of gas-phase turbulent kinetic energy are illustrated in Fig. 24. Effects of turbulence modulation are evident for both sprays near $x/d = 50$. Spray 1 is more lightly loaded,

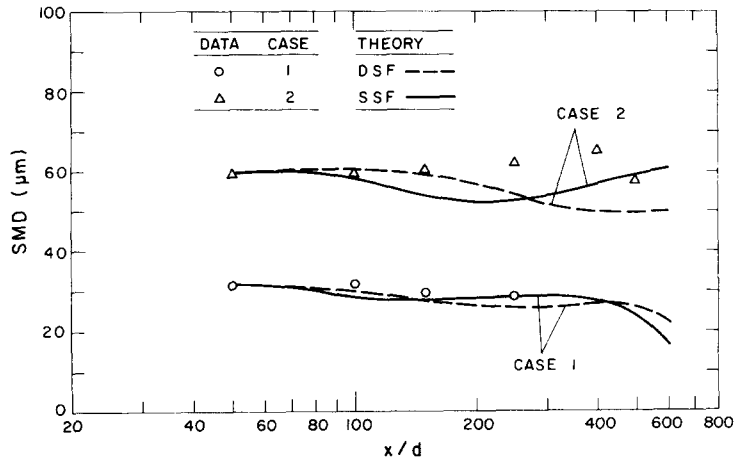

FIG. 23. SMD along the axis of round evaporating sprays. From Solomon *et al.*[34]

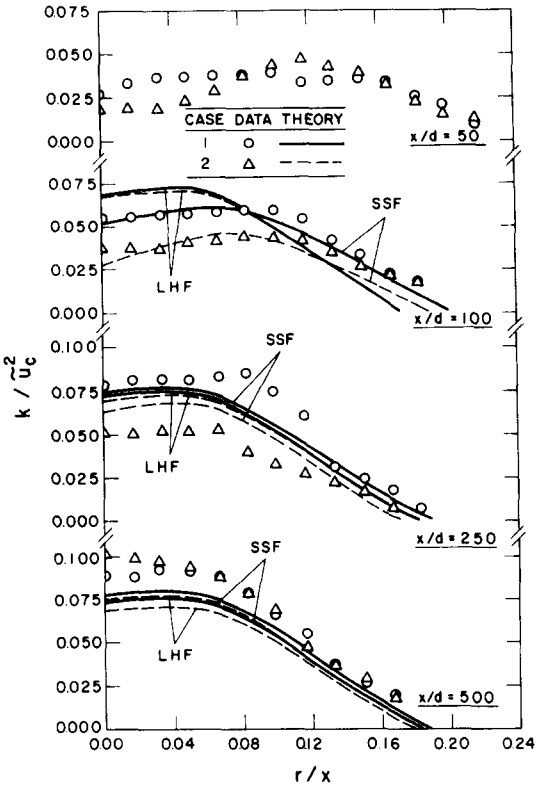

FIG. 24. Distribution of gas-phase turbulence kinetic energy in round evaporating sprays. From Solomon *et al.*[34]

this results in smaller reductions of k levels near the dense spray region and more rapid disappearance of turbulence modulation effects with increasing distance from the injector. These measurements only employed amplitude discrimination of the LDA to eliminate effects of drops on measurements of gas phase properties; therefore, uncertainties are introduced due to grazing collisions of large drops with the measuring volume. Modarress *et al.*,[92] as noted earlier, describe an improved phase discrimination system for continuous-phase LDA measurements; systems like this are recommended for quantitative work in the future. Nevertheless, large drops had very high slip velocities in the test sprays and it is difficult to see how extraneous signals from them could cause measurements of reduced turbulence levels. Thus the lower levels of k near the dense spray regions of the nonevaporating and evaporating sprays provide reasonably good evidence of the effects of turbulence modulation.

3.5. *Combusting Sprays*

The combusting spray experiments of Shuen *et al.*[35] involved ultra-dilute conditions throughout the flow. Initially monodisperse methanol drops were injected vertically upward at the base of a methane-fueled diffusion flame burning in still air. The methane flame had been extensively studied by Jeng and coworkers,[51,52,62] establishing predictive methods for the flow using the conserved-scalar formalism in conjunction with the laminar-flamelet approximation. The methanol drops only perturbed this flow; therefore, their environment was well known throughout the flame. Mean and fluctuating drop velocities were measured using LDA; drop sizes were measured using flash photography; and drop number fluxes were measured using Mie scattering. Drop histories to any point in the flow vary due to effects of turbulence; therfore, drop sizes are not monodisperse at any point other than the exit. This was not considered in the measurements: drop properties were simply averaged over all sizes at each point. Computations were averaged in the same manner so that predictions and measurements could be compared.

Only separated flow predictions will be reported in the following. For this ultra-dilute flow, drop properties are controlled entirely by interphase transport rather than mixing of the flow as a whole; therefore, the LHF method indicates that the drops evaporate completely very near the injector exit, which is clearly erroneous.

Initial conditions for separated flow analysis were measured one injector diameter from the burner exit. Mean streamwise velocity and all three components of velocity fluctuations were measured for the continuous phase. The measured rate of decay of k and the value of $\tilde{u}$ yielded ε. At the exit, $\tilde{f} = 1$ and $g = 0$ by definition. Drop diameters were constant. Mean and fluctuating streamwise and radial drop velocities and the drop number flux distribution were measured. Mean radial drop velocities were small and were estimated.

Depending on flame stability considerations, a fuel drop vaporizing in an oxidizing evironment can have several flame configurations, as follows: (1) the envelope flame configuration, where the drop is completely surrounded by a diffusion flame which is consuming its vapor; (2) a side- or wake-flame configuration, where the envelope flame extinguishes at the forward stagnation point but subsequently stabilizes at a point along the periphery or in the wake of the drop; and (3) the evaporation conditions, where the drop diffusion flame extinguishes entirely.[8] Drop transport rates are highest for the envelope flame condition, side flames are infrequently observed since they have limited ranges of stability, while wake flames and the evaporation configuration yield nearly the same drop transport rates. Thus, it is necessary to establish the presence or absence of envelope flames in order to estimate drop transport rates in combusting sprays.

The possible existence of envelope flames around each drop is a controverisal matter for analysis of combusting sprays.[17] Envelope flames are clearly not possible in fuel-rich regions but they could be present when drops interact with fuel-lean eddies. Szekely and Faeth[97] studied drops supported at various positions in a turbulent diffusion flame to provided some information concerning this issue. They found that dif-

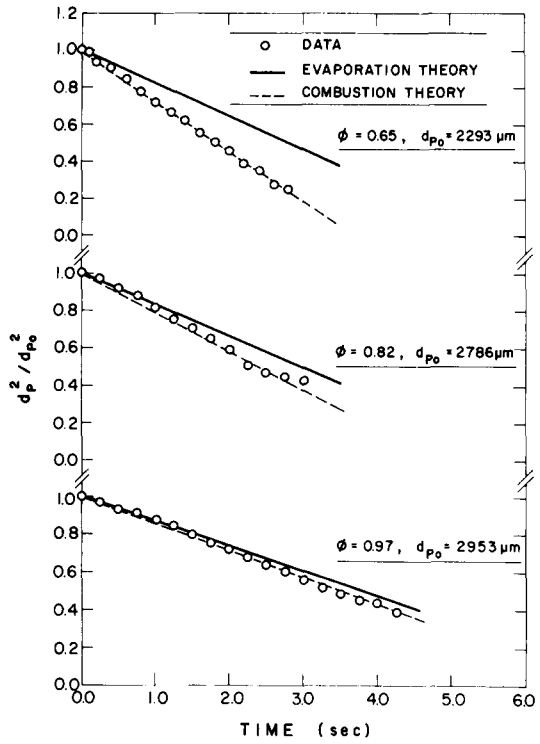

FIG. 25. Drop-life-history calibrations for combusting methanol drops. From Shuen *et al.*[35]

ferences in transport rates between evaporating and combusting drops were relatively small (less than 10–20%) until the mean fuel-equivalence ratio (the local fuel-air ratio divided by the stochiometric fuel-air ratio, often given as a percentage) of the flame environment dropped below 90%. Drops in the tests of Shuen *et al.*[35] penetrated beyond this condition, but the following predictions still neglect the effect of envelope flames. Additional calculations considering envelope flames to be present, for fuel-equivalence ratios less than unity, did not indicate significant effects of envelope flames. However, this may not always be the case. Predictions considering envelope flames are problematical since there is very little information available concerning their ignition and extinction properties in flame environments.[17]

There are substantial uncertainties in drop-life-history calculations in flames due to the wide variation of transport properties that are encountered. Therefore, calculations used in the separated-flow analyses were calibrated using measurements based on drops supported in the post-flame region of a flat-flame burner.[35] Similar to the drop evaporation calibrations of Solomon,[94] drop sizes and flow velocities were chosen in the calibration experiments so that the Reynolds number range of the dilute combusting spray was covered. The flat-flame burner was fueled with methane–air mixtures to simulate the dilute spray flame as well.

Predicted and measured drop life histories are illustrated in Fig. 25, for three fuel-lean equivalence ratios: ϕ = 0.65, 0.82 and 0.97. Predictions assuming envelope flames were present and absent are shown. Envelope flames were observed for these conditions and the predictions are matched accordingly, finding β = 0.3 in Eq. (23). The resulting comparison between predictions and measurements is excellent, providing some confidence in individual drop-life-history computations used in separated flow analysis of the dilute combusting sprays. Similar to the findings of Szekely and Faeth,[97] it is evident that there is not much difference in computations including or ignoring envelope flames for fuel equivalence ratios greater than 90%.

Measurements of mean gas-phase (time averaged) and drop (particle-averaged) velocities along the axis of the dilute combusting spray are illustrated in Fig.

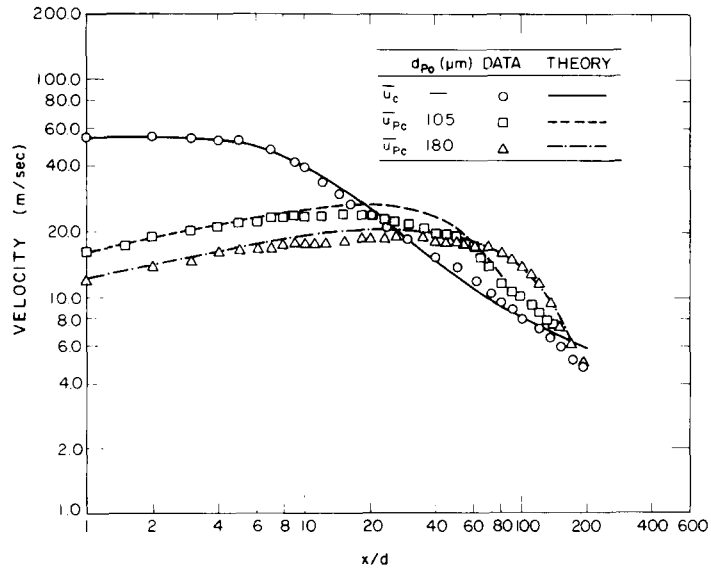

FIG. 26. Mean phase velocities along the axis of round, ultra-dilute, round combusting sprays. From Shuen *et al.*[35]

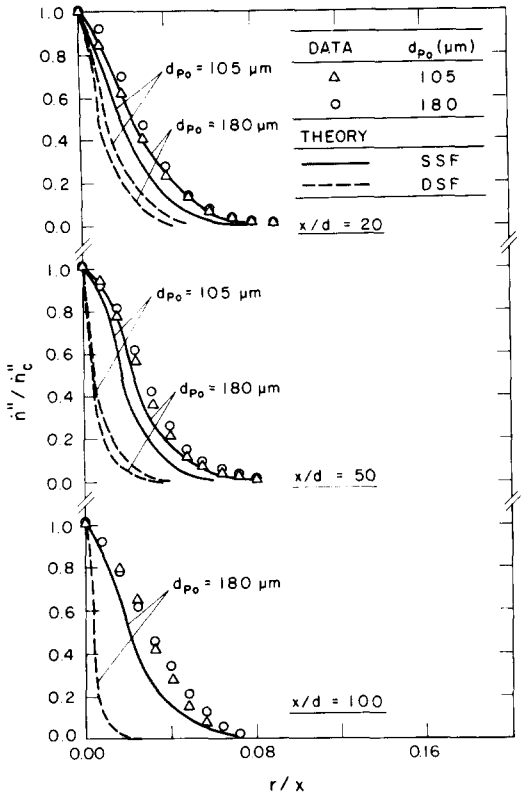

FIG. 27. Drop number flux distributions in round, ultra-dilute round combusting sprays. From Shuen *et al.*[35]

26. Drop velocities for both sprays tested are shown along with SSF predictions. Predicted gas velocities are Favre-avergaes; however, differences between time- and Favre-averaged mean velocities are not very large, as noted earlier. Gas velocities are greater than drop velocities at the burner exit, but decrease rapidly due to mixing with the surroundings. Near the injector, drops have significant inertia and their velocities only increase gradually due to drag from the gas. Near the tip of the flame ($x/d \sim 120$); however, drops become small and they rapidly approach gas velocities. The SSF analysis predicts these trends reasonably well.

Predicted (DSF and SSF methods) and measured mean drop number fluxes (both time averages) are illustrated in Fig. 27. The initially larger drops have wider profiles even though they are less responsive to turbulent dispersion. This occurs since they are able to penetrate farther into the flame zone before evaporating. SSF predictions provide the same ordering of spread rates and are in fair agreement with the measurements. The DSF predictions yield incorrect ordering of the spread rates and are not very effective, similar to the flows considered earlier.

Measured (time- and particle averages) and predicted (SSF method) phase velocity fluctuations along the axis are illustrated in Fig. 28. As before, gas velocity fluctuations were computed using the normal levels of anisotropy found near the axis of turbulent jets while drop velocity predictions result directly from the SSF analysis. Predicted gas phase velocity fluctuations are Favre-averages while the measurements are time averages. As noted earlier, Favre averages underestimate time-averaged fluctuating velocities in flames, by as much as 50% near the flame tip.[66] This effect, plus neglect of turbulence/buoyancy interactions, is probably responsible for the underestimation of gas-phase velocity fluctuations in Fig. 28, particularly near the tip of the flame.

Particle velocity fluctuations plotted in Fig. 28 show very high levels of anisotropy, much larger than predicted. Radial particle velocity fluctuations are predicted reasonably well, which is consistent with the satisfactory predictions of turbulent dispersion. Streamwise drop velocity fluctuations are substantially underestimated, however, probably due to the assumption of isotropic turbulence when eddy properties are selected for SSF analysis. Use of Favre-averaged velocities in the simulation also causes underestimation of time-averaged velocity fluctuations, as noted earlier. Near the burner exit, drop velocity fluctuations are small in comparison to the gas phase, due to drop inertia. At the end of drop lifetime (x/d *ca.*

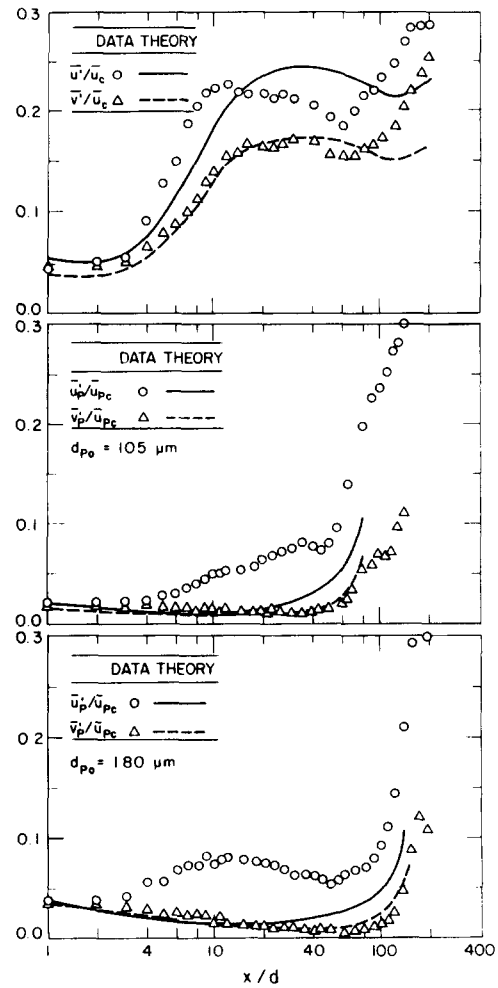

FIG. 28. Fluctuating phase velocities along the axis of round, ultra-dilute round combusting sprays. From Shuen *et al.*[35]

90–120), however, the remaining small drops can respond rapidly and approach flame properties.

3.6. *Particle-Laden Water Jets*

The next dilute dispersed jet that we shall consider involves particle-laden water jets injected vertically downward in still water, reported by Parthasarathy and Faeth.[36] Glass particles were used yielding a density ratio of 2.45:1. This density ratio regime is of some practical importance, since it is representative of portions of high-pressure combusting sprays. Furthermore, all terms in the B–B–O equation of motion of the particles are important. Finally, the increased response of particles in liquids, in comparison to particles in gases, provides relatively strong interaction between dispersed- and continuous-phase velocity fluctuations, highlighting evaluation of effects of anisotropy discussed thus far.

Two versions of the SSF analysis were considered during this study, as follows: (1) the baseline SSF analysis, and (2) a version allowing for anisotropy of continuous-phase velocity fluctuations when making random selection of velocities to determine eddy properties. In order to avoid additional approximations in the analysis, measurements of anistropy from the multi-phase jets were used directly to prescribe levels of anistropy. Methods used to select other parameters of the stochastic analysis were unchanged from the baseline SSF approach.

The particle laden jet was generated by a long length-to-diameter ratio tube, and the flow was nearly fully-developed at the tube exit. Phase velocities were measured using an LDA. Effects of grazing collisions of large particles were avoided when measuring continuous-phase velocities by using a phase-discriminating LDA configuration along the line of Modarress *et al.*[92] Particle number fluxes were measured using Mie scattering, similar to Shuen *et al.*[35]

Initial conditions for these flows were measured at $x/d = 8$, which was the closest position to the jet exit where adequate experimental uncertainties could be maintained. Mean and fluctuating phase velocities and the continuous-phase Reynolds stress, were measured. Dissipation, ε, was computed from the measured values of k, $\overline{u'v'}$ and the mean velocity gradient using Eq. (3). This position did not provide adequate spatial resolution to measure particle number fluxes; therefore, particles were assumed to be distributed uniformly over the region where they were observed. This agreed with the crude observations that could be made. Analysis of particle trajectories was calibrated using data obtained by the release of individual particles in still water. Baseline results were also obtained for a pure water jet from the same injector. The continuous-phase analysis was in good agreement with the baseline water jet measurements.

Predictions obtained using the baseline SSF approach were in reasonably good agreement with the measurements over the region of the flow measured,

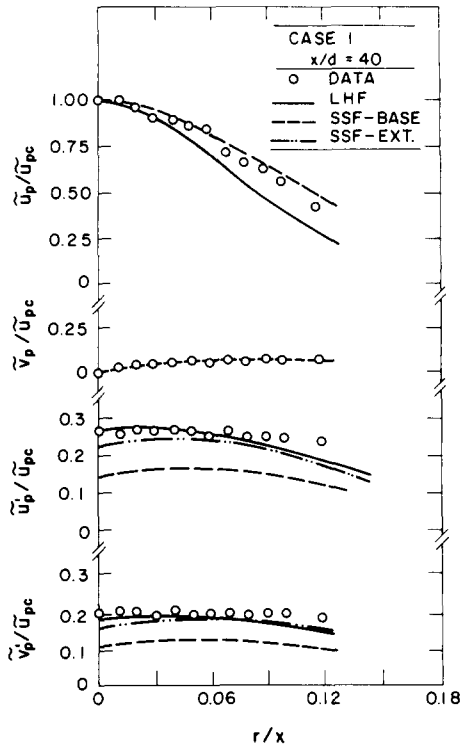

FIG. 29. Radial variation of mean and fluctuating properties in a particle-laden round turbulent water jet. From Parthasarathy and Faeth.[36]

$x/d \leq 40$, for all test conditions. LHF predictions were reasonably good in regions where relative velocities were small in comparison to continuous-phase velocities, e.g. small x/d near the axis.

Predictions and measurements of particle velocities from this study are particularly interesting. A portion of these results is illustrated in Fig. 29. LHF predictions of mean particle velocity at the axis were not very good, since relative velocities are significant in comparison to liquid velocities at this position. Results plotted in Fig. 29 show further increases in errors for predictions of mean particle velocities near the edge of the flow. Due to the method of normalizing the results plotted in Fig. 29, LHF predictions of particle velocity fluctuations appear to be reasonably good. Absolute agreement is not very good for the LHF method, however, due to deficiencies in prediction of centerline particle velocities, noted earlier. It can be seen that the anisotropic SSF (SSF-EXT) approach provides reasonably good predictions of streamwise particle velocity fluctuations, yielding a significant improvement over the baseline approach (SSF-BASE). This was accomplished with little effective change in estimates of turbulent dispersion, since continuous-phase flow properties near the edge of the jet dominate particle spread rates. The continuous-phase flow is nearly isotropic near the edge of the flow, corresponding to the assumptions used in past evaluations of the SSF approach. Thus, the effect of anisotropy is secondary with respect to turbulent

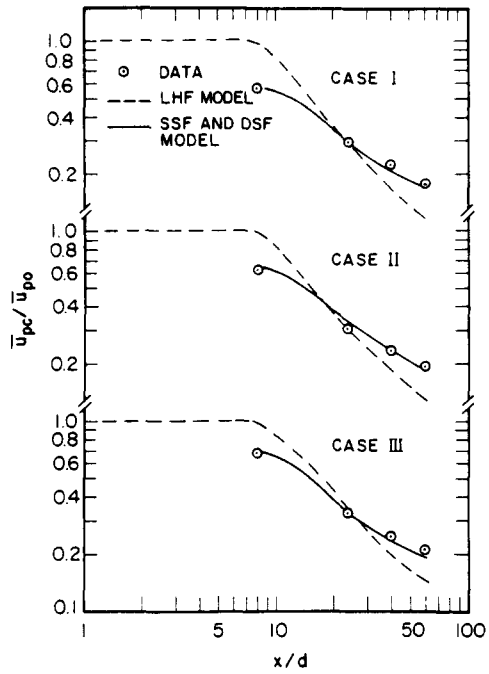

FIG. 30. Mean bubble-phase velocities along the axis of a round noncondensing bubbly jet. From Sun and Faeth.[37,38]

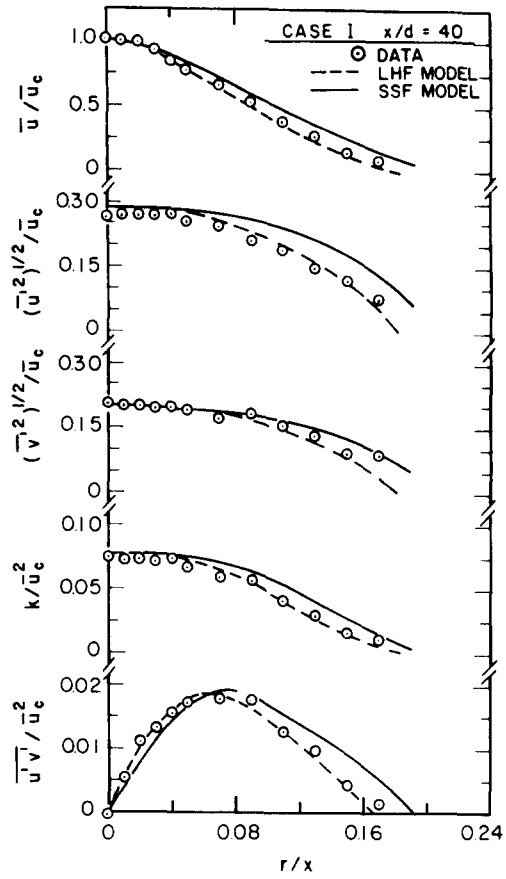

FIG. 31. Continuous-phase properties in a round noncondensing bubbly jet (case I). From Sun and Faeth.[37,38]

dispersion for the test results summarized in Table 1. This may not always be the case, however, and more complete analysis of continuous-phase turbulence properties, incorporating predictions of local anisotropy, appears to be warranted.

3.7. *Bubbly Jets*

3.7.1. *Measurements of Sun and Faeth*[37,38]

Present methods of analysis were largely developed for particle-laden jets and sprays; therefore, bubbly jets provide a challenging test of the approach. In this case, bubble inertia is negligible while virtual mass and Basset history forces are important. Thus, considering such flows provides an additional indication of the robustness of the analysis as well as insights gained by studying multiphase turbulent jets from a different perspective.

Two bubbly jet studies will be considered, as follows: (1) noncondensing bubbly jets, reported by Sun and Faeth;[37,38] and (2) condensing bubbly jets reported by Sun *et al.*[39] These studies were conducted using the same apparatus. The noncondensing bubbly jets, considered in this section, involved nearly monodispersed air bubbles in water, injected vertically upward in still water. Mean and fluctuating phase velocities were measured using LDA. Initial conditions for these flows were measured and prescribed at $x/d = 8$, similar to Parthasarathy and Faeth.[31]

Fig. 30 is an illustration of predicted (LHF, DSF and SSF methods) and measured mean bubble velocities along the axis. The Case I, II and III jets involved initial volume fractions of bubbles of 2.4, 4.8 and 9.1%. DSF and SSF predictions are similar in this case. LHF calculations were initiated at the jet exit and are similar to continuous-phase velocities, while the separated flow computations were initiated at $x/d = 8$, as noted earlier. Bubble velocities are lower than liquid velocities (represented by LHF predictions) near the injector due to the bubble formation system. Far from the injector, however, bubble velocities are greater than liquid velocities due to effects of buoyancy. Both separated-flow analyses represent this trend reasonably well.

Additional measurements of bubble phase properties will be deferred until the condensing bubbly jets are considered, since these measurements yield conclusions similar to the noncondensing flow and are more complete. Continuous-phase properties will be emphasized here, since the noncondensing bubbly jet experiments involved higher initial gas volume fractions than the condensing bubbly jets, which highlights effects of turbulence modulation.

Predicted (LHF and SSF methods) and measured continuous-phase velocities and the Reynolds stress for the Case I and III bubbly jets are illustrated in Figs 31 and 32. Estimates of velocity fluctuations were obtained from the predictions assuming the levels of

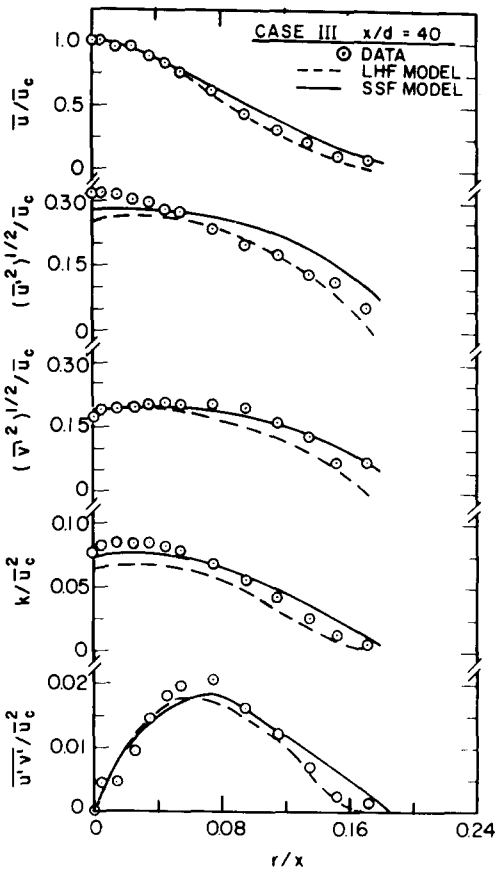

FIG. 32. Continuous-phase properties in a round noncondensing bubbly jet (case III). From Sun and Faeth.[37,38]

anisotropy observed near the centerline of single-phase jets,[53] e.g. $\bar{u}^2:\bar{v}'^2 = k:k/2$. The agreement between predictions and measurements is within experimental uncertainties for both the LHF and SSF methods. Near the axis of the Case I jet, levels of anisotropy are similar to single-phase jets. Turbulent fluctuations become more isotropic near the edge of the flow, which is also observed in single-phase jets.[53] However, the Case III jet, which is more heavily-loaded with bubbles, has significantly higher levels of anisotropy at the axis. Levels of anisotropy increased consistently with increasing distance from the injector and with increasing initial bubble loading.[38]

The increased anisotropy observed in Figs 31 and 32 was attributed to effects of turbulence modulation.[38] With increasing distance from the injector, the relative velocity between the phases becomes large in comparison to the maximum continuous-phase velocity, cf. Fig. 30, recalling that LHF predictions roughly correspond to continuous-phase velocities. Thus, turbulence generated by bubble drag tends to dominate shear prduction processes in the continuous-phsae, particularly near the axis where conventional turbulence production is small. The turbulence modulation terms of Table 2 were tested to see if they could represent this effect. A better match of predictions and measurements in Figs 31 and 32 was achieved, but other difficulties were encountered which will be discussed in connection with condensing bubbly jets. Definitive evaluation of the turbulence modulation terms could not be obtained in any event, since the effect was comparable to experimental uncertainties. The results suggest that measurements of turbulence modulation can be obtained in dilute dispersed flows with reasonable accuracy, however, by simply choosing conditions where relative velocities between the phases are large in comparison to continuous-phase velocities.

3.7.2. *Measurements of Sun* et al.[39]

This study employed the same apparatus as Sun and Faeth.[37,38] Methods of defining initial conditions and calibrating the bubble-life-history analysis were also the same. The condensing bubbly jets involved nearly monodisperse carbon dioxide bubbles in water, injected vertically upward in still water. The carbon dioxide dissolves in the water while dissolved air comes out of solution and accumulates in the bubbles. Thus, the bubbles never entirely disappear but reach terminal diameters roughly 20% of their initial diameter. Mean and fluctuating phase velocities were measured using LDA. Bubble diameters and number intensities were measured using flash photography. Bubble number intensity is defined as the number of bubbles along a cord-like path through the flow, per unit cross-sectional area of the path. This quantity can be related to the local void fraction of the flow

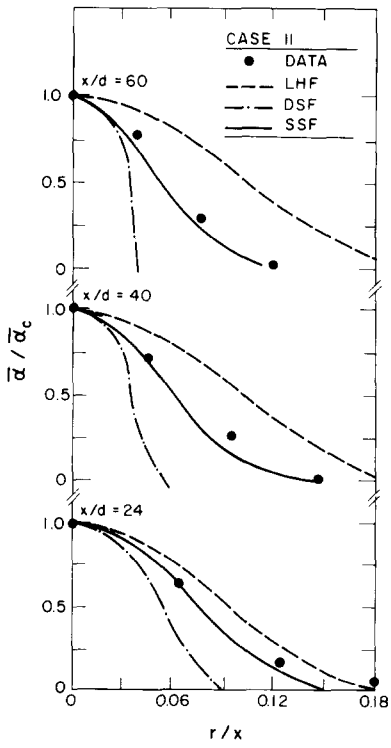

FIG. 33. Mean bubble number intensity distributions in round condensing bubbly jets. From Sun *et al.*[39]

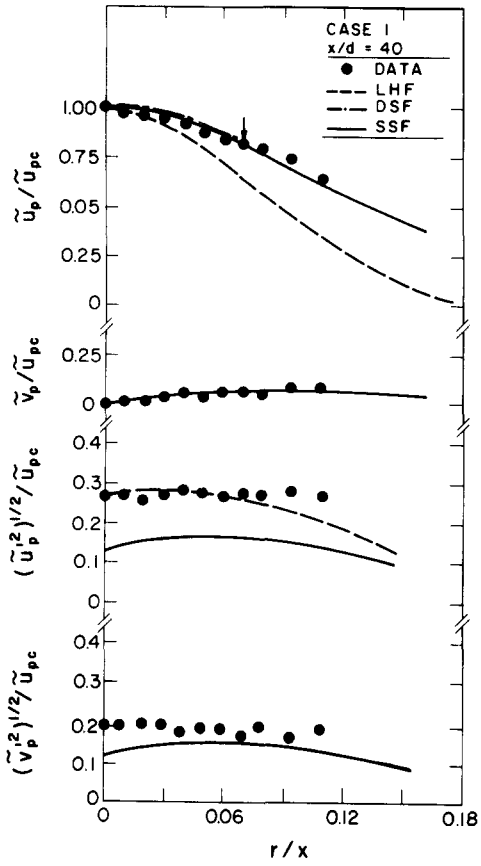

FIG. 34. Mean and fluctuating bubble velocities in round condensing bubbly jets. From Sun *et al.*[39]

and is easily computed from the analysis for comparison with measurements. The advantage of bubble number intensity is that it is less subject to experimental error than its deconvolution to give local void fractions.[39]

Typical predicted (LHF, DSF and SSF methods) and measured bubble number intensities for a condensing bubbly jet are illustrated in Fig. 33. In spite of the almost complete reversal of the phase densities, these results are very similar to the particle-laden jet results of Yuu *et al.*, ilustrated in Fig. 7. In general, the LHF and DSF methods over- and underestimate the extent of the bubble-containing region. For the bubbly jet, however, relative velocities are small near the injector and the LHF analysis provides fair predictions at the lowest axial station. The SSF method, however, provides reasonably good predictions of the transition between near-LHF conditions, in the vicinity of the injector, to the region where turbulent dispersion is important, at $x/d = 60$.

Typical measurements and predictions of bubble velocities are illustrated in Fig. 34. Predictions of the LHF and SSF analyses are shown, although LHF results closely correspond to the properties of the continuous phase. LHF predictions of fluctuating properties were found using the anisotopic ratios near the axis of single-phase jets.[53] SSF predictions were obtained directly from the calculations, averaged over all bubble sizes, similar to the measurements. DSF predictions of mean velocities were the same as SSF predictions, but this approach predicted a narrower two-phase region (ending at the arrow) as seen from Fig. 33. The DSF method provides no information concerning bubble velocity fluctuations.

Separated flow predictions of mean velocities are reasonably good. However, due to low liquid-phase velocities, relative velocities between the phases are significant due to effects of buoyancy; therefore, LHF predictions underestimate mean velocities. LHF predictions of bubble velocity fluctuations are in fortuitously good agreement with the measurements, in view of the poor predictions of mean velocities used to normalize the data. SSF predictions of bubble velocity fluctuations, however, tend to underestimate the measurements—particularly the streamwise component.

Two explanations were advanced for discrepancies between SSF predictions and measurements of bubble velocity fluctuations.[39] First of all, the assumption of monodisperse initial bubble sizes is not exact and slip velocities are strongly dependent on bubble size. This accounts for about half the discrepancy. The other factor is the isotropic turbulence assumption when randomly selecting eddy properties in SSF simulations, which has been discussed earlier. In the present case, bubbles respond rapidly to their local environment; thus effects of anisotropy of the continuous phase are substantial. This behavior is not represented by stochastic predictions, which are nearly isotropic, and are quite different from the particle-laden gas jet results in Section 3.2.5. The reason for this is the rapid adjustment of bubbles to local conditions in comparison to particles in gases. As a result, the assumption of isotropic turbulence in the stochastic analysis dominates the analysis of the bubble/turbulence interaction and causes the streamwise bubble velocity fluctuations to be underestimated when using the baseline approach—similar to results in Fig. 29 for particle-laden water jets.

Effects of turbulence modulation were also observed during this study, similar to those discussed in connection with Figs 31 and 32. This prompted a more extensive consideration of use of the turbulence modulation terms of the SSF analysis, listed in Table 3. Similar to the noncondensing bubbly jet study, use of these terms, with $C_{\varepsilon 3} < 0.2$, yielded improved predictions of continuous-phase velocity fluctuations, near the axis, when plotted like Figs 31 and 32. Including effects of turbulence modulation also increased the turbulent dispersion of bubbles in the region far from the injector. This improved the comparison between predicted and measured bubble number intensities far from the injector, where the baseline approach, illustrated in Fig. 33, is seen to underestimate the measurements. However, predictions of rates of spread and turbulence levels (near the edge of the bubble-containing region) of the con-

tinuous-phase were overestimated as a result—particularly for non-zero values of $C_{\varepsilon 3}$.

These effects of the turbulence-modulation terms of Table 3 follow from the strong contribution of the bubble source term in the k equation, which does not involve an empirical constant aside from neglecting the term entirely in the present simplified analysis. The difficulty appears to involve the multiple turbulent length scales introduced by the bubble phase. Contributions of bubbles to turbulence occur at smaller scales than the energy-containing range of the continuous phase. Thus bubble-generated turbulence enters the turbulent eddy cascade at small scales and dissipates more rapidly, tending to contribute less to turbulence properties important for mixing than is implied by the bubble source term in the k equation. It appears that properly treating effects of turbulence modulation must consider the turbulence spectrum of the continuous phase and the spectrum of turbulence generated by the relative motion of the dispersed phase. This aspect of turbulence modulation will be considered in Section 4, while alternative methods of modeling the effect will be discussed in Section 5.

4. TURBULENCE MODULATION

4.1. *Background*

Results for dilute dispersed flows considered thus far have highlighted effects of turbulent dispersion, and to a lesser degree, effects of nonlinear phase interactions. The findings suggest that turbulent dispersion is important and should be considered during comprehensive analysis of dilute dispersed flows.* The baseline stochastic-separated-flow analysis, described in Section 2.6, has demonstrated encouraging capabilities to treat effects of turbulence dispersion for dilute dispersed jets. The evaluation has ranged from particles (drops) in gases to bubbles in liquids. Results considered thus far, however, have not shed much light on effects of turbulence modulation, since the dilute dispersed flows that were studied only exhibited effects of turbulence modulation on the same order as experimental and theoretical uncertainties. Limited attempts to use the approach summarized in Table 3 to treat turbulence modulation, however, were not very successful.[36–39] In this section we consider past work which directly studied turbulence modulation, to gain a better understanding of potential sources of the difficulty. This background will then be used in Section 5, to help interpret several proposals for treating turbulence modulation in comprehensive analysis of dispersed flows.

*Effects of turbulent dispersion appear to be diminished in rapidly evaporating sprays, based on the findings of Gosman and Ioannides[83] and Solomon *et al.*[34] Therefore, it may prove possible to ignore turbulent dispersion for engineering calculations in some circumstances.

Recall that a narrow definition of turbulence modulation is being used here, namely, that the phenomenon is a direct effect of the dispersed phase on the turbulence properties of the continuous phase. This excludes indirect effects, where the presence of the dispersed phase modifies mean velocities of the continuous phase, and thus, processes of turbulence production and dissipation within the continuous phase itself. Such indirect effects are considered by tbe baseline analysis of Section 2.6. Instead, we are focussing on direct effects, such as turbulence within the wakes of dispersed phase elements and effects of the dispersed phase on the eddy structure of the continuous phase, i.e. on its energy spectrum, due to preferential interaction of the dispersed phase with eddies having a particular size.

Although turbulence modulation was not included in the predictions illustrated in Figs 5–34, its effects were observed in a portion of the experimental results. One change in continuous-phase turbulence properties, attributed to turbulence modulation, was reduced turbulence intensities and greater anisotropy of the turbulence in the vicinity of dense dispersed flows, cf. Fig. 20. Another was increased turbulence intensities in dilute regions of dispersed flows, when relative velocities between the phases were large in comparison to the velocity of the continuous phase, cf. Figs 31 and 32. For such conditions, effects of continuous-phase shear on turbulence properties become small in comparison to dispersed-phase interactions associated with turbulence modulation. Naturally, changes in continuous-phase turbulence properties can influence mixing and turbulent dispersion, particularly if the large-scale eddies which dominate these processes are affected. Thus, turbulence modulation is a key issue for achieving a better understanding of dilute dispersed flows.

Potential effects of turbulence modulation have been recognized for some time. Owen[98,99] and Hinze[2] review early work on the problem, in connection with measurements reported by Hino[100] and Kada and Hanratty.[101] The degree to which experimentally-observed changes in turbulence structure in these studies were due to direct turbulence-modulation, however, is questionable. Theoretical considerations of turbulence modulation include the work of Kuchanov and Levich[102] who analyzed the motion of a particle in homogeneous isotropic turbulence, at the Stokes limit, showing that energy dissipation due to particle lag can exceed viscous dissipation at large particle loadings. Owen[99] reached a similar conclusion after consideration of particle response to the motion of the fluid.

Hinze[2] describes several mechanisms of turbulence modulation, as follows: (1) an effect due to locally increased shear rates in the continuous phase, modifying the turbulent energy-spectrum of the continuous-phase in the wave number range corresponding to the distance between elements of the dispersed phase; (2) effects due to turbulence in the wakes of

individual elements of the dispersed phase, modifying the turbulent energy spectrum of the continuous-phase in the wave number range corresponding to the size of the dispersed-phase elements; (3) effects due to the volume occupied by the dispersed phase; and (4) the action of groups of particles upon the flow pattern of the continuous phase. The third effect is small in dilute dispersed flows, since dispersed-phase volume fractions are generally $< 1\%$, while the fourth effect is an indirect effect which is not turbulence modulation under the present narrow definition of the phenomenon; therefore, we shall concentrate on the first two effects in the following.

Hinze[2] suggests that the dispersed phase should influence the turbulence energy spectrum of the continuous phase in wave number ranges corresponding to the size and spacing of dispersed-phase elements. This generally corresponds to the high wave-number range of the spectrum of the continuous phase. Effects at wave numbers near the size of dispersed-phase elements are expected, since this is a representative scaling parameter for their near-wake turbulence. Effects at the scale of the spacing of dispersed-phase elements result from perturbation of mean shear rates at this length due to the motion of elements of the dispersed phase.[2] Furthermore, growing length scales in the wakes of dispersed-phase elements are probably limited to scales on the order of element spacing as well, due to incoherent merging of adjacent wakes.

Modification of the turbulent energy spectrum of the continuous phase at high wave numbers implies greater dissipation rates than a single-phase flow having comparable mean flow-properties.[2] This observation is supported by the findings of Owen,[99] Hino[100] and Kada and Hanratty.[101] as well as the direct analysis of Al Taweel and Landau[23] to be considered in Section 4.2.

The influence of turbulence modulation on other turbulence properties of the continuous phase, however, is more system dependent. For example, with increased loading of the dispersed phase, Solomon *et al.*[32-34] and Owen[99] find reduced turbulence intensities; Sun and Faeth,[37,38] Sun *et al.*,[39] Hino[100] and Kada and Hanratty[101] find increased turbulence intensities; while Hetsroni and Sokolov[55] find little effect on turbulence intensities. Increases and decreases of continuous-phase turbulence intensity can be rationalized by considering whether the dispersed phase is moving faster or slower than the continuous phase. Observation of no change in turbulence intensities can result when dispersed-phase/continuous-phase interactions are limited to high wave numbers and don't influence the large energy-containing eddies which dominate evaluation of properties like turbulence intensity.[2] The results of Hetsroni and Sokolov[55] could also be an artifact of their experimental technique. These measurements have been questioned due to effects of impaction of the dispersed phase (drops) on the hot wire used to measure continuous-phase turbulence properties.[8,17,18,103]

Experimental difficulties aside, Hinze[2] concludes that no generalization concerning effects of turbulence modulation on continuous-phase turbulence properties is possible. The specific properties of each dispersed flow must be considered. Clearly, elements that are important include the wave number range of the energy-containing eddies, the microscale of the continuous phase having the same mean shear but without the presence of the dispersed phase, and the wave number range directly influenced by turbulence modulation, e.g. the scales of dispersed-phase element size and spacing. Obviously, there are many possibilities for the relative locations of these scales. Furthermore, the relative magnitude of turbulence modulation is influenced by the mean shear of the continuous phase, which affects conventional turbulence processes, as well as the loading of the dispersed phase. Thus, any given set of experiments can only provide anecdotal information. In this sense, turbulence modulation is much like effects of turbulent dispersion, where the properties change with position even in a given flow, and certainly from one flow to another.

4.2. *Modulation of Turbulence Spectra*

Examining the response of the dispersed phase to turbulence fluctuations of the continuous phase provides insight concerning aspects of turbulence modulation. Such considerations are frequently incorporated into proposals for treating turbulence modulation in the context of a continuous-phase turbulence model. These proposals will be considered in Section 5. In the following, response properties are discussed, based on the analysis of Al Taweel and Landau.[23]

The analysis of Al Taweel and Landau[23] proceeds in two steps. The first considers the response of an isolated dispersed-phase element to sinusoidal oscillations of its surrounding continuous phase. The second uses Kolmogorov's concept of spectral energy transfer to evaluate continuous phase energy dissipation due to the finite response of the dispersed phase.

The response analysis follows Al Taweel and Carley.[104] This involves determining the response of an individual dispersed phase element (taken to be a sphere) to sinusoidal oscillations of the velocity of a constant property continuous phase, assuming negligible relative velocity between the phases in the mean. Analysis was limited to the linear (Stokes) flow regime, considering the complete B–B–O equation of motion (Eq. 15) with $\Delta_H = 1$, but using the Stokes expression for virtual mass of an oscillating particle. The response was characterized by the amplitude ratio and phase lag of particle and fluid velocities, as a function of the dimensionless frequency of oscillation of the continuous phase. The continuous-phase oscillation frequency was represented by the vibration number, defined as follows:

$$N_{vib} = \omega d_p^2/\nu. \quad (24)$$

Typical results of the response analysis of Al Taweel and Landau[23] are illustrated in Fig. 35. The normalized deviation of the dispersed phase velocity from the continuous-phase velocity, averaged over a period of oscillation, R_N is defined as follows:

$$R_N^2 = \overline{(u' - u_p')^2}/\bar{u}'^2. \quad (25)$$

This quantity is plotted as a function of N_{vib} for oil droplets in air and air bubbles in water in Fig. 35. At low frequencies, the dispersed-phase closely follows the continuous phase and $R_N \sim 0$. With increasing frequency, however, the motion of the two phases deviates and R_N increases. The magnitude of the deviation also depends on the density ratio of the phases; therefore, deviation begins at lower values of N_{vib} for oil drops in air (a large phase–density ratio) than for the more responsive air bubbles in water (a small phase–density ratio). Noting that the rate of energy dissipation per particle by this mechanism is the product of the drag force and relative velocity, averaged over a period of oscillation, yields the following average rate of energy dissipation per unit volume:

$$\varepsilon_p = 18 W \mu \varrho \bar{u}'^2 R_N^2/(d_p^2 \varrho_p) \quad (26)$$

where W is the mass of dispersed phase per unit mass of the continuous phase.

The expression for ε_p in Eq. (26) was used to determine the effect of a dispersed phase on the turbulent energy spectrum. The approach employed a generalization of Onsager's[105] cascade model for turbulent spectra due to Corrsin.[106] The analysis considers locally isotropic turbulence, noting that eddies of any wave number, $K = \omega/\bar{u}'$, receive energy from larger eddies, dissipating a portion of it by viscous dissipation and interaction between the phases, and transferring the remainder to eddies having higher wave numbers. Using Eq. (26) to represent dissipation due to phase interactions, the following expression is found for the turbulence spectrum (e.g. the fraction of turbulent energy associated with K, $E(K)$):

$$E(K) = \xi \varepsilon^{2/3} K^{-5/3}$$

$$\exp\left\{-\frac{3}{2}(K\eta)^{4/3} - \left(\frac{36\xi W\mu}{d_p^2 \varrho_p \varepsilon^{1/3}}\right) \times \int_0^K K^{-5/3} R_N(K)^2 \, dK\right\} \quad (27)$$

where

$$\eta = (\nu^3/\varepsilon)^{1/4} \quad (28)$$

is the Kolmogorov microscale, ξ is an empirically-determined spectrum constant having a value of $\sim 3/2$, and $R_N(K)$ is evaluated at wavenumber $K = \omega/\bar{u}'$.

The first term on the RHS of Eq. (27) is due to conventional viscous dissipation, leaving the $K^{-5/3}$ dependence in the inertial subrange (at small values of K) where viscous effects are not important.[106] Pao[107] finds this expression using a similar argument for single-phase flow. The second term on the RHS of Eq. (27) represents the effect of turbulence modulation. This term can be evaluated from the response function solution for R_N, although iteration is required to find ε when turbulence modulation is significant.[23] If R_N is set equal to unity, the analysis corresponds to a flow containing large particles that do not respond to turbulent fluctuations. Eq. (27) then reduces to a form very similar to that found by Baw and Peskin,[108] for this limit.

Al Taweel and Landau[23] compare Eq. (27) with measurements of energy spectra of the continuous phase for the particle-laden jet (oil drops in air) experiments of Hetsroni and Sokolov.[55] The comparison was encouraging; however, this confirmation is questionable due to errors in experimental results caused by drop impaction on the hot-wire sensors used during the study—noted earlier.

Some general results concerning effects of particles on continuous-phase turbulence spectra are reported in a later study by Al Taweel and Landau.[109] Figures 36 and 37 are representative findings of this study. Effects of particles in a fully developed turbulent flow within a round duct are considered, with single-phase spectra based on the measurements of Laufer.[110] Spectra vary across the duct, the position considered is near the wall of the duct, $(d - 2r)/d = 0.0082$. Eulerian spectra were used, rather than Lagrangian spectra following a particle implied by the analysis, for lack of an alternative; however, the two spectra are similar for fully-developed, homogeneous flow.[24,111] Results were computed for sand particles having a density ratio $\varrho_p/\varrho = 2050$ with respect to air. The response function for these particles is similar to that of oil drops in air, illustrated in Fig. 35.

The plots in Figs 36 and 37 show that the presence of particles damps turbulent fluctuations, particularly at high-wave numbers where the particles cannot respond quickly enough to follow the flow. Results in Fig. 36 show that effects of turbulence modulation increase with increased particle loading for a fixed particle size. In Fig. 37, the effect of particle size is

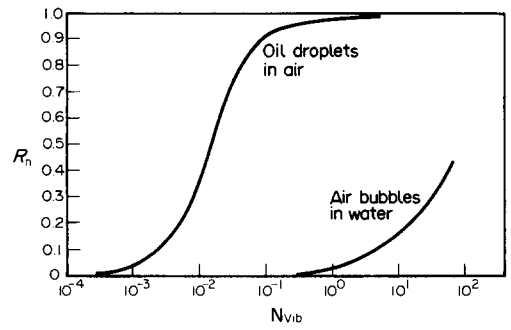

FIG. 35. Response of dispersed-phase particles to sinusoidal continuous-phase velocity fluctuations. From Al Taweel and Landau.[23]

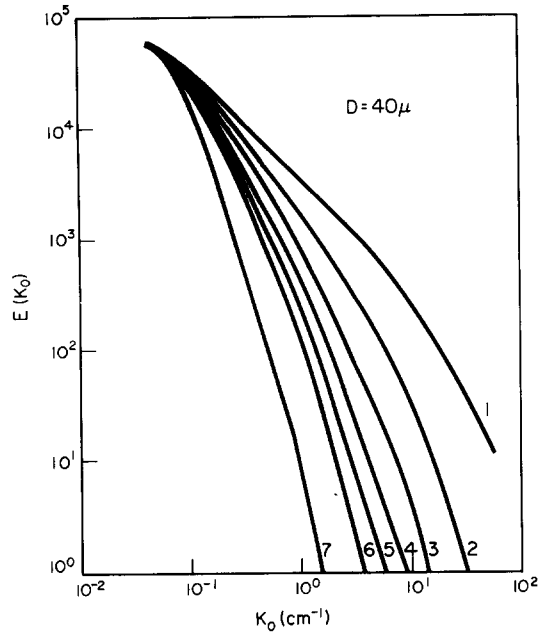

FIG. 36. Predicted effect of solids loading on turbulence modulation for a fixed particle size. Numbers on curves denote loading ratio, as follows: (1) 0.0, (2) 0.2, (3) 0.4, (4) 0.6, (5) 0.8, (6) 1.0 and (7) 2.0. From Al Taweel and Landau.[109]

considered, keeping the particle loading ratio constant at $W = 0.1$. At low wave numbers, the small particles cause less damping than large particles, since they respond more rapidly to the fluctuations of the flow. At high wave numbers, however, small particles result in increased damping. For the conditions shown, all particle sizes have $R_N \sim 1$ at high wave

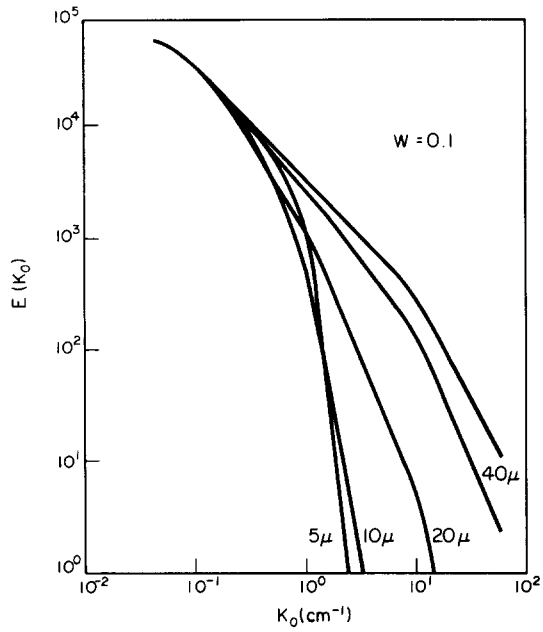

FIG. 37. Predicted effect of particle size on turbulence modulation for a fixed solids loading. From Al Taweel and Landau.[109]

numbers; thus, this effect is due to the greater surface area available with small particles at the same mass loading, i.e. the d_p^2 dependence of the turbulence modulation term in Eq. (27).

It is also evident from Figs 36 and 37, and anticipated by Hinze,[2] that the large-scale energy containing eddies are not strongly influenced by the presence of particles for these conditions. In jets, the large-scale eddies are primarily responsible for mixing and for effects of dispersion; therefore, modification of turbulence properties at high wave numbers due to turbulence modulation should not have a significant influence on these properties. Thus, a simple model of turbulent dispersion which does not consider the difference in scale between the energy-containing eddies and those which are damped by turbulence modulation, like the approach summarized in Table 3, is unlikely to be successful. This probably accounts for the difficulties encountered with this approach when applied to bubbly jets, discussed earlier. Proposals for overcoming this difficulty will be considered in the next section.

The approach described by Al Taweel and Landau[23] provides an interesting perspective on effects of turbulence modulation; however, their study has several limitations with respect to practical dispersed flows. First of all, the analysis is limited to relative oscillatory velocities within the linear Stokes regime, with negligible relative velocities between the phases in the mean. We have seen that such conditions are rarely found in practical dispersed flows, where effects of relative velocities are generally important and dispersed-phase Reynolds numbers are on the order of 100 (which is well beyond the Stokes regime). Thus, the response functions are used by Al Taweel and Landau[23] are not appropriate for these conditions. Rather, we are faced with potentially large-scale velocity fluctuations superimposed on a large mean relative velocity. Nagaraj and Gray[112] suggest a change in the response formulation to account for non-Stokesian fluctuations; however, they do not report results of such analysis.

A second limitation of the turbulence modulation analysis of Al Taweel and Landau[23] also relates to their neglect of dispersed-phase relative velocities in the mean. By this assumption, effects of growing wakes, due to particle motion, are not considered, although they clearly would modify the turbulence spectrum. Merging of these wakes on scales related to particle spacing is another aspect of the problem that cannot be considerd in the single-particle formalism considered in Ref. 23. In a sense, the crude approach for treating turbulence modulation, summarized in Table 3, attempts to treat such effects in a global way. However, this method does not account for the important effects of scale highlighted by the analysis of Al Taweel and Landau[23] and also clearly cannot address structural details of the continuous-phase turbulence, like its spectra. In view of the difficulties involved in the analysis of turbulence modulation for

conditions relevant to practical dispersed flows, experimental information ranging from near LHF conditions (in the mean) to typical slip conditions (for various particle loadings and spacings), would be most helpful for gaining a better understanding of turbulence modulation.

5. ALTERNATIVE ANALYSIS OF DILUTE DISPERSED FLOW

5.1. *Introduction*

The SSF analysis described in Section 2.6 has provided a unified, baseline approach to the dilute dispersed flows considered thus far. Several other methods have been proposed to treat such flows, however, and no review would be complete without considering them. A sample of recent analyses will be considered in this section. Dispersed-phase/turbulence interactions will be emphasized, particularly turbulence modulation, since many of these analyses incorporate more elaborate methods to treat this phenonmenon than have been discussed thus far.

The discussion will begin with analyses using the interpenetrating-continua formulation, since most work to date considering turbulence modulation has adopted this approach. The section concludes with discussion of recent discrete-element analyses which treat turbulence modulation.

5.2. *Interpenetrating-Continua Analyses*

5.2.1. *Introduction*

The method of interpenetrating continua has recently been reviewed by Drew,[21] therefore, the details of this approach will be omitted. Use of the interpenetrating continua formulation is particularly convenient when the dispersed phase is monodisperse. At this condition, the number of equations to be integrated is only roughly twice that of a single-phase flow. Furthermore, numerical solution of all the equations can proceed in a similar manner, avoiding the interaction problems of two different types of formulations, and bookkeeping problems for the dispersed phase, encountered in the Eulerian/Lagrangian formulation of discrete-element analysis. The approach also provides a convenient formalism for treating turbulence-modulation, which has attracted a number of workers interested in this phenomenon.

The method of interpenetrating continua also has several deficiencies which must be kept in mind when considering its use. Recall that this approach requires auxiliary information concerning the turbulent diffusivity of the dispersed phase. This is a serious limitation since turbulent dispersion is very complex, e.g. particle properties, turbulence properties and the relative velocities of the phases are all involved, which makes universal correlation of dispersion a monumental task. Another problem is the proliferation of continua, all requiring solution of full sets of governing equations, when polydisperse flows, or flows involving heating and phase changes of the dispersed-phase, are considered. A more fundamental difficulty involves application of continuum concepts to a dilute-dispersed phase, which can result in embarrassingly large incremental volumes for this component of the flow, cf. Marble,[6] Lumley[7] and Drew.[21]

5.2.2. *Mixing-length methods*

The analyses considered in the following were all limited to monodisperse dispersed phases. The methods can be distinguished by the approach used to treat continuous-phase turbulence properties, e.g. mixing-length methods, one-equation methods, and higher-order methods. We begin with mixing-length methods such as Melville and Bray[103] and Michaelides.[113] The following discussion will be limited to the work of Melville and Bray,[103] which is representative of the genre, since dilute dispersed jets were considered with particular reference to the measurements of Laats and Frishman.[28,29]

Melville and Bray[103] develop their analysis for conditions where interphase slip is small, employing constant eddy diffusivities for the momentum exchange of each phase and particle transport. The turbulent diffusivity of the continuous phase was corrected for the presence of the dispersed phase, considering two methods: (1) an approach due to Owen,[99] assuming complete response of the dispersed phase to turbulent fluctuations; and (2) and approach due to Abramovich.[114,115] They develop an expression for the eddy diffusivity based on an early result of Meek and Jones,[116] that the ratio of turbulent kinetic energies of the dispersed and continuous phases in homogeneous isotropic turbulence is $k_p/k = T_L/(T_L + t_p)$, where T_L is the streamwise Lagrangian integral time scale of the continuous phase, and t_p is the characteristic linear (Stokesian) response time of dispersed-phase elements, as follows:

$$t_p = d_p^2(2\varrho_p/\varrho + 1)/36\nu. \tag{30}$$

They also find that the ratio of the eddy diffusivities of the two phases is the same as k/k_p. The turbulent mass diffusivity of the dispersed phase is then computed by assuming a constant turbulent Schmidt number of 0.7.

Clearly, effects of turburlence modulation are dispersed throughout the formulation with this approach, making assessment of the various approximations very difficult. The predictions were compared with the measurements of Laats and Frishman,[28,29] with some success, but the generality of the approach has not been established. In fact Melville and Bray[103] suggest that methods incorporating higher-order turbulence closure should be considered for improved analysis of dispersed flows.

Most subsequent workers have adopted this suggestion.

5.2.3 *One-equation methods*

Danon *et al.*[117] describe a one-equation (k-length scale) model for two-phase jets, also at the limit of small relative velocities between the phases. The prescription for the length scale was not modified from normal use in single-phase constant-density jets. However, a particle source term was included in the governing equation for turbulence kinetic energy, in a manner which partially compensated for particle inertia. The analysis was evaluated using the data of Hetsroni and Sokolov.[55] The basic analysis was not in good agreement with the measurements, and could only be fitted by attributing unusually large effects of turbulence modulation to the dispersed flow. Later, it became evident that much of the difficulty was due to errors in the measurements, discussed earlier.[17] However, the approach of Ref. 117 has not been subsequently evaluated using more recent measurements.

5.2.4 *Higher-order methods*

Genchev and Karpuzov[118] consider particle-laden flow in a pipe using a two-equation model of turbulence. This involved modeled governing equations for k and the turbulence length scale, along the lines of Harlow and Nakayama.[119] The two-phase flow was limited to conditions where the dispersed phase completely responds to the mean (large-scale) motion, $\tilde{u}_i = \tilde{u}_{pi}$, but does not follow the large wave-number fluctuations of the turbulence, i.e. $\overline{u_i' u_{pi}'} \ll \overline{u_i'^2}$. Relative velocities at high wave numbers were assumed to be small; therefore, drag was computed at the linear (Stokes) limit. Typical of two-equation models, the dispersed-phase source term in the k equation was formally exact; however, the analogous term in the other equation (representing the dissipation length scale in this case) had to be modeled—introducing an unknown empirical constant. The discussion of Section 4.2 suggests that the turbulence modulation terms are oversimplified by this approach, since the differing scales of large-scale mixing and turbulence modulation on small scales are not distinguished. Genchev and Karpuzov[118] assume uniform concentration of the dispersed phase across the duct; therefore, effects of turbulent dispersion were not addressed. The analysis was not compared with measurements, thus the value of the new empirical turbulence modulation constant and the generality of the overall analysis are not known.

Elghobashi and coworkers[75,120] have developed one of the most elaborate two-equation models for dilute dispersed flows reported thus far. The approach is limited to the linear (Stokes) regime for both mean and fluctuating relative velocities, which is a logical limit for systematic development of theoretical understanding of effects of turbulent dispersion and modulation. A k–ε model of turbulence is used. The governing equations for k and ε are developed by Elghobashi and Abou-Arab,[75] by introducing time-averaged mean and fluctuating quantities and establishing closure of higher-order correlations, similar to turbulence models of single-phase flows. Effects of the dispersed phase are considered in this portion of the analysis using the linear (Stokes) approximation for drag.

Elghobashi and Abou-Arab[75] use a sophisticated procedure to treat turbulence modulation while accounting for the spectral properties of continuous phase turbulence. This step requires evaluation of the correlation between continuous-phase and relative velocity fluctuations, $\overline{u_i'(u_i' - u_{pi}')}$, which appears in the turbulence modulation terms when a linear drag law is used. The correlation was found using Chao's[121] results for the response of a particle to turbulent fluctuations. Chao's analysis is somewhat similar to the approach used by Al Taweel and Carley;[104] therefore, effects of mean relative velocity differences between the phases are ignored and the analysis is limited to the linear drag law for velocity fluctuations. With these approximations, Chao[121] obtained the following expression for the ratio of dispersed- and continuous-phase velocity fluctuations:

$$u_{pi}'^2/u_i'^2 = \int_0^\infty (\Omega_1/\Omega_2)\, f(\omega)\, \mathrm{d}\omega \tag{31}$$

where Ω_1 and Ω_2 are spectral response functions which depend on the characteristic response time of the particle, t_p; the density ratio of the phases, ϱ_p/ϱ; and the frequency of the turbulence, ω. The Lagrangian frequency function, $f(\omega)$, weights the response according to the turbulence spectrum of the continuous phase. This function was approximated differently in Refs 75 and 120. The most recent version,[120] approximated $f(\omega)$ following Hinze,[3] as follows:

$$f(\omega) = (2T_L/\pi)/(1 + \omega^2 T_L^2). \tag{32}$$

The local Lagrangian time scale, T_L, was evaluated assuming isotropic turbulence, according to Calabrese and Middleman,[122] as follows:

$$T_L = 5k/(12\varepsilon) \tag{33}$$

which is similar to the expression for t_e used in present SSF analysis, Eq. (14), except that the coefficient in Eq. (33) is roughly a factor of two larger than the coefficient of Eq. (14). The turbulence modulation term in the ε equation involves additional approximations, but includes effects associated with the correlation appearing in Eq. (31). This introduces a new empirical constant, $C_{\varepsilon 3}$, analogous to the turbulence modulation parameter of the particle source term of Table 3.

Elghobashi *et al.*[120] describe the turbulent disper-

sion portion of this analysis. This is based on a gradient diffusion approximation using a correlation for the dispersed phase Prandtl/Schmidt number due to Peskin.[123] This correlation was recently reviewed and recommended by Alonso.[124] The correlation can be written as follows:

$$1/\sigma_p = 1 - (kt_p^2/6v)/(t_p + T_L). \quad (34)$$

This form was reached by approximating the Lagrangian length scale, L_L, and Eulerian microscale, λ, as follows:

$$L_L = (2k/3)^{1/2} T_L \quad (35)$$

$$\lambda = (10v\, k/\varepsilon)^{1/2}. \quad (36)$$

Elghobashi *et al.*[120] extend the definition of the linear particle response time, t_p, to consider conditions beyond the linear Stokes drag regime; however, this extension is questionable since linear drag is assumed for all other aspects of the analysis. Furthermore, the Prandtl/Schmidt number correlation of Eq. (34) was developed for negligible relative velocities between the phases, e.g. there is no transit-time effect in the expression since dispersed-phase elements are always assumed to be captured by eddies. Thus, while consistent with a linear drag analysis at small slip, use of Eq. (34) to treat turbulent dispersion raises questions concerning the application of the method to most practical dispersed flows. This is one area where the mathematical simulation aspects of the SSF approach, (admittedly with a relatively crude model of continuous-phase turbulence properties similar to the interpenetrating continuum methods), is helpful.

The approach developed by Elghobashi and coworkers[75,120] is systematic, but it involves numerous modeling approximations and additional empirical constants which must be established by comparison with measurements. Work along these lines was initiated using the measurements of Modarress *et al.*[92,125] for a particle-laden jet in coflowing air within a duct. As noted earlier, however, these measurements are difficult to analyze quantitatively due to effects of unreported streamwise pressure gradients in the duct.[66,86] Furthermore, since a number of new empirical constants and modeling concepts are involved, definitive evaluation of this approach will require consideration of a more extensive data base.

Humphrey and coworkers[126,127] report a more simplified approach to treat turbulence modulation, using a k–ε model of turbulence in conjunction with the interpenetrating continua formalism. This analysis was also limited to the linear (Stokes) drag regime. Turbulent dispersion of the dispersed phase was modeled as in Elghobashi and coworkers,[75,120] using the dispersed-phase Prandtl/Schmidt number correlation of Peskin[123] and the same prescription for continuous-phase turbulence scales. The dispersed-phase momentum equation required an expression for the dispersed-phase turbulence kinetic energy, and the turbulence-modulation term required an expression for the dispersed-phase/continuous phase velocity fluctuation correlation. These quantities were found from the following expression

$$k_p/k = \overline{u_i' u_{pi}'}/(2k) = T_L/(T_L + t_p) \quad (37)$$

where t_p and T_L are found from Eqs (30) and (33). The first of these equations is identical to the finding of Meek and Jones,[116] used by Melville and Bray.[103] The assumption given by Eq. (37) provides the $\overline{u'u'_{pi}}$ correlation needed in the turbulence modulation term of the k equation; a more complex expression involving the ratio t_p/T_L, and the gradient of T_L, is used in the ε equation. Thus, this approach provides some consideration of effects of the differing scales of the eddies largely responsible for mixing and the high wave number eddies where effects of turbulence modulation are concentrated. Thus, when $t_p/T_L \ll 1$, the particle source term in the k equation approaches zero. The final formulation involves numerous model approximations which require evaluation with measurements. However, work along these lines has not been reported as yet.

The last interpenetrating continuum analysis applied to turbulence modulation that we shall consider involves the approach developed by Chen and Wood[128,129] and Chen.[130] This analysis is based on a multiscale k–ε turbulence model which is extended from the method developed by Hanjalac *et al.*[131] for single-phase turbulent flows. With this approach, two sets of governing equations are constructed for k and ε of the continuous phase. One set refers to the large-scale (production) region of the energy spectrum while the other treats the transfer region of the spectrum representative of the small-scale dissipative range of the eddies. The dispersed-phase is only assumed to interact with the small-scale portion of the spectrum, in keeping with the dispersed-phase response characteristics discussed in Section 3.7.2. This implies that the formulation is limited to conditions where the particle response is adequate to follow the large-scale eddies of the flow. However, there is no automatic provision to allow for varying dispersed-phase response: the dispersed-phase effect is always assigned to the transfer region of the spectrum. Like other interpenetrating-continua analyses, dispersed-phase Reynolds numbers are assumed to be in the linear (Stokes) regime. Dispersion is treated assuming a gradient-diffusion approximation, with the turbulent Prandtl/Schmidt number of the dispersed phase given by the following expression:

$$\sigma_p = 0.7(T_L' + t_p)/T_L' \quad (38)$$

where T_L' is the "macro" time scale of the flow. T_L' is related to k and ε of the production region of the turbulence spectrum in a similar way to T_L in Eq. (33). The prescriptions for the turbulence modulation terms in the k and ε equations for the dissipative region of the spectrum involve t_p and T_L' as well, cf. Refs 128–130 for the specific formulas.

Chen[130] evaluates the multiscale approach using measurements for particle-laden duct flows reported by Tsuji *et al.*,[132] Steimke and Dukler,[133] Lee and Durst,[134] and Kramer and Depew.[135] The comparison between predicted and measured mean phase velocities and streamwise fluctuating continuous-phase velocities was encouraging. This portion of the evaluation, however, did not involve information concerning variations in dispersed-phase concentrations to test the turbulent dispersion aspects of the analysis. Turbulent dispersion was considered using measurements of Memmott and Smoot[136] for a confined particle-laden jet. In this case, there was considerable uncertainty in defining initial conditions, the velocity data was judged not to be sufficiently reliable to compare with predictions, and coflowing jets in ducts are difficult to use for evaluation due to problems of small streamwise pressure gradients,[66] noted earlier. Keeping these limitations in mind, encouraging agreement between predictions and measurements was reported.

During Chen's[130] evaluation of the multiscale method, it was necessary to only consider conditions where the linear drag law was adequate. Extension to non-Stokesian drag must be considered before this approach can be applied to most practical dispersed flows. The extent to which the specific turbulence modulation terms in the analysis of Ref. 130 contributed to predictions of continuous phase properties is also not clear, e.g. the presence of particles significantly modified mean velocity profiles for the duct flows, which causes changes that are not turbulence modulation within the current narrow definition of this phenomenon. Finally, the prescription for turbulent dispersion used in this approach is relatively ad hoc. Further comparison of predictions and measurements is needed to test turbulent dispersion aspects of the analysis, using results from well-defined experiments.

5.3. *Discrete-Element Analyses*

Consideration of discrete-element analysis will be limited to stochastic methods since they provide a convenient formalism for considering effects of dispersed-phase/turbulence interactions—particularly turbulent dispersion. The following considerations are not comprehensive, but are meant to bring out features of recent SSF analysis that were not considered when the baseline approach was described in Section 2.6.

Buckingham[137,138] and Buckingham and Siekhaus[139] describe an SSF analysis for transient particle-laden flow in a duct, with application to problems of gun-barrel erosion. Clearly, this is a very complex transient flow and capabilities for evaluating the approximations of this method are limited. However, several features of this approach are of interest for subsequent development of SSF analysis.

In Buckingham's[138] approach, the assumption of uniform properties of finite-sized eddies is not used. Instead, the sampling procedure for instantaneous continuous-phase properties considers both the Gaussian PDF of velocity fluctuations and the autocorrelation function of the flow. This is accomplished by weighting each random selection with past values so that the choices satisfy the autocorrelation function. Continuous-phase turbulence properties were found from a k–ε turbulence model. However, instead of estimating the autocorrelation function from the turbulence model, results from Betchov and Lorenzen[140] and Uberoi and Freymuth[141] were used. The use of empirical data for the correlation limits the generality of the method, however, this deficiency should be removable using scales which can be approximated from the turbulence model. In addition, the approach must also be extended to consider transit-time effects if it is to be applied to most practical cases, where the relative velocities of the phases are significant. Finally, whether use of a dispersed-phase/fluid autocorrelation is warranted (in preference to the uniform-eddy approximation) must still be established.

Another interesting feature of the analysis of Refs 137–139 involves the use of "importance sampling," cf. Faist and Muckerman,[142] for a description of the technique and related references. This methodology weights random sampling so that important portions of the PDF can be more rapidly resolved, accelerating the convergence of stochastic methods. Exploitation of these techniques would reduce one of the main deficiences of SSF analysis, namely, the increased computation time required to obtain statistically-significant results in comparison to DSF methods (however both methods would benefit from use of importance sampling).

The turbulence modulation approach used in Refs 137–139 is speculative and has not been evaluated. Effects of both particle inertia and acoustical energy loss modifications due to the presence of particles were considered, neglecting slip for the latter correction.

The present baseline SSF approach has already been described. From the discussion of Section 4, a major deficiency of the turbulence modulation portion of the analysis is lack of consideration of the response properties of the dispersed phase. Actually, when turbulence modulation is ignored, as in the baseline analysis, one essentially is assuming that the particles only modify the high wave number portion of the spectrum and don't influence the large-scale eddies responsible for turbulent dispersion and mixing. In view of our current limited understanding of turbulence modulation, this is perhaps the best course of action, for the present, for dilute dispersed flows.

Recently, Mostafa and Mongia[93] report an SSF analysis of particle-laden jets which is very similar to the present baseline approach. The main modifications involve the treatment of dispersed-phase drag in

the mean momentum conservation equation, and a different approach for the turbulence modulation terms in the k and ε equations. In this analysis, S_{pu} is linearized, similar to DSF analysis, as follows:

$$\bar{S}_{pu} = \sum_{k=1}^{n} s_{puk} (\bar{u} - \bar{u}_p)_k / V_j \quad (39)$$

where

$$s_{puk} = (\dot{n}\pi d_p^2 C_D |\vec{u} - \vec{u}_p|)_k / 8. \quad (40)$$

Mostafa and Mongia[93] continue the linear approximation when driving the turbulence modulation portion of the equation and assume that s_{pui} is a constant when averaging after multiplying the instantaneous momentum equation by u_i'. The turbulence modulation term then only involves the continuous phase/relative velocity fluctuation correlation, $\overline{u_i'(u_i' - u_{pik}')}$, e.g. a linear drag approximation. This correlation is modeled in the same manner as Humphrey and coworkers[126,127] in their linearized interpenetrating continua approach, as follows:

$$\overline{u_i'(u_i' - u_{pik}')} = 2kt_{pk}/(T_L + t_{pk}). \quad (41)$$

The dispersed-phase response time was evaluated allowing for nonlinear drag, as follows:

$$t_{pk} = (4d_p \varrho_p / (3C_D \varrho |\vec{u} - \vec{u}_p|))_k. \quad (42)$$

T_L was evaluated from an equation like Eq. (33), but with the coefficient reduced by roughly 15%. Finally, the turbulence modulation terms are prescribed as follows:

$$\bar{S}_{pk} = -\sum_{k=1}^{n} 2k(s_{pu} t_p / (T_L + t_p))_k \quad (43)$$

$$\bar{S}_{p\varepsilon} = -C_{\varepsilon 3} \varepsilon S_{pk} / k. \quad (44)$$

The equation for $\bar{S}_{p\varepsilon}$ follows from the usual assumption that dissipation of ε by a particular mechanism is proportional to the corresponding dissipation term in the k equation.

These modifications simplify evaluation of the three dispersed-phase source terms in particle-laden flows, in comparison to the approach summarized in Table 3. Furthermore, effects of scale are incorporated in the turbulence modulation terms. This has been achieved, however, at the expense of linearizing the drag expression and a somewhat inconsistent treatment of the $\overline{u S_{pu}}$ correlation, e.g. assuming that s_{pu} can be treated as a constant even though effects of fluctuations in this term are comparable to the term that was considered. Results illustrated in Fig. 17 indicate that linearizing the mean drag, similar to the DSF approach, makes a significant change in mean velocity predictions in some instances. Whether such differences are significant in comparison to other uncertainties in SSF analysis remains to be seen. The effect of linearization and other approximations in the turbulence modulation terms is also unknown.

Mostafa and Mongia[93] evaluated their analysis using the particle-laden jet measurements of Shuen *et al.*[31] The turbulence model constants were the same as Table 3, except that a value of $C_{\varepsilon 3} = 1$ was established by matching predictions and measurements for one particle-laden jet test condition of Ref. 31. Measured initial conditions were used, except for ε which was estimated as described in Section 3.2.5. Best agreement between predictions and measurements for the pure air jet measured during these tests was achieved using a slightly different procedure for finding ε than Shuen *et al.*[31] The agreement between predicted and measured mean particle velocities was not very good, suggesting underestimation of particle drag. This is probably due to the linearization of the drag analysis, discussed earlier; Shuen *et al.*[31] encountered similar difficulties (cf. Fig. 16) with their calculations using the DSF approach where drag is computed in the same way. Mostafa and Mongia[93] conclude that analysis including their turbulence modulation terms yielded improved predictions of continuous-phase properties. However, differences between results with and without these terms are comparable to experimental uncertainties. Shuen *et al.*[31] found similar levels of improvement using the approach summarized in Table 3. Thus, these observations are not definitive, due to limitations of the experiments.

We have seen that many proposals have been made to model turbulence modulation in the context of higher-order turbulence models. Unfortunately, existing data involves uncertainties concerning turbulence modulation that are too large to provide a definitive test of these methods. New experiments, for simple flows, where turbulence modulation is a more dominant effect and can be measured accurately, are still needed. This recommendation was also made by Hinze[2] some time ago. It appears likely that an effective approach toward treating turbulence modulation will consider the response of the disperse phase, the spectral properties of the continuous phase in the frequency domain, and nonlinear drag interactions beyond the linear (Stokes) regime. Other issues, raised by Hinze,[2] which have not been considered by any turbulence modulation proposals to date, involve wake effects and perturbation of continuous-phase shear. These effects result from finite relative velocities between the phases. They potentially contribute to continuous-phase turbulence properties at much larger scales—comparable to the spacing of dispersed-phase elements and closer to the energy-containing range of the spectrum. The spacing of dispersed-phase elements is still generally small in comparison to flow widths, and thus the scale of the largest eddies. However, contributions of such effects appear to be comparable to turbulence modulation effects related to the dispersed-phase response to continuous-phase velocity fluctuations which have been emphasized thus far.

It is also clear that past work on turbulence modulation has largely emphasized phenomena associated with dispersed-phase drag. Effects of turbulence mo-

dulation on scalar transport are also potentially important and should receive more attention—particularly for flame environments. This, and other aspects of turbulence modulation, present challenging problems for workers in the area of dilute dispersed flows.

6. DENSE-DISPERSED JETS

6.1. *Introduction*

Some aspects of dense dispersed jets have been considered thus far, based on observations near the boundaries of dilute dispersed jets. In this section, we will consider additional information obtained by direct observation and analysis of dense dispersed jets. Aspects of dense dispersed flows are treated in more detail in reviews by Sirignano,[11] Bracco,[12,13] Faeth,[17] Lefebvre,[18,19] Elkotb,[20], Drew,[21] Harrje and Reardon,[143] Griffen and Muraszew[144] and references cited therein.

The scope of the present discussion will be primarily limited to dense sprays produced by round pressure-atomizing injectors. Bracco and his associates[12,13,87,145–150] have studied this flow configuration; therefore, much of the material in the following has been drawn from their work. Naturally, this omits direct consideration of the wide variety of pressure- and air-atomizing injectors encountered in practice. However, many fundamental aspects of the dense region of sprays near the injector are similar for all systems.

In the following, we first treat general background concerning dense-spray processes. This involves breakup regimes, flow patterns, breakup processes and collisions between drops. The section concludes with a brief description of dense-spray models which have been developed thus far, primarily examining the work of Bracco and his associates.[12,13,149,150]

6.2. *Background*

6.2.1. *Breakup regimes*

One of the first things that must be determined for a multiphase flow is the flow regime.[151] Atomizer flows involve breakup regimes of liquid jets as well as various flow patterns within the spray. Ranz,[152] describes four flow regimes of liquid jet breakup, as follows: drip, Rayleigh breakup, wind-induced breakup, and atomization. The drip regime involves the slow formation of large drops immediately at the jet exit, which then fall as a single stream. Rayleigh breakup is caused by surface tension effects. Rayleigh breakup occurs many jet diameters from the injector exit and yields a stream of drops having diameters larger than the jet diameter. Wind-induced breakup is due to instabilities caused by the relative motion of the gas and liquid, stabilized to some extent by surface tension. Wind-induced breakup occurs many diameters from the jet exit and yields drop diameters ranging from the jet diameter to about one order-of-magnitude smaller. The atomization regime is characterized by jet breakup immediately at the jet exit, at least at the surface which is generally the only directly visible portion of the flow. Flow in the atomization regime yields drops whose average diameter is much smaller than the jet diameter.

Only the wind-induced and atomization breakup regimes lead to a dense spray region, unless an array of injectors is used. Ranz[152] prescribes criteria for these breakup regimes for round liquid jets, based on the liquid and gas Weber numbers of the flow, defined as follows:

$$We_{(f\,or\,g)} = \varrho_{(f\,or\,g)} u_0^2 d/\sigma \tag{45}$$

The criteria for wind-induced breakup are $We_f > 8$, $0.4 < We_g < 13$; while the criteria for the atomization regime are $We_f > 8$, $We_g > 13$. These assessments are only approximate; for example, Miesse[153] finds transition to the atomization regime at $We_g > 40$. Identification of a flow regime is also the subjective opinion of an individual investigator about the appearance of a physical process.[151] Thus, some investigators identify two wind-induced breakup regimes, while others are satisfied with only one.[154] Finally, factors other than We_g and We_f have been found to influence breakup regime boundaries, e.g. injector Reynolds numbers, ambient flow properties (cross-flow), injector length-to-diameter ratio, density ratio of the phases and cavitation within the injector, to name only a few.[12,13]

Flash photographs ($\sim 1\,\mu$sec flash duration) of liquid jets in the wind-induced breakup and atomization regimes are illustrated in Figs 38–40. Test conditions involve a water jet injected vertically downward into air at normal temperature and pressure. The injector was a long length-to-diameter ratio passage having a smooth entry to avoid effects of cavitation. The initial jet diameter was 10 mm, yielding jet Reynolds numbers on the order of 10^6. Naturally this passage is much larger than typical injectors, however, the flow exhibits regime transitions similar to small injectors and the large scale allows features of the flow to be seen more clearly. Four pictures are shown for each test condition, near the exit and centered at $x/d = 50$, 100 and 150. The lowest position appearing in the photographs is nearly 2 m from the injector exit.

Conditions of wind-induced breakup are illustrated in Figs 38 and 39. The flow in Fig. 38 corresponds to the first wind-induced breakup regime, defined by Reitz.[154] Breakup occurs far from the injector, yielding drops whose diameters are similar to the jet diameter. Breakup is attributed to surface tension, augmented by the motion of the surrounding gas.

An interesting feature of the results illustrated in Fig. 38 is that the liquid surface exhibits fine-grained roughness near the injector but becomes smoother

FIG. 38. Flash photographs of a pressure-atomized spray for first wind-induced breakup conditions.

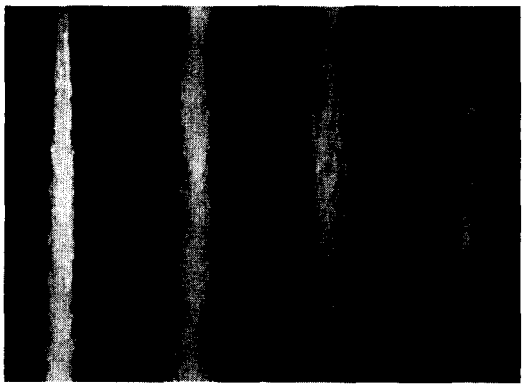

FIG. 40. Flash photographs of a pressure-atomized spray for atomization breakup conditions.

(with large-scale irregularities appearing) far from the injector. A shift of the turbulence spectra of both phases, toward lower wave numbers, is probably involved in this phenomenon. Liquid phase turbulence properties near the injector exit are governed by the tube flow. However, once the flow leaves the injector, liquid velocities become more uniform since the gas cannot retard the surface velocity as effectively as the passage wall. This reduces turbulence production in the liquid, causing the turbulence to decay with the high wave number end of the spectrum disappearing first. The developing flow in the gas phase also favors the smallest scales near the injector exit. If liquid velocities were higher so that drops formed from the surface, smaller asperities would lead to smaller drops, suggesting small drops being rapidly dispersed by the turbulence near the edge of the flow. The extent to which liquid-phase turbulence generally influences drop sizes in typical injectors is still open to question, however, since most pressure-atomizing injectors have short passages with little time available for turbulence to develop.[12,13]

Higher liquid velocities yield conditions for the second wind-induced breakup regime.[154] This flow is illustrated in Fig. 39. Breakup occurs far from the injector and yields drops having diameters much smaller than the jet diameter. Decay of liquid surface roughness is also evident here, with large-scale disturbances reminiscent of Fig. 38 appearing in the all-liquid core, far from the injector.

FIG. 39. Flash photographs of a pressure-atomized spray for second wind-induced breakup conditions.

With an additional increase in the jet velocity, the flow enters the atomization regime, pictured in Fig. 40. The atomization regime is defined by breakup of the liquid surface immediately at the tube exit. All higher flow rates would look the same. Drops found near the tube exit are probably small. The wispy appearance of the drop-containing region, much like a single-phase flow seeded with tracer particles, is evidence of this. Clear areas of drop intermittency penetrate the drop-containing region. However, near the jet exit, the extent of penetration is quite small, suggesting an underlying all-liquid core similar to Figs 38 and 39. The depth of penetration increases with distance from the injector, but drop intermittency is not seen at the axis until $x/d \sim 150$–200, suggesting that the liquid core is very long for these conditions. Chehroudi *et al.*[150] and Hiroyasu *et al.*[155] provide more quantitative evidence of an extended contiguous liquid core for the atomization regime. We will consider their results shortly.

6.2.2. *Flow patterns*

Operating conditions for the wind-induced breakup regime are relatively narrow;[154] therefore, the most important regime for dense-spray phenomena of pressure-atomized sprays is the atomization regime. Flows within this breakup regime also exhibit several multi-phase flow patterns located in different regions of the spray. A sketch illustrating these patterns (based on the observations of Bracco and coworkers[12,13,149,150] and the large-scale sprays pictured in Figs 38–40) appears in Fig. 41.

The process illustrated in Fig. 41 begins with an all-liquid flow in a passage and finally evolves to a dilute spray. Once the dilute-spray approximations are acceptable over the entire cross-section of the flow, we reach the region where dilute spray analysis is normally used. However, a dilute-spray region

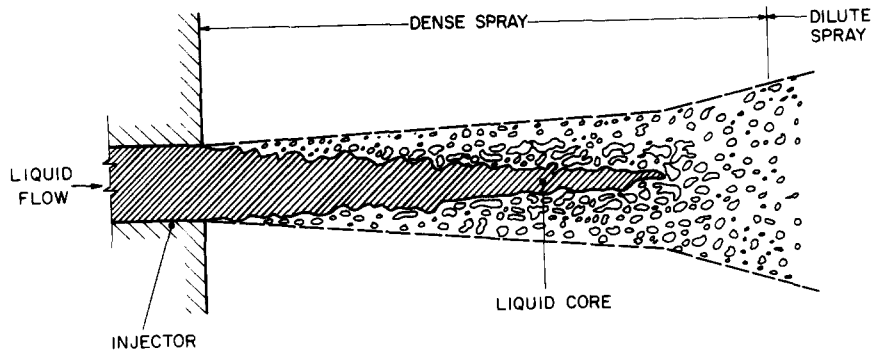

FIG. 41. Sketch of the near-injector region of a pressure-atomized spray for atomization breakup conditions.

always is present near the periphery of the flow, even upstream of the streamwise position where all the flow is dilute.

As the liquid leaves the injector, it enters a region defined as a churn flow pattern by Bracco.[12,13] This region includes the all-liquid core and other irregularly-shaped liquid elements near the axis of the flow. The terminology "churn flow" is drawn from usage for multiphase flow in tubes, where it refers to a flow pattern involving large irregular volumes of the ultimately dispersed flow near the axis.[151] In this sense, the churn flow descriptor is appropriate, however, criteria for flow regime transitions to and from the churn flow pattern of tube flow are naturally different. O'Rourke and Bracco[87] describe churn flow for sprays as a region where the volume fraction of liquid is greater than the gas, so that the liquid cannot be considered to be dispersed in the gas phase. Rather large liquid elements are present in churn flow, including the all-liquid core, favored by the high liquid fraction. The momentum exchange capabilities of the gas phase in this region is relatively limited, since gas density and its volume fraction are small; therefore, relative velocities between the phases are small in normal situations where streamwise pressure gradients are negligible. Thus, the large liquid elements are relatively stable in this region.

As the void fraction continues to increase by mixing, the large liquid elements pass into slower-moving gas where they become unstable and break up into ligaments and drops. This signals the onset of the dense-spray flow pattern. In the dense-spray region liquid fractions are relatively high; there is a wide diversity of drop sizes, shapes and velocities; and effects of collisions are probably significant. As the void fraction continues to increase, potential effects of collisions become small, and the liquid elements become small enough to approximate spheres. We then enter the dilute-spray region.

The churn-flow pattern descriptor is not very widespread as yet for sprays with many simply considering both the churn- and dense-spray flow patterns as the dense-spray region, e.g. all portions of the flow which are not dilute dispersed flows. We shall adopt this terminology except when it is important to consider the specific properties of the churn and dense-spray regions.

Observations of pressure-atomized sprays in the atomization regime do not reveal the features of the churn and dense spray flow patterns, since these regions are obscured by drops present in the dilute region, cf. Fig. 40. However, other evidence has been obtained suggesting the presence of a contiguous liquid core extending some distance from the injector. Hiroyasu *et al.*[155] measured the electrical resistance between the injector exit and a screen across the flow which could be traversed in the streamwise direction. It was assumed that the current carried by an unconnected region of the flow would be small, yielding the length of the contiguous liquid core. Chehroudi *et al.*[150] criticized this experiment and repeated the measurements using an extrapolation procedure to find the end of the contiguous core. A correlation of both these results yields the following expression:[12,150]

$$L_{fc}/d = C_c(\varrho_f/\varrho_\infty)^{1/2} \tag{46}$$

where C_c is a constant in the range 7–16, the lower value being due to the more recent measurements. Use of Eq. (46) places the length of the contiguous core in the range L_{fc}/d = 200–430 for the conditions of Fig. 40. From the flash photographs, the lower value of this range seems quite reasonable.

Additional verification of the density ratio effect included in Eq. (46) would be desirable. However, if we accept the correlation, liquid core lengths are quite significant even at high pressures. For example, at 100 atm., which is typical of Diesel engine pressures, $L_{fc}/d \sim$ 20–40 if the ambient gas is at room temperature and longer at elevated ambient temperatures. Earlier measurements and analysis of combusting pressure-atomized sprays at these conditions suggest spray lengths on the order of $x/d \sim 100$, with density ratio scaling roughly the same as Eq. (46).[68] This suggests that processes associated with the churn and dense-spray flow patterns occupy a significant volume of the liquid-containing regions of combusting pressure-atomized sprays.

The character of the churn and dense-spray flow

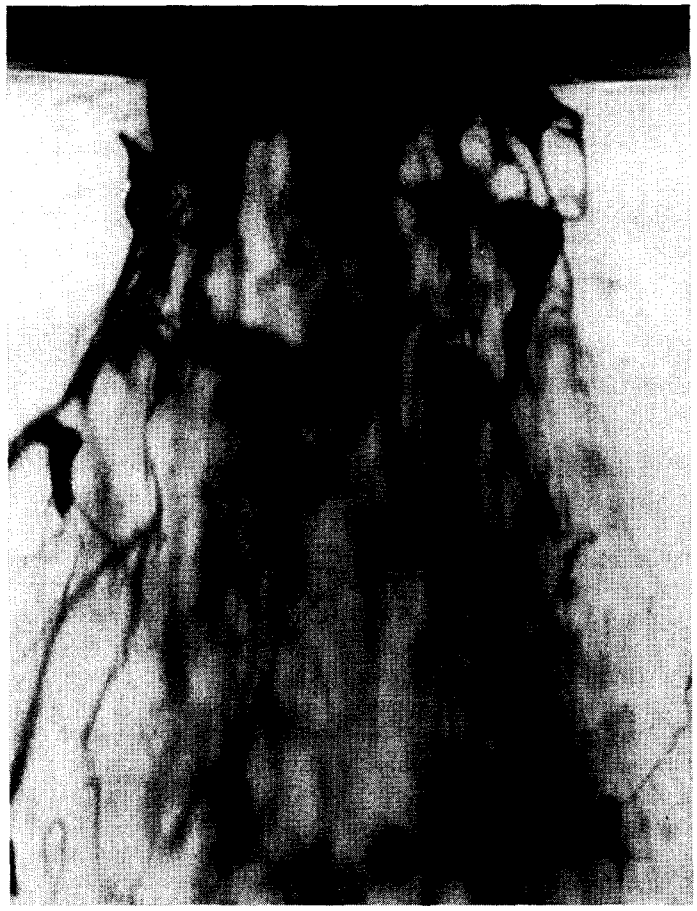

FIG. 42. Flash photograph of the flow at the exit of an air-atomizing injector.

patterns can be seen in the flash photograph (1 μsec flash duration) which appears in Fig. 42. The photograph illustrates the flow at the exit of the internally-mixed air-atomizing injector used by Solomon *et al.*[32,33] Thus, the liquid core is within the injector while the smallest drops, having diameters less than 10 μm, are not resolved. The spray was well-atomized, yielding an SMD of 30 μm at $x/d = 50$, which corresponds to the downstream end of the dense-spray region.

The churn and dense-spray flow patterns illustrated in Fig. 42 involve dispersed-phase elements having very complex shapes, e.g. ligaments, irregular drops, etc., which persist throughout the dense spray region. Similar observations of irregular structures near the exit of air-atomizing injectors abound.[18,143,144] It seems reasonable to assume that properties of the churn and dense-spray regions of pressure atomized sprays are similar. Therefore, while it is tempting to think of a dense spray as a close-packed collection of spherical drops, this picture is clearly not accurate. Irregular dispersed-phase elements are an essential part of dense sprays.

6.2.3. *Breakup processes*

The churn and dense-spray flow patterns begin as all-liquid flows in a passage and eventually evolve into a dilute spray consisting of a rather widely spaced array of polydisperse drops. Thus, by definition, these regions involve breakup processes. A number of phenomena are involved, e.g. aerodynamic breakup or stripping of small drops from the core, liquid sheets or large drops; splitting of sheets into ligaments; breakup of ligaments into drops; breakup of large drops into smaller ones; and probably drop shattering by collisions between drops.[143,144] The following considerations will be limited to stripping mechanisms, cf. Harrje and Reardon,[143] and Griffin and Muraszew[144] and references cited therein for a more complete treatment of breakup processes.

Bracco and coworkers[12,13] have considered effects of aerodynamic breakup mechanisms in the atomization regime. Emphasis was placed on breakup of the surface of the liquid core very near the injector exit, applying earlier results of Castleman,[156] Taylor[157] and Ranz.[158] This involves the unstable growth of surface waves, whose wavelengths become shorter and growth rates increase with increasing relative velocities. Shorter waves can appear closer to the injector exit, eventually signalling the onset of the atomization regime, where breakup of the surfaces appears to occur right at the exit. This theory involves some empiricism, but provides a framework for estimating

the initial average drop size and the angle of divergence of the drop-containing region.[12,13]

An interesting result of the aerodynamic breakup theory is that drops found near the injector exit are generally rather small in comparison to mean drop sizes measured farther downstream in sprays.[12] For example, O'Rourke and Bracco[87] evaluated tests conducted by Hiroyasu and Kodota[159] using aerodynamic breakup theory. They estimated an initial SMD of 6 μm, while mesurements farther downstream yielded an SMD of 42 μm. Simplified computations by O'Rourke and Bracco,[87] assuming that the entire spray broke up into small drops at $x/d = 10$, indicated that collisions and coalescence of drops could explain this behavior, e.g. the large drop densities favor large drop collision rates.

Subsequent work has confirmed some of these features of liquid-core breakup and the importance of drop collisions for the near-injector region of pressure-atomized sprays.[12,13] Measurements of drop diameters near the jet exit were compared with estimates based on aerodynamic breakup theory. Uncorrected use of the aerodynamic breakup theory gave correct trends, for these drop size measurements, concerning effects of jet velocity and liquid properties. However, trends concerning gas density were wrong and predictions underestimated measured drop diameters by roughly a factor of three. The fact that the region of observation was near the edge of the flow, rather than near the surface, was felt to be the cause of these discrepancies; thus, allowing for collisions between drops during their migration from the surface to the edge of the flow provided improved estimates of the measurements.[10,11] Another factor is that momentum exchanges between the gas and drops near the surface will decrease the continuous-phase velocity gradient at the surface—tending to increase drop size at their point of formation.

Chatwani and Bracco[149] recently extended the analysis of O'Rourke and Bracco.[87] The objective was to allow for the effect of gradual stripping of drops from the liquid core, rather than the original assumption that the liquid was all in the form of drops at a plane $x/d \sim 10$. The core was treated as a geometrical feature, since it could not be resolved with the rather coarse numerical grid used. Furthermore, the analysis involves numerous other approximations and empirical aspects that must be tested with measurements. However, limited comparisons with available measurements far from the injector, reported by Wu *et al.*,[147] were encouraging. Additional development of the approach is needed, since this analysis incorporates consideration of many of the flow processes and patterns encountered in dense sprays.

We have seen that breakup of the liquid core and drop collisions are important features of dense sprays. Circumstances are also encountered where secondary breakup of drops becomes important. This is particularly true for high pressure combusting sprays.[8] In this case, as the drop surface temperature increases, conditions near the thermodynamic critical point are approached. Reduced surface tension at near-thermodynamic-critical conditions causes loss of stability of the drop, leading to secondary breakup or shattering.

Past studies of drop breakup have generally involved subjecting drops to abrupt changes of relative velocity. Use of shock wave disturbances, has yielded the following criterion for breakup:[143]

$$We_{p\text{crit}} = Re_p^{1/2}/2 \tag{47}$$

where

$$We_p = \varrho|\vec{u}_p - \vec{u}|^2 d_p/(2\sigma) \tag{48}$$

and the drop Reynolds number is also based on the relative velocity. For values of We_p near the limit, "bag" breakup occurs, while for larger values breakup occurs by liquid stripping or shearing from the drop periphery. There is controversy concerning the breakup criterion of Eq. (47), particularly the need to include effects of the relative acceleration of the phases.[143] However, the bag-breakup limit provides a reasonable estimate of conditions where shattering must be considered, certainly no worse than uncertainties concerning the structure of dense sprays.

It is often assumed that drop breakup is abrupt in sprays, however, this is not always the case. Wolf and Anderson[160] provide expressions for the breakup time and the mean drop size after bag breakup. For present purposes, the following simpler breakup–time expression for the stripping mode, found by Ranger and Nicholls,[161] is adequate:

$$t_b|\vec{u}_b - \vec{u}|(\varrho/\varrho_f)^{1/2}/d_p = 4. \tag{49}$$

Equation (49) can be rearranged to give a measure of the streamwise distance traveled by the drop during breakup, as follows:

$$u_p t_b/d = 4(d_p/d)(\varrho_f/\varrho)^{1/2} u_p/|\vec{u}_p - \vec{u}|. \tag{50}$$

At low pressures, Eq. (50) suggests that large drops will break up over distances of ~ 10 injector diameters, e.g. $\varrho_f/\varrho = 1000$, $d/d_p = 10$ and $\vec{u}_p \gg \vec{u}$. This is a relatively small fraction of the drop-containing region even for combusting sprays, where this region extends to $x/d = 100$–1000. However, these distances are not at all comfortably small in comparison to the extent of the dense spray region. Thus, the dynamics of breakup of drops may have to be considered, similar to breakup of the liquid core, for accurate treatment of the dense-spray region.

For high pressure combustion processes, the length of the liquid containing region and the magnitude of the relative velocities become smaller. It is difficult to make a reasonable quantitative estimate of the relative length of breakup from Eq. (50), however, past structure calculations have suggested that breakup and drop lifetimes are comparable.[17] Further study of breakup at high pressure conditions is needed, since drop size is a critical issue concerning

the applicability of LHF analysis at such conditions.[17] More information on the breakup of irregular dispersed phase elements, like ligaments, would also be desirable.

6.2.4. *Collisions*

Bracco and coworkers[12,13] suggest that drop collisions are important in dense sprays. While collisions can be a mechanism of drop growth, they can also contribute to drop breakup. Furthermore, collisions have also been suggested as the mechanism responsible for the rapid radial growth of the drop-containing region observed at times in dense sprays.[32,33] In such cases, collisions probably contribute to the spread of the dispersed phase since they are an effective way to convert streamwise momentum to radial momentum. Finally, one criterion for the dilute dispersed-flow region is that effects of collisions are negligible.

Hinze,[3] presents an estimate of the number of collisions per unit time and volume, assuming uniform-sized particles, as follows:

$$\dot{n}_p \sim \bar{u}_r(1 - \alpha)^2/d_p^4 \qquad (51)$$

where a coefficient of order unity has been omitted to simplify the expression. Term $\bar{u}_r$ is the mean relative velocity between particles and α is the void fraction. Formally, mean velocities of the particles would be similar for monodisperse particles and $\bar{u}_{pr}$ is best approximated by the particle velocity fluctuations. Particle velocity fluctuations depend on the particle response to the gas phase in a complex way, as we have seen. A conservative estimate is to assume that slip is negligible and the gas and particle velocity fluctuations are identical. For the more realistic case of a polydisperse spray, collision rates will be higher than such estimates, since large particles have significant relative velocities in comparison to the gas phase, and thus the small particles.

The strong dependence of particle collision rates on d_p in Eq. (51) reveals why collisions were important near aerodynamic breakup processes yielding small drops. In contrast, the dilute-dispersed flow analyses considered in Section 3, involved flows where void fractions generally exceeded 99–99.9%. In these cases the numerator of the right hand side of Eq. (51) becomes small for the range of particle sizes of interest and collisions can be ignored.

O'Rourke and Bracco[87] develop a method for treating collisions in the context of discrete-element analysis. This method is based on proposals for computing collision processes in rain clouds by Brazier-Smith *et al.*,[163] Ogura and Takahashi,[164] and references cited therein. Results of collisions can lead to the proliferation of new drop groups for discrete element analysis; therefore, this was controlled by modifying the properties of colliding groups, while satisfying conservation principles. This collision model is only one aspect of a very complex analysis, however, and specific evaluation of its performance has not been reported.

6.3. *Dense-Spray Analysis*

6.3.1. *LHF analysis*

The flow near the injector for atomization conditions clearly involves numerous complex phenomena. There are several flow patterns, while transitions between patterns are not well-defined in all instances. Rather than being well-defined spheres, liquid elements in the flow are irregular in shape. Breakup of liquid elements (the all-liquid core, ligaments, drops) occurs by several mechanisms which can extend over appreciable distances in the flow. Furthermore, collisions between liquid elements are probably frequent but collision processes and their outcome have received relatively little attention. The examples given are only representative of some of the major problems, the list could be easily extended.

Since these phenomena are complicated, prospects are not good for developing detailed analysis of near-injector processes in the near future. Important elements of the flow must be studied explicitly in order to develop an adequate science base for rational formulation of such analysis. However, recent observations suggest an alternative that could provide a better understanding of at least some spray phenomena in the near-injector region. This involves the use of the LHF approximation to treat mixing properties, void structure and entrainment in the near-injector region of pressure-atomized sprays. The LHF approximation has been used to study various aspects of Diesel sprays, e.g. penetration, spray trajectories, etc., for some time, and has strong advocates for such use.[8,17]

Wu *et al.*[146,147] carried out more detailed measurements of pressure-atomized spray structure than in the past, finding results which are supportive of the use of LHF analysis at elevated pressures. In particular, photographs of spray boundaries suggested that LHF analysis provides reasonable estimates of the lateral spread of the edge of the spray. The flash photograph appearing in Fig. 40 tends to confirm this idea as well, since the deep-penetrating zones of drop intermittency present a single-fluid picture rather than a continuous phase being traversed by drops having large relative velocities. Measurements of velocities in pressure-atomized sprays, using LDA, were also given as evidence that LHF ideas might be pertinent in the near-injector region.[147]

These findings are support for the use of LHF analysis, however, they can be questioned. Small drops are generally present near the edge of pressure-atomized sprays. Drops of this size would be expected to act like tracer particles and spread according to LHF ideas. However, the light-scattering methods used to photograph these flows were not quantitative in terms of particle concentrations; therefore, we have no idea whether a significant mass flow rate of drops

was responsible for the photographic determinations of the edge. Thus, the results do not show whether larger drops or liquid elements under the surface layer of small drops are satisfying LHF approximations. The LDA measurements have uncertainties as well. Measurements were limited to regions far from the injector, $x/d > 300$; therefore, they have only a weak bearing on near-injector processes.[147,149] Additionally, only amplitude discrimination was used to distinguish phase velocities; therefore, the results are likely to be biased by the large number of small drops (which tend to satisfy the LHF approximation) present in such flows.

Evidence suggesting that LHF analysis is deficient for sprays is widespread as well. Results discussed in Section 3 show significant effects of relative velocities in almost every dilute spray where detailed measurements were made. The large spread rates observed in the dense regions of sprays from twin-fluid injectors, far beyond expectations of a single-phase turbulent jet, also cannot be explained by LHF analysis. These difficulties are apparent in the Figs 18, 22 and 42. However, it could be argued that most of the test conditions that were considered were chosen to highlight effects of turbulent dispersion; therefore, they are not necessarily representative of practical sprays. Furthermore, all the results were at atmospheric pressure and the deficiencies of LHF analysis may be reduced at elevated pressures.

Past work, however, also suggests difficulties with LHF analysis of pressure-atomized sprays at elevated pressures. Mao *et al.*[68] studied combusting pressure-atomized sprays and found that LHF analysis overestimated rates of spray development, even at pressures approaching 100 atm. Similar to all dense spray measurements (particularly at high pressures), however, their experimental findings involved substantial uncertainties. Additionally, their computations concerning effects of finite interphase transport rates ignored effects of drop shattering; which could be very important at high pressures where the stabilizing effect of surface tension decreases as the drop surface nears its thermodynamic critical point.[17] This is relevant since secondary breakup into smaller drops would favor LHF analysis. Finally, quantitative deficiencies aside, the LHF analysis did provide the correct trends of the effect of pressure on the measurements of Mao *et al.*[68] and were certainly not devoid of value concerning the mixing properties of the flow.

Clearly, work thus far has failed to resolve the controversy concerning application of LHF analyses to the dense regions of pressure-atomized sprays, particularly at elevated pressures. If the method is applicable for these flows it would be helpful for gaining a better understanding of dense sprays, with little empiricism beyond that needed for analysis of single-phase turbulent flows. Another advantage is that LHF analysis requires very little information concerning initial conditions of the analysis, offering good prospects for practical applications.

6.3.2. *Separated-flow analysis*

Even if LHF analysis yields useful information concerning the overall mixing properties of dense sprays, this will not provide sufficient detail for many purposes. The major deficiency is that LHF analysis does not provide information concerning dispersed-phase properties that is needed to specify initial conditions for the analysis of dilute sprays. Naturally, lack of physical understanding concerning processes responsible for dispersed-phase properties near the end of the dilute spray region, also limits capabilities to control the design of sprays. Separated-flow analysis is required to reveal properties of this nature. Past work along these lines is considered in the following.

Bracco and coworkers[12,13,87,148,149] have developed probably the most comprehensive model of dense spray processes, however, many of its features have not been specifically evaluated by comparison with measurements. The analysis is limited to the dense- and dilute-spray portions of the flow. The churn flow region is treated as a boundary condition. The analysis is formulated similar to dilute-spray analysis, but it incorporates features to treat dense-spray phenomena.

While the spray equation, similar to Williams,[22] is displayed with the formulation of Bracco and coworkers,[12,13,87] the spray equation is not solved explicitly. The formulation solved corresponds to a discrete-droplet approach. Thus a Eulerian formulation is used for the continuous phase while a Lagrangian formulation is used for the dispersed phase. Initial work treated turbulent dispersion using the approach described by Dukowicz,[80] with empirical turbulent diffusivities for the dispersed phase. More recent versions correspond to a stochastic separated-flow model, with random selection of eddy velocities, specifying that drops interact with particulate eddies for a computed correlation time.[148,149] The details of drop/eddy interactions differ from the approach used for the SSF analysis described in Section 2.6, however, and original sources should be considered for the specifics of this approach. Effects of high liquid fractions on drop transport rates are considered using empirical expressions developed from measurements of particle-laden fluidized beds.[87] It was found, however, that these corrections were not very significant for liquid fractions less than 10%, which is the region where computations have been made thus far. The governing continuous-phase equations account for the volume occupied by liquid, which is straightforward but not very important in the same regime. As noted earlier, the analysis allows for collisions using methods developed originally to describe processes in rain clouds.[163,164]

Initial conditions were specified across a plane near the injector, *ca.* $x/d = 10$, during initial calculations with the dense-spray analysis.[87,148] At this point it was assumed that all the liquid in the spray was broken up into drops having initial diameters given by the near-

injector estimate of the aerodynamic breakup analysis. This is not very realistic in view of the character of the churn flow region; therefore, more recent work has considered the presence of the liquid core, while ignoring the remaining portions of the churn-flow region. This was done by representing the core as a line source of drops having a length correlated similar to Eq. (46) and shaped like a cone. Aerodynamic breakup theory was used to estimate drop diameters while mass conservation in the liquid core gave drop mass fluxes as a function of distance from the injector. While these are plausible approximations, useful for considering potential effects of the liquid core, the approach is clearly not a complete representation of physical processes in the churn-flow region.

The churn-flow region presents particular problems for separated flow analysis. In this region, the gas phase is initially the dispersed phase while the liquid is the dispersed phase near the end of the region. Thus, dispersed flow analysis, where transport within the dispersed phase is ignored, is not particularly convenient.

Multiphase flows involving transitions from one dispersed phase to another are often best handled by the interpenetrating continua methods.[21] With this approach transport within each phase is considered so that the analysis proceeds smoothly through the variation of liquid volume fraction. The main problem with this approach is that interphase transport and processes, like turbulent dispersion, must be modeled. Nevertheless, application of the interpenetrating continua method to the churn-flow region of sprays deserves more attention than in the past.

7. CONCLUSIONS

1. Effects of finite interphase transport rates and turbulent dispersion were important in the dilute dispersed flows considered here; therefore, the LHF method, which ignores finite interphase transport rates and the DSF method, which ignores turbulent dispersion, were not very effective.

2. The SSF method, which treats both finite interphase transport rates and dispersed-phase/turbulence interactions (using random walk computations for dispersed phase motion and transport) yielded encouraging results for the present dilute dispersed flows. Flows considered included particle-laden gas jets, nonevaporating sprays, evaporating sprays, ultra-dilute combusting sprays, particle-laden liquid jets, noncondensing bubbly jets and condensing bubbly jets, which represents a wide variety of phase interactions and fluid properties.

3. The conserved-scalar formalism and a relatively unsophisticated k–ε-g turbulence model were used to estimate continuous-phase properties during present computations of dilute dispersed flows. This approach should be extended to consider anisotropic velocity fluctuations and correlations between density (mixture fraction) and velocity fluctuations, since evidence was found that dispersed-phase/turbulence interactions were influenced by these properties.

4. Effects of turbulence modulation (modification of continuous-phase turbulence properties by the dispersed phase) were observed near regions of dense dispersed flow and in regions of dilute dispersed flows where relative velocities were comparable to continuous-phase velocities. Current methods of estimating effects of turbulence modulation are not well-developed and deserve further study. Properly treating finite relative velocities and differences between the scale of the energy-containing eddies of the continuous phase and turbulence scales introduced by the motion of the dispersed phase are particular concerns.

5. Existing information on combusting dilute dispersed flows is very limited and more measurements are needed. For the non-premixed and ultra-dilute combusting sprays considered here, drops largely evaporated in regions where no oxidant was present. However, drops were observed to penetrate the flame zone; therefore, more theoretical and experimental information is needed concerning the initiation and stability of drop envelope flames for conditions representative of combusting sprays.

6. Dense sprays involve irregular liquid elements (ligaments, etc.) and significant effects of collisions and breakup. The complexities of these phenomena limit prospects for the development of detailed separated flow analyses of dense sprays in the near future. Recent work, however, suggests that LHF analysis might be effective for estimating the mixing and turbulent dispersion properties of the dense-spray region of pressure atomized sprays, in spite of deficiencies noted earlier in dilute sprays. Additional measurements are needed to definitively evaluate this suggestion.

7. Separated flow models incorporating features of stochastic analysis have been developed recently which are proving helpful in gaining a better understanding of dense spray processes. Many elements of these models, however, have not been evaluated due to deficiencies in available measurements. Future progress in this area is very much contingent on expanding the limited data base currently available for testing new theory.

In general, theoretical proposals to treat various aspects of sprays are far more numerous than measurements needed to evaluate these ideas and to highlight phenomena not yet considered in contemporary analysis. Greater emphasis on measurements in sprays and related dispersed flows is clearly needed.

Acknowledgements—The author's research on multiphase transport processes was sponsored by the National Aeronautics and Space Administration, Grant No. NAG 3-190, under the technical management of R. Tacina of the

Lewis Research Center; the Office of Naval Research, Contract No. N00014-80-C-0517 and N00014-85-C-0148, under the technical management of R. D. Ryan, M. K. Ellingsworth and L. Parnell; and the Air Force Office of Scientific Research, Grant No. AFOSR-85-0244, under the technical management of J. Tishkoff; and the Army Research Office, Contract No. DAAL03-86-K-0154, under the Technical Management of D. Mann.

REFERENCES

1. Soo, S. L. *Fluid Dynamics of Multiphase Systems*, Blaisdel, Waltham (1967).
2. Hinze, J. O. *Prog. Heat Mass Transfer* **6**, 433 (1972).
3. Hinze, J. O. *Turbulence*, 2nd Edn, pp. 427 and 724–734, McGraw-Hill, New York (1975).
4. Goldschmidt, V. W., Householder, M. K., Ahmadi, G. and Chuang, S. C. *Prog. Heat Mass Transfer* **6**, 487 (1972).
5. Peskin, R. L. *AIChE Symp. Ser.* 147, **71**, 52 (1975).
6. Marble, F. E. *A. Rev. Fluid Mech.* **2**, 397 (1970).
7. Lumley, J. L. *Turbulence*, P. Bradshaw (Ed.), pp. 289–324, Topics in Appl. Mech., Vol. 12, Springer-Verlag, Berlin (1978).
8. Faeth, G. M. *Prog. Energy Combust. Sci.* **3**, 191 (1977).
9. Clift, A. K., Grace, J. R. and Weber, M. E. *Bubbles, Drops and Particles*, pp. 185–319, Academic Press, New York (1978).
10. Law, C. K. *Prog. Energy Combust. Sci.* **8**, 171 (1982).
11. Sirignano, W. A. *Prog. Energy Combust. Sci.* **9**, 291 (1983).
12. Bracco, F. V. *Recent Advances in Gas Dynamics*, C. Casci (Ed.), Plenum Publishing Corp., New York (1983).
13. Bracco, F. V. Modeling of engine sprays, *SAE Pap. No. 850394* (1985).
14. Chigier, N. A. *Prog. Energy Combust. Sci.* **2**, 97 (1976).
15. Crowe, C. T. *J. Fluids Engng.* **104**, 197 (1982).
16. Faeth, G. M. Recent advances in modeling particle transport properties and dispersion in turbulent flow, *Proceedings of ASME-JSME Thermal Engineering Joint Conference*, Vol. II, pp. 517–534, New York (1983).
17. Faeth, G. M., *Prog. Energy Combust. Sci.* **9**, 1 (1983).
18. Lefebvre, A. H. *Prog. Energy Combust. Sci.* **6**, 233 (1980).
19. Lefebvre, A. H. Atomization performance of gas turbine fuel injectors, *Proceedings of Central States Meeting*, The Combustion Institute, Pittsburgh (1986).
20. Elkotb, M. M. *Prog. Energy Combust. Sci.* **8**, 61 (1982).
21. Drew, D. A. *Ann. Rev. Fluid Mech.* **15**, 261 (1983).
22. Williams, F. A. Some theoretical aspects of spray combustion, *ASME Pap. No. 85-WA/HT-44* (1985).
23. Al Taweel, A. M. and Landau, J. *Int. J. Multiphase Flow* **3**, 341 (1977).
24. Snyder, W. H. and Lumley, J. L. *J. Fluid Mech.* **48**, 41 (1971).
25. Yuu, S., Yasukouchi, N., Hirosawa, Y. and Jotaki, I. *AIChE Jl* **24**, 509 (1978).
26. McComb, W. D. and Salih, S. M. *J. Aerosol Sci.* **8**, 171 (1977).
27. McComb, W. D. and Salih, S. M. *J. Aerosol Sci.* **9**, 299 (1978).
28. Laats, M. K. and Frishman, F. A. *Fluid Dynamics*, **5**, 333 (1970).
29. Laats, M. K. and Frishman, F. A. *Heat Trans. Sov. Res.* **2**, 7 (1970).
30. Levy, Y. and Lockwood, F. C. *Combust. Flame* **40**, 333 (1981).
31. Shuen, J.-S., Solomon, A. S. P., Zhang, Q.-F. and Faeth, G. M. *AIAA Jl* **23**, 396 (1985).
32. Solomon, A. S. P., Shuen, J.-S., Zhang, Q.-F. and Faeth, G. M. *AIAA Jl* **23**, 1548 (1985).
33. Solomon, A. S. P., Shuen, J.-S., Zhang, Q.-F. and Faeth, G. M. *AIAA Jl* **23**, 1724 (1985).
34. Solomon, A. S. P., Shuen, J.-S., Zhang, Q.-F. and Faeth, G. M. *J. Heat Transfer* **107**, 679 (1985).
35. Shuen, J.-S., Solomon, A. S. P. and Faeth, G. M. *AIAA Jl* **24**, 101 (1986).
36. Parthasarathy, R. N. and Faeth, G. M. Structure of turbulent particle-laden water jets in water, *Int. J. Multiphase Flow*, in press.
37. Sun, T.-Y. and Faeth, G. M. *Int. J. Multiphase Flow* **12**, 99 (1986).
38. Sun, T.-Y. and Faeth, G. M. *Int. J. Multiphase Flow* **12**, 115 (1986).
39. Sun, T.-Y., Parthasarathy, R. N. and Faeth, G. M. *J. Heat Transfer* **108**, 951 (1986).
40. Gany, A., Mannheimer-Timnat, T. and Wolfshtein, M. *Acta astronaut.* **3**, 241 (1976).
41. Harlow, F. H. and Amsden, A. A. *J. comput. Phys.* **17**, 19 (1975); ibid. **18**, 440 (1975).
42. Peskin, R. L. and Kau, C. J. *J. Fluids Engng.* **101**, 319 (1979).
43. Moore, E. F. and Davis, R. W. Numerical computation of particle trajectories: a model problem, *Joint Fluid Mechanics, Plasma Dynamics and Laser Conference*, ASME, New York (1985).
44. Davis, R. W., Moore, E. F. and Crowe, C. T. *Proceedings of the Third International Conference on Numerical Methods in Laminar and Turbulent Flows*, C. Taylor and B. A. Schrefler (Ed.), pp. 279–290, Pineridge Press, Swansea (1983).
45. Lockwood, F. C. and Naguib, A. S. *Combust. Flame* **24**, 109 (1975).
46. Bilger, R. W. *Prog. Energy Combust. Sci.* **1**, 87 (1976).
47. Bilger, R. W. *Combust. Flame* **30**, 277 (1977).
48. Liew, S. K., Bray, K. N. C. and Moss, J. B. *Combust. Sci. Technol.* **27**, 69 (1981).
49. Liew, S. K., Bray, K. N. C. and Moss, J. B. *Combust. Flame* **56**, 199 (1984).
50. Pope, S. B. *AIAA Jl* **16**, 279 (1978).
51. Jeng, S.-M. and Faeth, G. M. *J. Heat Transfer* **106**, 721 (1984).
52. Jeng, S.-M. An investigation of structure and radiation properties of turbulent buoyant diffusion flames, Ph.D. Thesis, The Pennsylvania State University, University Park (1984).
53. Wygnanski, I. and Fiedler, H. E. *J. Fluid Mech.* **38**, 577 (1969).
54. Becker, H. A., Hottel, H. C. and Williams, G. C. *J. Fluid Mech.* **30**, 285 (1967).
55. Hetsroni, G. and Sokolov, M. *J. appl. Mech.* **93**, 315 (1971).
56. Birch, A. D., Brown, D. R., Godson, M. G. and Thomas, J. R. *J. Fluid Mech.* **88**, 431 (1978).
57. Chevray, R. and Tutu, N. K. *J. Fluid Mech.* **88**, 133 (1978).
58. Shearer, A. J., Tamura, H. and Faeth, G. M. *J. Energy* **3**, 271 (1979).
59. Mao, C.-P., Szekely, G. A., Jr. and Faeth, G. M. *J. Energy* **4**, 78 (1980).
60. Gore, J. P. and Faeth, G. M. *J. Heat Transfer*, **109**, 165 (1987).
61. Gore, J. P. and Faeth, G. M. *AIAA Jl*, **25**, 339 (1987).
62. Jeng, S.-M., Chen, L.-D. and Faeth, G. M. *Nineteenth Symposium (International) on Combustion*, pp. 1077–1085, The Combustion Institute, Pittsburgh (1982).
63. Jeng, S.-M. and Faeth, G. M. *J. Heat Transfer* **106**, 891 (1984).

64. GORE, J. P. and FAETH, G. M. Structure and spectral radiation properties of turbulent ethylene/air diffusion flames, *Twenty-First Symposium (International) on Combustion,* The Combustion Institute, Pittsburgh, in press.
65. BILGER, R. W. *AIAA Jl* **20**, 962 (1982).
66. FAETH, G. M. and SAMUELSEN, G. S. *Prog. Energy Combust. Sci.* **12**, 305 (1986).
67. ABDEL-KHALIK, S. I., TAMARU, T. and EL-WAKIL, M. M. *Fifteenth Symposium (International) on Combustion,* pp. 389–399, The Combustion Institute, Pittsburgh (1975).
68. MAO, C.-P., WAKAMATSU, Y. and FAETH, G. M. *Eighteenth Symposium (International) on Combustion,* pp. 337–347, The Combustion Institute, Pittsburgh (1981).
69. GORDON S. and MCBRIDE, B. J. Computer program for calculation of complex chemical equilibrium compositions, rocket performance, incident and reflected shocks and Chapman-Jouget detonations, *NASA SP-273,* Washington (1971).
70. PRAUSNITZ, J. M. and CHUEH, P. L. *Computer Calculations for High Pressure Vapor-Liquid Equilibria,* Prentice-Hall, Englewood Cliffs (1968).
71. JONES, W. P. Models for turbulent flows with variable density, *Prediction Methods for Turbulent Flow,* Hemisphere Publ. Corp., Washington (1980).
72. JONES, W. P. and WHITELAW, J. H. *Combust. Flame* **48**, 1 (1982).
73. TCHEN, C. M. Mean value and correlation problems connected with the motion of small particles suspended in a turbulent fluid, Ph.D. Thesis, University of Delft, The Hague (1947).
74. HJELMFELT, A. T. and MOCKROS, L. F. *Appl. scient. Res.* **6**, 149 (1966).
75. ELGHOBASHI, S. E. and ABOU-ARAB, T. W. *Phys. Fluids* **26**, 931 (1983).
76. YUDINE, M. I. *Adv. Geophys.* **6**, 185 (1959).
77. CSANADY, G. T. *J. atmos. Sci.* **20**, 201 (1963).
78. JUREWICZ, J. T. and STOCK, D. E. A numerical model for turbulent diffusion in gas–particle flows, *ASME Pap. 76-WA-FE-33* (1976).
79. ABBAS, A. S., KOUSSA, S. S. and LOCKWOOD, F. C. *Eighteenth Symposium (International) on Combustion,* pp. 1427–1438, The Combustion Institute, Pittsburgh (1981).
80. DUKOWICZ, J. K. *J. comput. Phys.* **35**, 229 (1980).
81. HUTCHINSON, P., HEWITT, G. F. and DUKLER, A. E. *Chem. Engng. Sci.* **26**, 419 (1971).
82. BROWN, D. J. and HUTCHINSON, P. *J. Fluids Engng.* **101**, 265 (1979).
83. GOSMAN, A. D. and IOANNIDES, E. Aspects of computer simulation of liquid-fueled combustion, *AIAA Pap. No. 81-0323* (1981).
84. SHUEN, J.-S., CHEN, L.-D. and FAETH, G. M. *AIChE Jl* **29**, 167 (1983).
85. SHUEN, J.-S., CHEN, L.-D. and FAETH, G. M. *AIAA Jl* **21**, 1483 (1983).
86. ZHANG, Q.-F., SHUEN, J.-S., SOLOMON, A. S. P. and FAETH, G. M. *AIAA Jl* **23**, 1123 (1985).
87. O'ROURKE, P. J. and BRACCO, F. V. *Inst. mech. Engr.* Pub. ISBN 0852984693, 101 (1980).
88. ODAR, F. and HAMILTON, W. S. *J. Fluid Mech.* **18**, 302 (1964).
89. MOORE, D. W. *J. Fluid Mech.* **23**, 749 (1965).
90. SHUEN, J.-S., SOLOMON, A. S. P., ZHANG, Q.-F. and FAETH, G. M. A theoretical and experimental study of turbulent particle-laden jets, *NASA CR-168293* (1983).
91. GOSMAN, A. D., LOCKWOOD, F. C. and SYED, S. A. *Sixteenth Symposium (International) on Combustion,* pp. 1543–1555, The Combustion Institute, Pittsburgh (1977).
92. MODARRESS, D., TAN, H. and ELGHOBASHI, S. *AIAA Jl* **22**, 624 (1984).
93. MOSTAFA, A. A. and MONGIA, H. C. On the turbulence-particles interaction in turbulent two-phase flows, *AIAA Pap. No. 86-0215* (1986).
94. SOLOMON, A. S. P. A theoretical and experimental investigation of turbulent sprays. Ph.D. Thesis, The Pennysylvania State University, University Park (1984).
95. TISHKOFF, J. M., HAMMOND, D. C., JR. and CHRAPLYVY, A. R. Diagnostic measurements of fuel spray dispersion, *ASME Pap. No. 80-WA/HT-35* (1980).
96. FOUNTI, M., HUTCHINSON, P. and WHITELAW, J. H. Measurements and calculations of a kerosene fueled flow in a model furnace, *Rep. FS/79/19,* Mechanical Engineering Department, Imperial College, London (1979).
97. SZEKELY, G. A., JR. and FAETH, G. M. *Combust. Flame* **49**, 255 (1983).
98. OWEN, P. R. *J. Fluid Mech.* **20**, 225 (1964).
99. OWEN, P. R. *J. Fluid Mech.* **39**, 407 (1969).
100. HINO, M. *ASCE J. Hydrol.* HY **4**, 161 (1963).
101. KADA, H. and HANRATTY, T. C. *AIChE Jl* **6**, 624 (1960).
102. KUCHANOV, S. I. and LEVICH, V. G. *Sov. Phys.-Dokl.* **12**, 549 (1967).
103. MELVILLE, W. K. and BRAY, K. N. C. *Int. J. Heat Mass Transfer* **22**, 279 (1979).
104. AL TAWEEL, A. M. and CARLEY, J. F. *Chem. Prog. Symp. Ser.* **67** (116), 124 (1971).
105. ONSAGER, L. *Phys. Rev.* 68, 286 (1945); *Nuovo Cim.,* Suppl. 6, No. 2, 279 (1949).
106. CORRSIN, S. *Phys. Fluids* **7**, 1156 (1964).
107. PAO, Y.-H. *Phys. Fluids* **8**, 1063 (1965).
108. BAW, P. S. H. and PESKIN, R. L. *J. bas. Engng.* **93**, 631 (1971).
109. AL TAWEEL, A. M. and LANDAU, J. *J. Engr. Sci.* **4**, College of Engr., Univ. of Riyadh, 97 (1978).
110. LAUFER, J. The structure of turbulence in fully developed pipe flow, *NACA Rep. 1174* (1954).
111. KOMASAWA, I., KUBOI, R. and OTAKI, T. *Chem. Engng. Sci.* **29**, 641 (1974).
112. NAGARAJ, N. and GRAY, D. J. Particle/droplet characterization in multiphase aerodynamic flows, *AIAA Pap. No. 86-0455* (1986).
113. MICHAELIDES, E. E. *Int. J. Multiphase Flow,* **10**, 61 (1984).
114. ABRAMOVICH, G. N. *Sov. Phys.-Dokl.* **15**. 101 (1970).
115. ABRAMOVICH, G. N. *Int. J. Heat Mass Transfer* **14**, 1039 (1971).
116. MEEK, C. C. and JONES, B. G. *J. atmos. Sci.* **30**, 239 (1973).
117. DANON, H., WOLFSHTEIN, M. and HETSRONI, G. *Int. J. Multiphase Flow* **3**, 233 (1977).
118. GENCHEV, ZH. D. and KARPUZOV, D. S. *J. Fluid Mech.* **101**, 833 (1980).
119. HARLOW, F. H. and NAKAYAMA, P. I. *Phys. Fluids* **10**, 2323 (1967).
120. ELGHOBASHI, S., ABOU-ARAB, T., RIZK, M. and MOSTAFA, A. A. *Int. J. Multiphase Flow* **10**, 697 (1984).
121. CHAO, B. T. *Osterr. Ing. Arch.* **18**, 7 (1964).
122. CALABRESE, R. V. and MIDDLEMAN, S. *AIChE Jl* **25**, 1025 (1979).
123. PESKIN, R. L. *Proceedings of the First International Symposium on Stochastic Hydraulics,* pp. 251–267, University of Pittsburgh Press, Pittsburgh (1971).
124. ALONSO, C. V. *ASCE Trans.* **107**, 733 (1981).
125. MODARRESS, D., WUERER, J. and ELGHOBASHI, S. An experimental study of a turbulent round two-phase jet, *AIAA Pap. No. 82-0964* (1982).
126. POURAKMADI, F. and HUMPHREY, J. A. C. *Int. J. Physi-*

cochem. Hydrodynamics **4**, 191 (1983).
127. CROWDER, R. S. III, DAILY, J. W. and HUMPHREY, J. A. C. *J. Pipelines* **4**, 159 (1984).
128. CHEN, C. P. and WOOD, P. E. *Can. J. chem. Engng.* **63**, 349 (1985).
129. CHEN, C. P. and WOOD, P. E. Turbulence closure modeling of the dilute gas-particle axisymmetric jet, *AIChE Jl*, in press.
130. CHEN, C. P. Calculation of confined gas-particle two-phase turbulent flows, *AIAA Pap. No. 86-0219* (1986).
131. HANJALAC, K., LAUNDER, B. E. and SCHIESTAL, R. *Turbulent Shear Flows II*, pp. 36–49, Springer-Verlag, Berlin (1980).
132. TSUJII, Y., MOREKAWA, Y. and SHIOMI, H. *J. Fluid Mech.* **139**, 417 (1984).
133. STEIMKE, J. L. and DUKLER, A. E. *Int. J. Multiphase Flow* **9**, 751 (1983).
134. LEE, S. L. and DURST, F. *Int. J. Multiphase Flow* **8**, 125 (1982).
135. KRAMER, T. J. and DEPEW, C. A. *J. bas. Engng.* **94**, 492 (1972).
136. MEMMOTT, V. J. and SMOOT, L. D. *AIChE Jl* **24**, 466 (1978).
137. BUCKINGHAM, A. C. Turbulent density gas coupling with weak statistical coupling, *AIAA Pap. No. 79-1484* (1979).
138. BUCKINGHAM, A. C. *AIAA Jl* **19**, 501 (1981).
139. BUCKINGHAM, A. C. and SIEKHAUS, W. J. Interaction of moderately dense particle concentrations in turbulent flow, *AIAA Pap. No. 81-0346* (1981).
140. BETCHOV, R. and LORENZEN, C. *Phys. Fluids* **17**, 1503 (1974).
141. UBEROI, M. S. and FREYMUTH, P. *Phys. Fluids* **13**, 2205 (1970).
142. FAIST, M. B. and MUCKERMAN, J. T. *J. chem. Phys.* **69**, 4087 (1978).
143. HARRJE, D. T. and REARDON, F. H. (Ed.) Liquid propellant rocket combustion instability, pp. 37–102, *NASA SP-194*, Washington (1972).
144. GRIFFIN, E. and MURASZEW, A. *The Atomisation of Liquid Fuels*, John Wiley and Sons, New York (1953).
145. REITZ, R. D. and BRACCO, F. V. *Phys. Fluids* **25**, 1730 (1982).
146. WU, K.-J., SU, C.-C., STEINBERGER, R. L., SANTAVICCA, D. A. and BRACCO, F. V. *J. Fluids Engng.* **105**, 406 (1983).
147. WU, J.-J., SANTAVICCA, D. A., BRACCO, F. V. and COGHE, A. *AIAA Jl* **22**, 1263 (1984).
148. MARTINELLI, L., REITZ, R. D. and BRACCO, F. V. *AIAA Prog. Astronaut. Aeronaut.* **95**, 484 (1984).
149. CHATWANI, A. V. and BRACCO, F. V. Computation of dense spray jets, *3rd International Conference on Liquid Atomisation and Spray Systems*, Imperial College, London (1985).
150. CHEHROUDI, B., ONUMA, Y., CHEN, S.-H. and BRACCO, F. V. On the intact core of full-cone sprays, *SAE Pap. 850126* (1985).
151. COLLIER, J. G. *Convective Boiling and Condensation*, 2nd Edn, pp. 8–23, McGraw-Hill, New York (1981).
152. RANZ, W. E. *Can. J. Chem. Engng.* **36**, 175 (1958).
153. MIESSE, C. C. *Ind. Engng. Chem.* **47**, 1690 (1955).
154. REITZ, R. D. Atomization and other breakup regimes of a liquid jet, Ph.D. Thesis, Princeton University (1978).
155. HIROYASU, H., SHIMIZU, M. and ARAI, M. *Proceedings of 2nd International Conference on Liquid Atomization and Spray Systems*, Madison, WI (1982).
156. CASTLEMAN, R. A., JR. The mechanism of atomization accompanying solid injection, *NACA Rep. 440* (1932).
157. BATCHELOR, G. K. (Ed.) *Collected Works of G. I. Taylor*, Cambridge University Press, Cambridge (1958).
158. RANZ, W. E. *Can. J. Chem. Engng.* **36**, 175 (1958).
159. HIROYASU, H. and KADOTA, T. *SAE Trans.* **83**, 2615 (1974).
160. WOLFE, H. E. and ANDERSON, W. H. Kinetics mechanism and resulting drop sizes of aerodynamic breakup of liquid drops, *Aerojet Gen. Rep. No. 0395-04 (18) SP*, Sacramento (1964).
161. RANGER, A. A. and NICHOLLS, J. A. *AIAA Jl* **7**, 285 (1969).
162. LOEB, L. B. *The Kinetic Theory of Gases*, pp. 31–39, Dover Publications, London (1961).
163. BRAZIER-SMITH, P. R., JENNINGS, S. G. and LATHAM, J. *Proc. R. Soc. Lond.* **A326**, 393 (1972).
164. OGURA, Y. and TAKAHASHI, T. *J. atmos. Sci.* **30**, 262 (1973).